



University of Tennessee, Knoxville
**TRACE: Tennessee Research and Creative
Exchange**

Doctoral Dissertations

Graduate School

12-2020

Multi-layer Utilization of Beamforming in Millimeter Wave MIMO Systems

Mustafa S. Aljumaily

University of Tennessee, Knoxville, mlatief@vols.utk.edu

Follow this and additional works at: https://trace.tennessee.edu/utk_graddiss

 Part of the [Digital Communications and Networking Commons](#)

Recommended Citation

Aljumaily, Mustafa S., "Multi-layer Utilization of Beamforming in Millimeter Wave MIMO Systems. " PhD diss., University of Tennessee, 2020.
https://trace.tennessee.edu/utk_graddiss/6057

This Dissertation is brought to you for free and open access by the Graduate School at TRACE: Tennessee Research and Creative Exchange. It has been accepted for inclusion in Doctoral Dissertations by an authorized administrator of TRACE: Tennessee Research and Creative Exchange. For more information, please contact trace@utk.edu.

To the Graduate Council:

I am submitting herewith a dissertation written by Mustafa S. Aljumaily entitled "Multi-layer Utilization of Beamforming in Millimeter Wave MIMO Systems." I have examined the final electronic copy of this dissertation for form and content and recommend that it be accepted in partial fulfillment of the requirements for the degree of Doctor of Philosophy, with a major in Computer Engineering.

Husheng Li, Major Professor

We have read this dissertation and recommend its acceptance:

Hairong Qi, Seddik Djouadi, Xiaopeng Zhao

Accepted for the Council:

Dixie L. Thompson

Vice Provost and Dean of the Graduate School

(Original signatures are on file with official student records.)

Multi-layer Utilization of Beamforming in Millimeter Wave MIMO Systems

A Dissertation Presented for the
Doctor of Philosophy
Degree

The University of Tennessee, Knoxville

Mustafa Sadiq Latief Al Jumaily
December 2020

Copyright © by Mustafa Sadiq Latief Al Jumaily, 2020
All Rights Reserved.

To my Family, Friends, and Country

Acknowledgments

First, I would like to thank the Iraqi Government and the Higher Committee for Education Development in Iraq (HCED) for this opportunity to pursue my PhD degree fully funded by their scholarship program. Also, I would like to thank my family for their support and patience during my long years of study, without your support I would never went this far. Special Thanks to my advisor Professor (Husheng Li) for his kind guidance, support, and mentorship. Finally, I would like to thank all the friends who have been with me since the beginning and believed in me all the time.

Thanks so much.

Abstract

mmWave frequencies ranging between (30-300GHz) have been considered the perfect solution to the scarcity of bandwidth in the traditional sub-6GHz band and to the ever increasing demand of many emerging applications in today's era. 5G and beyond standards are all considering the mmWave as an essential part of their networks. Beamforming is one of the most important enabling technologies for the mmWave to compensate for the huge propagation loss of these frequencies compared to the sub-6GHz frequencies and to ensure better spatial and spectral utilization of the mmWave channel space. In this work, we tried to develop different techniques to improve the performance of the systems that use mmWave. In the physical layer, we suggested several hybrid beamforming architectures that both are relatively simple and spectrally efficient by achieving fully digital like spectral efficiency (bits/sec/Hz). For the mobility management, we derived the expected degradation that can affect the performance of a special type of beamforming that is called the Random Beamforming (RBF) and optimized the tunable parameters for such systems when working in different environments. Finally, in the networking layer, we first studied the effect of using mmWave frequencies on the routing performance in an ad-hoc type of networks compared to the performance achieved when using sub-6 GHz frequencies. Then we developed a novel opportunistic routing protocol for Mobile Ad-Hoc Networks (MANET) that uses a modified version of the Random Beamforming (RBF) to achieve better end to end performance and to reduce the overall delay in delivering data from transmitting nodes to the intended receiving nodes. From all these designs and studies, we conclude that mmWave frequencies and their enabling technologies (i.e. Beamforming, massive MIMO, ...etc.) are indeed the future of wireless communications in a high demanding world of Internet of Things (IoT), Augmented Reality (AR), Virtual Reality (VR), and self driving cars.

Table of Contents

1	Introduction	1
1.1	Motivation	1
1.2	Concept of Beamforming	2
1.3	Beamforming in the Physical Layer	3
1.4	Mobility Effect on Random Beamforming	5
1.5	Routing Protocols using mmWave	10
2	Hybrid Beamforming in Massive-MIMO mmWave Systems	13
2.1	Using LU Decomposition	13
2.1.1	System Model	14
2.1.2	Simulation Results	19
2.1.3	Comparing with Other Matrix Factorization Methods	19
2.2	Using Convex Optimization and Machine Learning	24
2.2.1	Introduction	24
2.2.2	Convex Optimization Using CVX	25
2.2.3	System Model	26
2.2.4	Simulation Results	28
2.3	Beamforming with DeepMIMO for mmWave Networks	30
2.3.1	System Model	31
2.3.2	Deep MIMO Dataset and Simulation process	32
3	Performance of Random Beamforming in Mobile mmWave Systems	47
3.1	System Model	48

3.1.1	Downlink Broadcasting MIMO System that uses mmWave	48
3.1.2	System Throughput	49
3.1.3	Random Beamforming	50
3.2	Outage Probability Due to Mobility	51
3.2.1	Mobility Assumptions	51
3.2.2	Degradation Analysis	52
3.3	System Parameters Optimization	60
3.3.1	Frame-Duration Optimization	60
3.3.2	Beam-Width Optimization	61
3.4	Numerical Results	61
4	Routing Protocols in Mobile Ad-Hoc Networks Using Millimeter Wave	76
4.1	MANET Routing Algorithm with mmWave	77
4.1.1	Performance Evaluation Metrics	81
4.1.2	mmWave Frequencies in the NS3 Simulator	82
4.1.3	Performance Evaluation	82
4.2	Opportunistic Routing Protocol For Ad-Hoc Networks Using mmWave and Random Beamforming	91
4.2.1	Introduction	91
4.2.2	System Model	93
4.2.3	Opportunistic Routing in MANET Using mmWave	95
4.2.4	Performance Evaluation	97
4.2.5	Interference Analysis	97
4.2.6	Expected Per-Hop Throughput	100
4.2.7	Average Delay Per Hop	101
4.2.8	End to End Performance	103
4.2.9	Conclusions	105
	Bibliography	107
	Vita	118

List of Tables

2.1	Simulation Parameters	20
2.2	Approximation Techniques Comparison	29
2.3	Simulation Parameters	34
3.1	Mathematical Derivation Parameters	62
3.2	Simulation Parameters	71
4.1	Simulation Scenario Parameters	85
4.2	Performance Evaluation Parameters	98

List of Figures

1.1	Hybrid Beamforming Architecture	7
1.2	Possible Performance degradation resulted from mobility when using the random beamforming	7
2.1	Two structures of hybrid precoding in mmWave MIMO systems using different mapping strategies: each RF chain is connected to N_t antennas in (b) and to N_t/N_{RF}^t antennas in (c).	15
2.2	Comparison of two analog RF precoder structures.	15
2.3	Examples of the channel realizations used in the experiments	20
2.4	16X4 MIMO system achievable spectral efficiency comparison for single user	21
2.5	64X16 MIMO system achievable spectral efficiency comparison for single user	21
2.6	144X36 MIMO system achievable spectral efficiency comparison for single user	22
2.7	16X4 MIMO system achievable spectral efficiency comparison for 5 user . . .	22
2.8	64X16 MIMO system achievable spectral efficiency comparison for 5 user . .	23
2.9	144X36 MIMO system achievable spectral efficiency comparison for 5 user .	23
2.10	Suggested system structure in the Transmitter and the same is used in the receiver	29
2.11	16X4 MIMO system achievable spectral efficiency comparison among different approximation techniques and the fully digital precoder	29
2.12	16X4 MIMO system achievable spectral efficiency comparison	34
2.13	16X4 MIMO linear regression results for the training data	35
2.14	16X4 MIMO linear regression results for the validation data	36
2.15	16X4 MIMO linear regression results for the testing data	37

2.16	16X4 MIMO linear regression results for all the data set	38
2.17	64X16 MIMO System Achievable Spectral Efficiency Comparison	39
2.18	144X36 MIMO System Achievable Spectral Efficiency Comparison	39
2.19	16X4 MIMO System Achievable Spectral Efficiency Comparison for 10 users	40
2.20	64X16 MIMO System Achievable Spectral Efficiency Comparison for 10 users	40
2.21	144X36 MIMO System Achievable Spectral Efficiency Comparison for 10 users	41
2.22	Both LU-decomp. and ML-aided for single user and 64X16 MIMO System Achievable Spectral Efficiency Comparison	41
2.23	Coordinated Beamforming System Model	43
2.24	A top View of the street, buildings, and the Base stations distribution	44
2.25	UE Mobility Speed Effect on the Achievable Spectral Efficiency	45
2.26	Achievable Spectral Efficiency with Nadam optimizer	45
2.27	Achievable Spectral Efficiency with MSLE loss function	46
3.1	Possible Performance degradation resulted from mobility when using RBF. .	53
3.2	Beam Area with Side Borders.	53
3.3	Beam Approximate Shape with the Edge Probability Calculation Parameters	56
3.4	Relationship Between UE location and probability of leaving the Beam: (a) UE far enough from the Beam Border so that the probability of leaving the beam is too small. (b) UE is closer to the beam border which increases the probability of leaving the beam during the RTT. (c) UE is very close to the beam border, which increases the probability of leaving the beam even more.	57
3.5	Assumed Triangular Distribution of the Beam Leaving Probability	58
3.6	Probability of leaving the Beam Area for Walking Users for different beam angles	62
3.7	Probability of leaving the Beam Area for Running Users for different beam angles	63
3.8	Probability of leaving the Beam Area for Biking Users for different beam angles	64
3.9	Probability of leaving the Beam Area for Users Riding a Car for different beam angles	65

3.10	Expected Throughput Degradation for different Walking Speeds.	66
3.11	Expected Throughput Degradation for different Running Speeds.	67
3.12	Expected Throughput Degradation for different Biking Speeds.	68
3.13	Expected Throughput Degradation for different Car Speeds.	69
3.14	Throughput Degradation Resulted from Simulated Mobility for Random Speeds, Directions, and Distances between BS and UE	71
3.15	Optimal Frame Duration for Different Outage Probability Percentages with Walking Speed Range UEs	72
3.16	Optimal Frame Duration for Different Outage Probability Percentages with Running Speed Range UEs	73
3.17	Optimal Beam Angle for Different Outage Probabilities with Walking UEs . .	74
3.18	Optimal Beam Angle for Different Outage Probabilities with Running UEs .	74
4.1	Path Loss Comparison for different Channel models and Distances	83
4.2	mmWave modules in the ns3 Simulator	83
4.3	Packets Received for Different Wi-Fi MANET Routing Protocols	85
4.4	Packets Received for different mmWave MANET (with RMa Channel Model) Routing Protocols	86
4.5	Average Delivery Ratio for both Wi-Fi MANET and mmWave MANET (with RMa Channel Model) Routing Protocols	86
4.6	Packets Received for different mmWave MANET (with UMA Channel Model) Routing Protocols	87
4.7	Average reception rate for different routing protocols for mmWave UMa channel	87
4.8	Packets Received for Different Wi-Fi MANET Routing Protocols with 4kbps transfer rate and 128 Byte packet size	89
4.9	Packets Received for different mmWave MANET (with UMa Channel Model) Routing Protocols with 4kbps transfer rate and 128 Byte packet size	89
4.10	Average Delivery Ratio for both Wi-Fi MANET and mmWave MANET (with UMa Channel Model) Routing Protocols with 4kbps transfer rate and 128 Byte packet size	90

4.11 Tx Power of each UE and its Effect on the Delivery Ratio	90
4.12 Expected number of nodes per beam for different beam angles and node densities	98
4.13 An illustration of possible Interference	102
4.14 Achievable Throughput per Hop (in Mbps) for Different Hop Distances . . .	102
4.15 Average Delay (in seconds) per Hop for Different Hop distances (in meters) .	104
4.16 End to End Throughput (in Mbps) for Different Simulation Scenarios	104
4.17 End to End Delay (in seconds) for Different Simulation Scenarios	106

Chapter 1

Introduction

1.1 Motivation

The motivations to work on mmWave frequencies are so many and obvious as the mmWave is now considered an essential part of the 5G wireless communications and all the generations coming after it [70]. In our work, we studied the use of mmWave frequency bands (mainly the 28GHz band) in the three main networking layers (physical, data link, and networking) with different perspectives and tools but with common goal. Our goal in this work is to demonstrate the superiority and benefits that comes with the mmWave utilization in different network layers and the expected gain that these frequencies provide to the end users in different applications that are bandwidth and speed hungry [1, 12, 11]. Beamforming is considered now as one of the main enabling technologies for wireless communication networks that use mmWave [7, 9]. Different methods in building beamforming systems have been studied and the hybrid type was shown to be the most suitable one from a hardware cost and feasibility point of view. Different hybrid beamforming architectures were suggested in [7, 9] for different applications and use cases and their advantages over the state of the art architectures were explained. Fifth generation of wireless communications or (5G) is promising tens of times faster communications and cheaper megabits per seconds compared to the 4G LTE networks [1]. To achieve such promises, 5G architecture depends to a large extent on the densification of cell towers and base stations and the use of beamforming. Mobility of users while communicating to the cell towers that uses beamforming requires

the beams to track users movement and location or use adaptive beamforming techniques. Mobility effect on a special type of beamforming (called random beamforming [49]) was studied in the papers [8, 5] and the parameters of the network were optimized for different situations. Routing in a multihop wireless networks was also studied in [10, 6]. In [10], a new opportunistic routing protocol for mobile ad hoc networks was suggested and compared with the state of the art protocols. On the other hand, in [6] we studied the effect of using mmWaves in an ad hoc networks and compared the performance with other well known routing protocols using the ns3 simulator and the channel measurements from the NYU university.

1.2 Concept of Beamforming

Beamforming is the process of sending and receiving data in beams in specific directions in the 3D plane of the area between the transmitter and receiver devices. It can be described as a spatial filtering operation that use an array of radiators to capture or radiate energy in a specific direction over its aperture [47]. The improvement achieved over omnidirectional transmission/reception is called the transmit/receive gain. In Multiple-In Multiple-Out (MIMO) systems, beamforming can be achieved by electronic beam steering using a phased array, which is a multi-element radiation device with a specific geometric configuration. The output spatial power distribution, termed as the array radiation pattern, is determined by the vector sum of the fields radiated by individual elements. It can be expressed in terms of the individual element radiation pattern and the array factor, which is a function of the array geometry and amplitude/phase shifts applied to individual elements [47].

In mmWave band, the gain realized through antenna beamforming can compensate for the excessive path and penetration losses. The millimeter wave channel characteristics, to a large extent, dictate the choice of physical (PHY) layer and medium access control (MAC) layer schemes as well as the hardware implementation. From this perspective, multiple antenna technology is a key enabler to efficiently utilize the millimeter wave band as it can increase the link capacity by employing directional communication. The small wavelengths

in the millimeter wave regime has facilitated array architectures embedded into portable devices with a compact form factor, making beamforming an attractive proposition [47].

1.3 Beamforming in the Physical Layer

Millimeter wave (mmWave) frequency band has been considered as a vital part of the current and future communications systems. The huge available bandwidth of mmWave allows data rates of multi-gigabits per second, an end to end delay of milliseconds, and massive machine-type communications (mMTC) as suggested in the 5G standard [1]. Despite all these benefits, mmWave suffers from many problems related to the weak reflection from surfaces, several orders of magnitude pathloss compared with microwave signals, and huge atmospheric absorption compared with other traditional frequencies in the sub-6GHz band. All these limitations encourage the use of beamforming techniques, to send narrow beams instead of omnidirectional transmissions, which becomes a common sense when designing mmWave systems [24]. Many techniques have been used to design beamforming systems, whereas only a few of them are practically feasible. Fully digital beamforming has been proven to be impractical for commercial systems, because of the high cost and power consumption issues [24]. Therefore the hybrid beamforming is a cost-effective replacement to achieve high spectral efficiency ($bits/sec/Hz$) in the mmWave band [86]. Hybrid beamforming design has been focused on optimizing one of the following three aspects: improving spectral efficiency to make it as close as possible to the fully digital one, increasing computational efficiency by using some convex relaxation techniques, or ensuring hardware efficiency by reducing the number of phase shifters to the minimum while maintaining the other aspects. The tradeoffs among these competing goals have been the main issue in this field in the recent years [86, 85, 87] and [24, 87, 74, 83, 76, 74, 75, 56]. One of the early designs of hybrid beamforming systems was suggested in [24], where they exploited the spatial structure of mmWave channels in formulating the precoding (at the transmitter) and combining (at the receiver) as a sparse reconstruction problem. Alternating minimization for hybrid precoding [86, 85] is another well known technique that has been evolving over years and proven to attain a better efficiency than [24]. In their work, they treated the hybrid precoder (it has

been common to use precoder and beamformer interchangeably in the literature) as a matrix factorization problem [86]. They suggested two different structures as fully connected and partially connected structures for both single and multiple user cases. It has been studied on how many phase shifters are required for the system to reduce the system cost and hardware complexity in [87]. On the other hand, the phase shifter resolution and its effect on the achievable spectral efficiency have been studied in [74, 83]. These works tried to minimize the cost of the system by using limited resolution phase shifters, which is more practical than assuming infinite or high resolution phase shifters as assumed in other researches. In [76], a special codebook design for the hybrid beamforming systems was suggested, which takes the special directional characteristics of mmWave channels in consideration. Hybrid beamforming structure was proven to achieve (almost) the same performance as the fully digital beamforming scheme in [74]. The only condition to achieve that is to have the number of RF chains to be equal to or more than twice of the number of data streams [74]. That work was generalized for multiuser case in [75], with the same relationship between the number of RF chains and the number of data streams. A more comprehensive survey about the traditional designs for hybrid beamforming can be found in [56]. Simple diagram that explains the general components of the beamforming system in both the transmitter (precoder) and the receiver (the combiner) devices is shown in figure 1.1:

Using matrix factorization in designing hybrid beamforming systems have been suggested in many recent studies as in [60, 88]. In [60], they propose a method to design a hybrid beamforming system (precoder and combiner) for multistream transmission in massive MIMO systems, by directly decomposing the predesigned unconstrained digital precoder/combiner of a large dimension MIMO system. They got a spectral efficiency that is pretty close to the optimal fully digital ones by using a singular value decomposition (SVD) based technique to secure an initial point sufficiently close to the global solution of the original nonconvex problem. Even though their algorithm is taking many iterations to converge and its complexity is very high. On the other hand, authors of [88] suggest a systematic design framework for hybrid beamforming for multi-cell multiuser massive MIMO systems over mmWave channels. These channels are characterized by sparse propagation paths and the framework relies on the decomposition of analog beamforming vectors and

path observation vectors into Kronecker products of factors being uni-modulus vectors. Their channel estimation method is derived specifically for their beamforming model where it estimates the angles-of-arrival (AoA) of data and interference paths by analog beam scanning and data-path gains by analog beam steering [88]. To design a hybrid precoder and combiner that achieve as close as possible spectral efficiency to the optimal fully digital ones, we assume that each device that wants to transmit a data will send a pilot signal (that is well known for all devices in the network) and will receive the response of the possible receiver devices that includes the channel matrix information. Once the channel matrix is estimated (using the pilot feedback), we can calculate the fully digital precoder (and combiner in the receiver side) matrix easily. From those matrices (namely called the F_{opt} in the transmitter side and the W_{opt} in the receiver side) we can derive the digital baseband and the analog RF matrix that can be used directly in the hybrid beamforming process. We prove through simulation that our designs (decomposition, machine learning aided, and the DeepMIMO based design) can reach high performance compared to the fully digital ones and that the resulted matrices from these designs are obeying the hardware limitations of each suggested design.

1.4 Mobility Effect on Random Beamforming

Random Beamforming (RBF) for Multiple Input, Multiple Output (MIMO) communication systems has been studied for a long time [73, 49, 48, 25]. Many channel models have been suggested for such beamforming scheme such as the Uniform Random Single-Path (UR-SP) and Uniform Random Multiple-Path (UR-MP) for mmWave frequency bands as in [49, 48] respectively. The Random Beamforming for MIMO systems that uses mmWave generally focuses on utilizing the sparsity in the arrival angle domain and the partial downlink Channel State Information (CSI) of the mmWave to prove that with enough number of users, we can achieve a linear sum rate scaling with respect to the number of antennas in the Base Station (BS) [49]. Based on that, Cellular systems with reduced feedback from the user equipment (UE) to the base station (BS) can be built in order to get faster systems with less overhead, and reasonable performance. In millimeter waves systems, the need for speed and overhead reduction has increased especially that the goal of the system is to get a multi-Gigabits per

second throughput in a semi optical crowded environments with an end-to-end delay in the order of milliseconds. The existing work about the RBF for mmWaves is considering only the stationary (no mobility) scenarios for UEs in each cell. So, the effect of mobility on the overall performance is investigated here in order to get more practical insights about the system performance for mobile users. See figure 1.2 for possible mobility scenario effect.

The investigation of mobility effect on system throughput is of a special importance for the broadcast systems using random beamforming scheme. In the existing random beamforming schemes, the BS randomly forms a beam, which is expected to point to a UE (opportunistically), with the assumption that there are sufficiently many UEs in each beam area of the BS. The UEs send back feedbacks (i.e. SNR), such that the BS can pick the UE with the highest signal-to-noise ratio (SNR). Then the BS sends the data to the UE along the same beam direction. However, if the UE is mobile, the beam may be misaligned during the data transmission period (see figure 1.2), since the UE is no longer at the original location. The faster the UE moves, the more the possibility of the beam misses the UE, thus causing significant performance loss.

Some of the previous works in this field include studying the mobility effects on the millimeter waves communication systems from Channel State Information (CSI) point of view. In [51], authors suggest that the normal walking speed in mmWave channel is stationary during the IEEE 802.11ad frame duration. whereas there is 2.0 to 4.0 dB degradation of the average Block Error Rate (BLER) performance for the narrow band transmissions [51]. Other work to study the non stationary nature of UE and its effect on the overall system performance was done in [52]. This work also included suggesting new models to describe the scenario specific geometric properties of the mmWave systems like [52]. Their measurement experiments show the feasibility of millimeter-wave small cells but at the same time the high time variance of the propagation channel resulted from the mobility [52]. In [61], authors suggest an approximation model, based on the Quasi-Stationary (QS) assumptions, in order to speed up the computation in the Markovian framework, and they use that model to calculate the average system throughput for both static and mobile users. They also take the probability of handover for mobile users between different Base Stations in consideration.

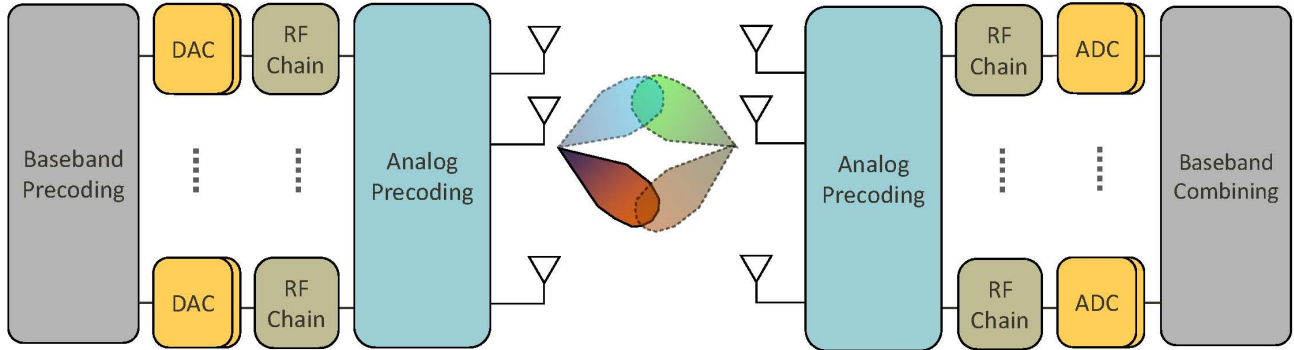


Figure 1.1: Hybrid Beamforming Architecture

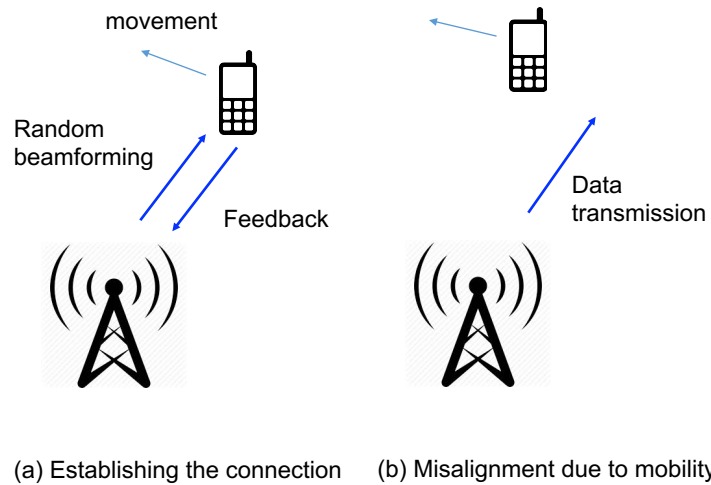


Figure 1.2: Possible Performance degradation resulted from mobility when using the random beamforming

The first part of chapter 3 is to study the mobility effect from different perspective [8]. Taking the same assumptions in [73] and [48] for system model and assuming many UE's with different mobility possibilities ranging from walking and running to biking and riding a car speed ranges. In each case we studied the effect of the beam width, the distance between BS and the mobile UE, the direction of movement of the UE, and the possible distance that the UE can move during the round trip time (RTT) of the messages from UE to BS and coming back. The effect of each of these factors was studied alone and then were combined together to get a closed form expression that gives a better idea about how much the throughput of the system can be affected because of the users mobility [8]. The other possible effects of mobility like blockage (both from the user itself (self blockage) or from other obstacles in the environment), the doppler shift results from horizontal and vertical movement of UE during mobility, and user scheduling if there are many users in each beam coverage area are good directions for further future works.

After studying the mobility effect and derive it both mathematically and through extensive simulation in [8], optimizing other system factors (like the frame duration and the beam angle) for RBF in mobile scenarios was studied as well in [5]. The goal of the work in [5] was to provide the best possible service to mobile users in the systems using RBF. Taking in consideration the typical coverage distance for Base Stations in an Ultra Dense Networks [30] (i.e. no more than 200 meters), and the results of the work in [8], we derived the best frame duration and the beam width for each outage probability [5].

Many researchers have been working on determining the optimal length of frames for different system applications and scenarios as in [80, 42, 4]. Minimizing the frame duration in large wireless networks (with multi-hops) have been found to be equivalent to the packet throughput maximization in [80]. In other words, authors in [80] minimized the frame duration in order to maximize packet throughput while optimizing the multicast trees of the network to be used by the packet streams [80]. They maximized the traffic throughput of the network by minimizing the total number of time slots in each frame [80]. Although they got good results, their assumptions can not be generalized for all scenarios as it can depend on other system factors like the number of users, the available bandwidth, and the type of application the system used for.

Usually there is a difference between the transmitted frame duration by the primary sender (communication initiator) and the secondary sender (the receiver) and it can waste the frequency channel. This was studied in [42] where such difference and its effect on the overall system throughput was reduced. To solve such a problem, the secondary sender was set to adjust the length of its frame to the length of the primary sender's frame by selecting frames used for frame aggregation properly [42]. Even though the delay and the wasted time were reduced, and the system throughput was improved, but no closed form solution was derived for the optimum frame length in terms of the differences in slots durations.

Authors in [4] went a step further in their study and suggested a closed form estimation for the optimum frame length for Frame Slotted ALOHA protocol in Radio Frequency Identification (RFID) systems. They do so by optimizing the Time-Aware Framed Slotted ALOHA (TAFSA) efficiency, which takes in consideration the differences in the slot durations. Despite the many attempts to optimize the frame duration, but there is no (one fits all) optimal frame duration for all scenarios. In the second part of our work, we optimized several parameters including the frame duration for MIMO systems that uses Random Beamforming algorithm in the downlink broadcast communication systems that use mmWave frequency band. In the optimization process, the derived expected degradation (outage expectations) resulted from user mobility that was published in [8] was used for different system parameters and scenarios.

In beamforming, we can set the beam width based on different factors. Deciding the optimal beam width for the directional Beamforming in mmWave systems has been studied extensively recently as in [62, 63]. In [62] Small Cell Networks (SCNs) with relaying capabilities (among UEs) that used mmWave frequencies was studied. The overall system throughput is optimized as a result of a coordinated meta-heuristically optimized beamwidth/alignment-delay approach. It has been shown that unless beamwidths for each transmitter-receiver pair are carefully chosen, many situations occur where there is considerable multiuser interference (MUI) even in TDMA systems [62]. The same authors of [62] proposed a novel framework [63] where they combine Matching Theory and Swarm Intelligence together to dynamically and efficiently pair vehicles and optimize both transmission and reception beamwidths in [63]. Both the Channel State Information (CSI)

and the Queue State Information (QSI) have been used in establishing the vehicle-to-vehicle (V2V) communication links [63]. In our work, the optimization of the beamwidth is done to utilize the hidden dependencies among the various parameters of the system when using RBF with mmWave and mobile users.

1.5 Routing Protocols using mmWave

Mobile Ad-hoc Networks (MANETs) have been studied for many years and they are the networks formed solely from mobile User Equipment (UE) that are cooperating to exchange data in an Infrastructure-less environment [55]. MANET can be used for many applications include the tactical edge operations, disastrous areas, and in the congested environments like campuses and stadiums where many users are willing to exchange information directly with each other or using others' devices as routers. Fifth generation (5G) of wireless communications is intended to provide much higher data rates and much lower end-to-end over-the-air (OTA) latency [84]. Some prospective applications for the 5G (beside the traditional cellular communications) are the wireless virtual reality (VR), Augmented Reality (AR), Device to Device (D2D) communications in the network edges, and the autonomous vehicles in the Vehicular Ad-hoc Networks (VANET) [22, 84], which can be part of an infrastructural or infrastructure-less networks. Millimeter wave frequencies (mmWave) are expected to have a major role in the networks that use 5G and beyond standards [66]. They have their advantages of huge available bandwidth (several GHz) and reduced delay, while they also have some limitations that are related to the limited transmission range, and the need for transmitting narrow beams to cover larger distances. The work in chapter four is intended to test the performance of a mobile ad-hoc network that consists of only mmWave user equipment (UE) without eNodeB (or gNodeB as suggested recently by the 3GPP [54]). The delivery ratio of data that is transmitted between any two mobile nodes in the network is of a significant importance for the feasibility and stability of the mmWave MANET applications. This type of networks with dynamic topology (because of mobility and lack of Infrastructure) is unsuitable for traditional end-to-end routing algorithms, and

that is why many MANET routing protocols have been proposed to control forwarding data from any node to any other node in the multi-hop MANET network [55].

Traditional routing protocols for ad-hoc networks are usually dependent on the broadcast nature of wireless signals in the sub-6 GHz band [3]. With the mmWave's directional antennas and beamforming, this argument about wireless signals is no longer true. To compensate for such a shortage, mmWave devices use many approaches to scan the entire environment around them like beam sweeping, random beamforming (RBF), et al. [69] and send narrow directional beams towards the intended destination nodes to mitigate the large propagation path loss.

Mobile Ad hoc Networks (MANET) have been attracting a lot of research attention for many years now. Many routing protocols were proposed for these networks, and the ones that are analyzed in this work [64, 20, 18] are among the most famous ones. Besides interesting in providing efficient data forwarding protocols in these networks, ensuring link availability and network stability have been studied as well in [36, 37]. Optimizing routes to achieve the ergodic rate density (ERD) in each link has been proven in [67], though they considered as the upper bound that can be achieved and some sub-optimal and more realistic protocols have also be presented in [67].

Many geographic based routing protocols have been proposed for such mobile ad-hoc networks as in [21, 43]. In [21], a parallel routing protocol (PRP) for MANET was proposed, where multiple data packets over disjoint paths can be routed simultaneously. Though they assume that each node in the network can maintain updated information about its own location in the virtual grid of the network using GPS which is not always available for such nodes in reality. In [43], several different routing protocols for MANET were analyzed and their performance was compared for special MANET networks that are used for video streaming with all of its special requirements. It was found that video streaming is possible for such networks using the traditional routing protocols with acceptable quality [43]. Although, they show that the performance of any routing protocol varies depending on the network scenario and the type of video traffic used.

In [79], they use a stochastic geometry approach to characterize the one-way and two-way communication characteristics and especially the Signal to Interference Ratio (SIR),

and the Interference to Noise Ratio (INR) distributions of a mmWave ad-hoc network with directional antennas, random blockage model, and ALOHA channel access. Another work that tried to utilize the mmWave in MANET was done in [15] where they proposed an Optimal Geographic Routing Protocol (OGRP) and a directional Medium Access Control (MAC) protocol for MANET with small range using directional antennas. Though, that work did not analyze or compare the performance of the suggested protocol with other protocols that are normally working in Wi-Fi networks. Other than that, there have been no efforts to study the effect of using mmWave on the performance of the MANET in the literature. This motivated us to study the effect of using mmWaves in MANET scenarios in the first part of chapter four and then suggest a novel opportunistic routing protocol for MANET networks for special usage [10] in the second part of it.

Chapter 2

Hybrid Beamforming in Massive-MIMO mmWave Systems

2.1 Using LU Decomposition

Beamforming is considered as one of the most important enabling techniques for mmWave with massive-MIMO communication systems. Fully digital beamforming has been proven to be infeasible from the hardware point of view. Analog Beamforming, on the other hand, can not achieve as good spectral efficiency as required for the high throughput applications expected for the next generation of wireless communications. So, the hybrid beamforming, as a combination of digital baseband and analog RF phase shifters, has been considered the common sense when designing beamforming systems. Achieving a performance that is close to the fully digital beamformers has been the goal of many studies recently. In this chapter, the hybrid beamforming is suggested to be built by decomposing the Fully digital optimal beamforming matrix into two matrices for the digital and the analog parts of the hybrid beamformer using the matrix factorization method called LU-Decomposition. Then we test the results to make sure they obey the hardware limitations of the system. Our results show that it is possible to build a very efficient hybrid beamformer with such simple method and to get as close performance to the fully digital one as possible. This work has been published partially in [7].

2.1.1 System Model

Traditionally, there are many methodologies to construct hybrid precoding (beamforming) systems based on the approach of connecting the RF chains with the phase shifters. The architecture that is used in our work is shown in Fig. 2.1 as in [85]. This design has been proven to be further simplified, when the digital and analog components of the beamformer are connected as in Fig. 2.2 (b) from [86] with double phase shifters. Such systems can achieve a specific throughput that is limited by the hardware of massive MIMO systems. Many attempts to improve such systems' performance have been carried out (as explained in the introduction); however, none of them could attain the same efficiency as the fully digital precoders. Taking in considerations that none of the previously suggested systems could reach exactly the same efficiency achievable by the fully digital beamformers, we suggest a simple matrix decomposition (LU decomposition) method to produce a digital and analog matrices that can achieve almost the same spectral efficiency as the fully digital beamforming systems while being subject to the hardware limitations.

The received signal according to the system shown in Figures 2.1 and 2.2 for the general case (multiple users) in an OFDM hybrid beamforming MIMO system is given by:

$$\mathbf{y}_{k,f} = \mathbf{W}_{\text{BB},k,f}^H \mathbf{W}_{\text{RF},k}^H \left(\mathbf{H}_{k,f} \sum_{k=1}^K \mathbf{F}_{\text{RF}} \mathbf{F}_{\text{BB},k,f} \mathbf{s}_{k,f} + \mathbf{n}_{k,f} \right) \quad (2.1)$$

where $\mathbf{s}_{k,f} \in \mathbb{C}^{N_s}$ is the transmitted symbol vector for the k -th user on the f -th subcarrier such that:

$$E[\mathbf{s}_{k,f} \mathbf{s}_{k,f}^H] = \frac{1}{KN_s F} I_{N_s}. \quad (2.2)$$

Here $\mathbf{F}_{\text{BB},k,f} \in \mathbb{C}^{N_{\text{RF}}^t \times N_s}$ is the digital baseband precoder (at the transmitter). $\mathbf{W}_{\text{BB},k,f} \in \mathbb{C}^{N_{\text{RF}}^r \times N_s}$ is the digital baseband combiner (at the receiver). $\mathbf{F}_{\text{RF}} \in \mathbb{C}^{N_t \times N_{\text{RF}}^t}$ is the analog RF precoder at the transmitter. $\mathbf{W}_{\text{RF},k} \in \mathbb{C}^{N_r \times N_{\text{RF}}^r}$ is the analog RF combiner at the receiver. Both \mathbf{F}_{RF} and \mathbf{W}_{RF} are subcarrier independent operations. $n_{k,f} \in \mathbb{C}^{N_r}$ is the adaptive noise with Independent and identically distributed (i.i.d.) Gaussian distribution $\mathcal{N}(0, \sigma^2)$. k is the number of users. f is the number of subcarriers of the OFDM. The other assumptions about these values are that they are subject to the hardware constraints $KN_s \leq N_{\text{RF}}^t \leq N_t$ and

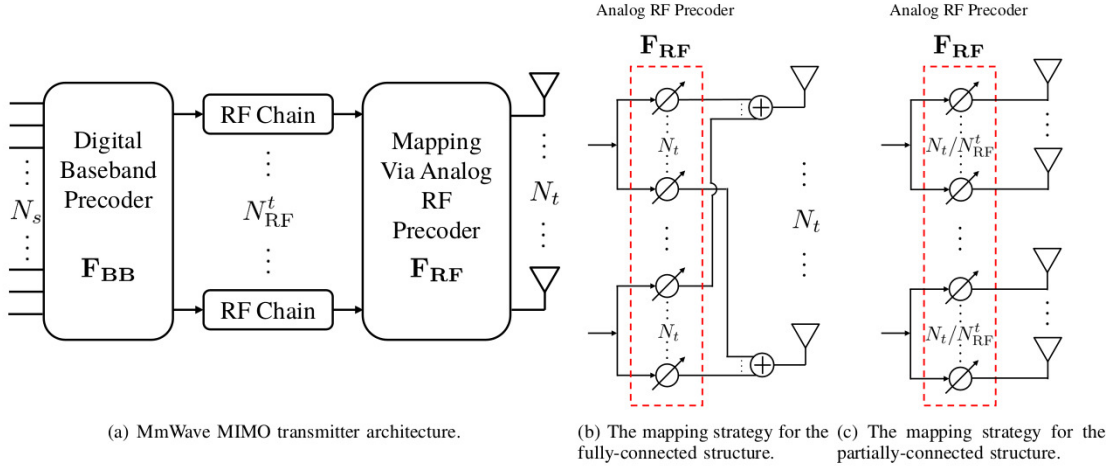


Figure 2.1: Two structures of hybrid precoding in mmWave MIMO systems using different mapping strategies: each RF chain is connected to N_t antennas in (b) and to N_t/N_{RF}^t antennas in (c).

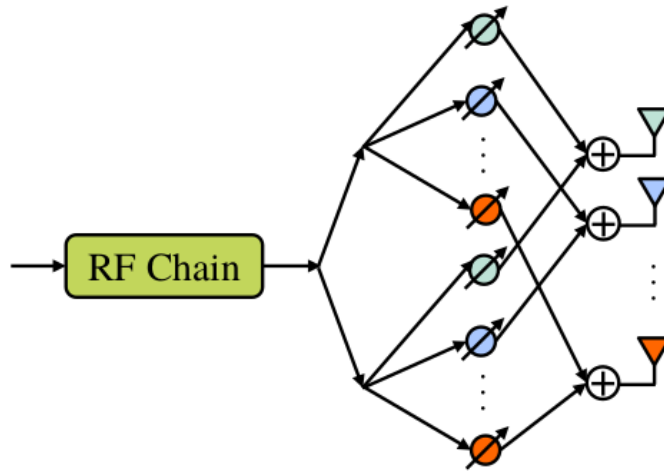
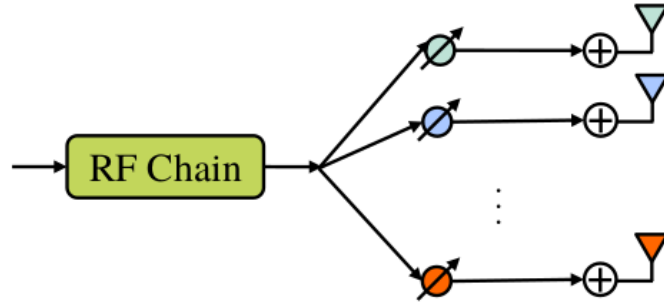


Figure 2.2: Comparison of two analog RF precoder structures.

$N_s \leq N_{RF}^r \leq N_r$ for K users [86]. The mmWave MIMO channel between the BS and the k -th user in the f -th subcarrier, denoted as $H_{k,f}$, can be characterized by the Saleh-Valenzuela model:

$$\mathbf{H}_{k,f} = \gamma_k \sum_{i=0}^{N_{cl,k}-1} \sum_{l=1}^{N_{ray,k}} \alpha_{il,k} \mathbf{a}_r(\theta_{il,k}) \mathbf{a}_t^H(\phi_{il,k}) e^{-j2\pi i f / F}, \quad (2.3)$$

where γ_k is the normalization factor given by

$$\gamma_k = \sqrt{\frac{\rho_k N_t N_r}{N_{cl,k} N_{ray,k}}}. \quad (2.4)$$

$N_{cl,k}$ is the number of clusters. $N_{ray,k}$ is the number of rays in each cluster. ρ_k is the path loss between the BS and the k -th user. $\alpha_{il,k}$ is the gain of the l -th ray in the i -th propagation cluster. $\mathbf{a}_r(\theta_{il,k})$ is the receive array response vector. $\mathbf{a}_t(\phi_{il,k})$ is the transmit array response vector. $\theta_{il,k}$ is the Angle of Arrival (AoA), and $\phi_{il,k}$ is the Angle of Departure (AoD). The underlying problem is to design the hybrid beamforming transceivers to achieve the maximum spectral efficiency (or the rate) for the possible digital and analog components, which can be expressed as

$$\begin{aligned} & \max_{F_{RF}, F_{BB}, W_{RF}, W_{BB}} R \\ \text{s.t. } & Tr(F_{RF} F_{BB} F_{BB}^H F_{RF}^H) \leq P \\ & \|F_{RF}(i, j)\|^2 = 1, \forall i, j \\ & \|W_{RF}(i, j)\|^2 = 1, \forall i, j \end{aligned} \quad (2.5)$$

where the data rate R is given by:

$$R = \log_2(|I_{N_s} + \frac{\rho}{N_s} \mathbf{R}_n^{-1} \mathbf{W}_{BB}^* \mathbf{W}_{RF}^* \mathbf{H} \mathbf{F}_{RF} \mathbf{F}_{BB} \mathbf{F}_{BB}^* \mathbf{F}_{RF}^* \mathbf{H}^* \mathbf{W}_{RF} \mathbf{W}_{BB}|) \quad (2.6)$$

The problem has been proven in [86] [85] and [24] to be reduced to the following form:

$$\begin{aligned}
& \min_{F_{RF}, F_{BB}} \|F_{opt} - F_{RF}F_{BB}\|_f \\
& \text{s.t. } F_{RF} \in A \\
& \|F_{RF}F_{BB}\|_f^2 = N_s
\end{aligned} \tag{2.7}$$

where A represents the unit modulus constraint (which is not a convex and need to be relaxed or changed), and F_{opt} is the fully digital beamforming matrix and considered as the optimal upper bound we need to reach. F_{opt} in the transmitter and W_{opt} in the receiver are comprised of the first N_s columns of V and U resulted from the singular value decomposition (SVD) of the channel matrix H respectively [86]. The second constraint is the power constraint of the transceiver. In other words, the problem is to minimize the difference between the results of the precoder and combiner and the optimal fully digital beamformer. Also the hybrid precoder design for multicarrier and multiuser systems using alternating minimization and double phase shifters (DPS), as shown in Fig. 2.2, can be reduced to the following:

$$\begin{aligned}
& \min_{F_{RF}, F_{BB}} \|\mathbf{F}_{opt} - \mathbf{F}_{RF}\mathbf{F}_{BB}\|_f \\
& \text{subject to } \|(\mathbf{F}_{RF})_{i,j}\| \leq 2
\end{aligned} \tag{2.8}$$

which is a convex optimization problem (for both the precoder at the transmitter and the combiner at the receiver) [86]. The same applies for W_{opt} , W_{RF} , and W_{BB} in the receiver side. When designing a hybrid precoder and combiner, we are trying to minimize the difference between the F_{opt} and the product of the F_{RF} and F_{BB} in the transmitter and the difference between W_{opt} and the product of the W_{RF} and the W_{BB} in the receiver, respectively. In the transmitter, this can simply be done by decomposing the F_{opt} into two matrices using the LU decomposition method [2] (and the same applies for the combiner in the receiver). While the original LU decomposition method was only used for square matrices and produced two $n \times n$ square matrices as well, the extensions of it can be used for any rectangular matrix [19]. When an $n \times m$ rectangular matrix get decomposed to a lower triangle (L) and upper triangle (U) matrices, it produces an $n \times n$ L matrix and an $n \times m$ U matrix. For our system, this means that the F_{RF} (corresponding to L matrix in our case) should obey the condition that $N_t = N_{RF}^t$ which is also true according to our assumptions in section II-A. Also, complying

with the condition in equation 2.8 was tested (in simulation) for many channel realizations for both the precoder and combiner matrices and for single and multiple users. The results were always fit with the condition in equation 2.8. The algorithm 1 is briefly explaining the decomposition and producing the hybrid beamformer matrices processes:

Algorithm 1 Hybrid Beamforming Using LU Decomposition Method

- 1: The BS Sends Pilot Signals to aquire the channel matrix H .
 - 2: The BS performs the Singular Value Decomposition as following:
 - 3: $[U, S, V] = svd(H(:, :, k))$
 - 4: $F_{opt}(:, :, k) = V([1 : N_t], [1 : N_s])$
 - 5: $W_{opt}(:, :, k) = U([1 : N_r], [1 : N_s])$
 - 6:
 - 7: **for** $k=1:K$ users **do**
 - 8: $[(F_{RF})_{i,j}, (F_{BB})_{i,j}] = LU((F_{opt})_{i,j})$
 - 9: $[(W_{RF})_{i,j}, (W_{BB})_{i,j}] = LU((W_{opt})_{i,j})$
 - 10: **if** $\|(F_{RF})_{i,j}\| > 2$ **then**
 - 11: $\|(F_{RF})_{i,j}\| = 2$
 - 12: $F_{BB} = F_{RF}^{-1}F_{opt}$
-

where K is the number of users, H is the channel matrix, N_t is the number of transmitting antennas, N_r is the number of receiving antennas, N_s is the number of data streams, W_{opt} is the fully digital matrix in the combiner side, W_{RF} is the analog RF matrix in the combiner side, and the W_{BB} is the digital baseband matrix in the combiner side. The condition in the end of the algorithm is to gaurantee the fitting with the hardware limitations and the condition in equation 2.8. Finally, if the power constraint in 2.9 is not satisfied by the outputs of the LU decomposition, then a normalization process is applied as in 2.10:

$$\|\mathbf{F}_{RF}\mathbf{F}_{BB}\|_F^2 \leq KN_sF \quad (2.9)$$

$$\hat{\mathbf{F}}_{BB} = \frac{\sqrt{KN_sF}}{\|\mathbf{F}_{RF}\mathbf{F}_{BB}\|_F} \mathbf{F}_{BB} \quad (2.10)$$

2.1.2 Simulation Results

Extensive simulation was done for different MIMO scenarios and for both single and multiple users according to the parameters listed in table 2.1.

The results are averaged over the number of channel realizations (1000 channel realizations in our experiment) to make sure that this suggested algorithm is working for different channel conditions and different users. Some examples of the channel realizations are shown in fig. 2.3.

Achievable spectral efficiencies versus different values of Signal to Noise Ratio (SNR) results are listed in the figures 2.4, 2.5 and 2.6 for the single user achievable spectral efficiency and in the figures 2.7, 2.8, and 2.9 for multiple users (5 users in our case). Our LU-Decomposition method is compared with some well known techniques over the same channels for fair comparison.

It is clear that the achievable spectral efficiency of our suggested design of the hybrid beamforming system is almost the same as the optimal fully digital one for both the single user and multiple users scenarios. In all cases our systems achieved better than some of the state of the art systems from [86, 85, 24] and the convex optimization from equation 2.8.

2.1.3 Comparing with Other Matrix Factorization Methods

After studying the LU decomposition method performance, we tried to apply the same algorithm on the beamforming matrices but using different factorization methods like QR decomposition [28] and the Cholesky decomposition [71]. Knowing that there are some time complexity differences among these methods, we performed several trials for different single user and many users cases. According to this book [39], the LU decomposition complexity of an $m \times n$ matrix is $2n^3/3$ with partial pivoting, it is $n^3/3$ for the Cholesky factorization and it is $2n^2(m - (n/3))$ for the QR decomposition. In reality, and using the system with the features listed in the table 2.1, the difference between the QR and the LU decomposition was always in the range of (1μ second). The Cholesky method only works for square matrix which is a rare case in practical beamforming systems that we are working on.

Table 2.1: Simulation Parameters

Parameter	Value
Number of data Streams N_s	4
Number of Clusters N_c	5
Number of Rays per cluster N_{ray}	10
Number of Users K	1 and 5
MIMO Structures	16X4, 64X16, and 144X36
Number of Channel Realizations	1000

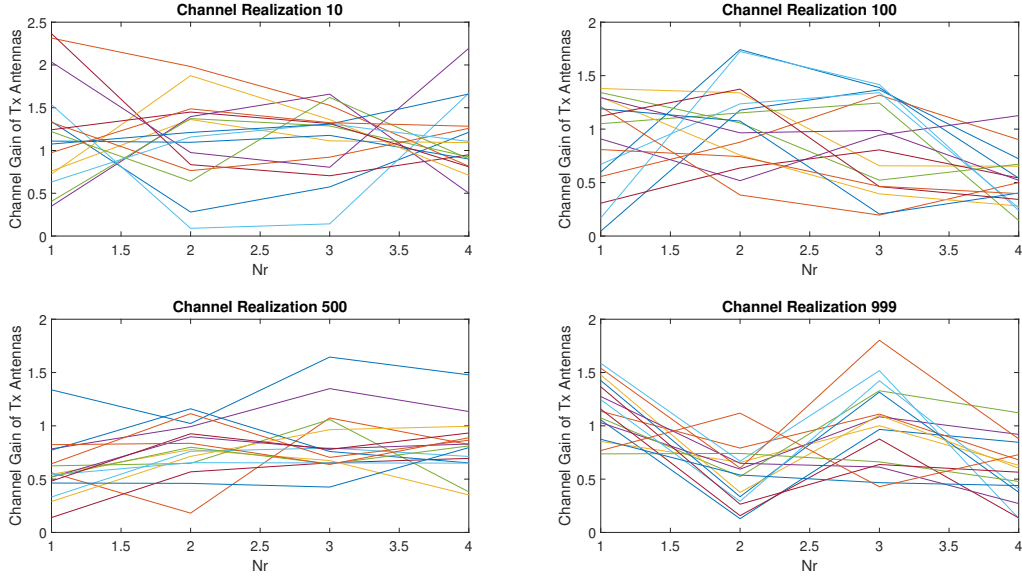


Figure 2.3: Examples of the channel realizations used in the experiments

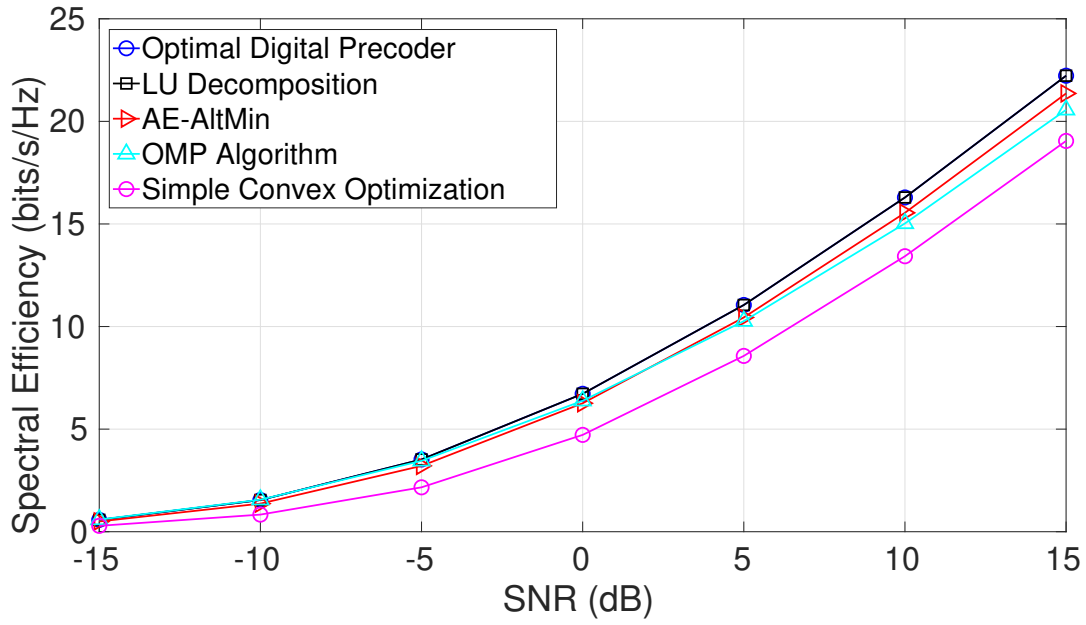


Figure 2.4: 16X4 MIMO system achievable spectral efficiency comparison for single user

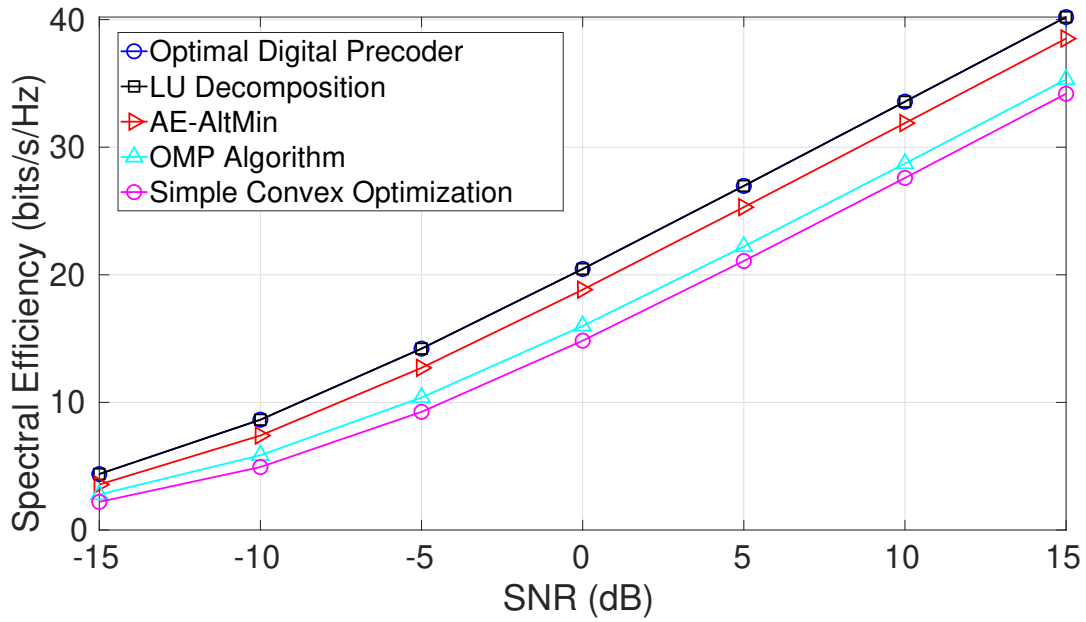


Figure 2.5: 64X16 MIMO system achievable spectral efficiency comparison for single user

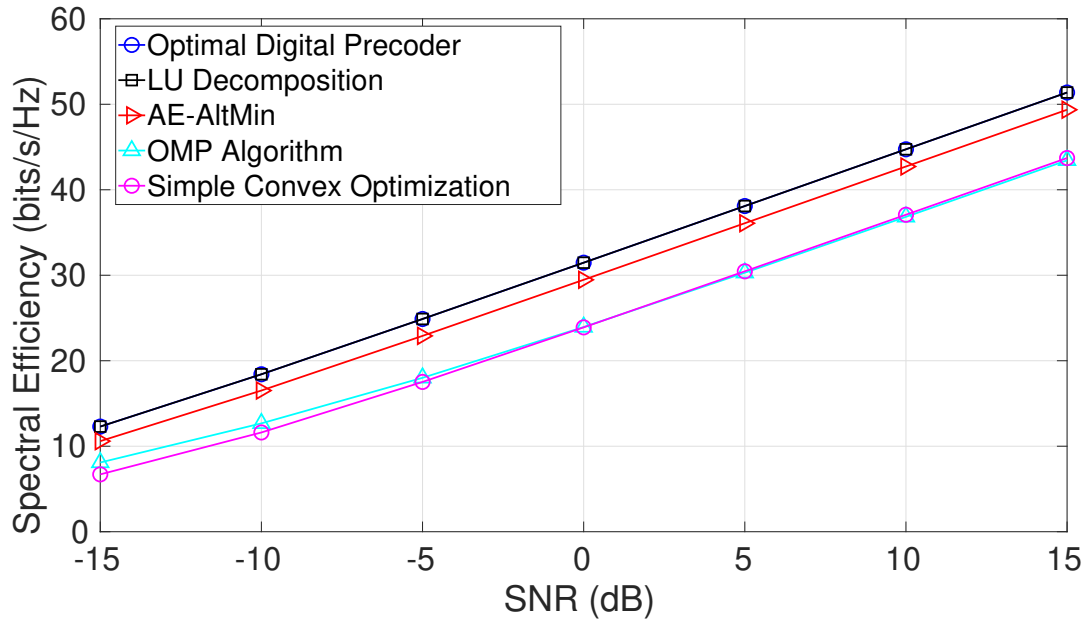


Figure 2.6: 144X36 MIMO system achievable spectral efficiency comparison for single user

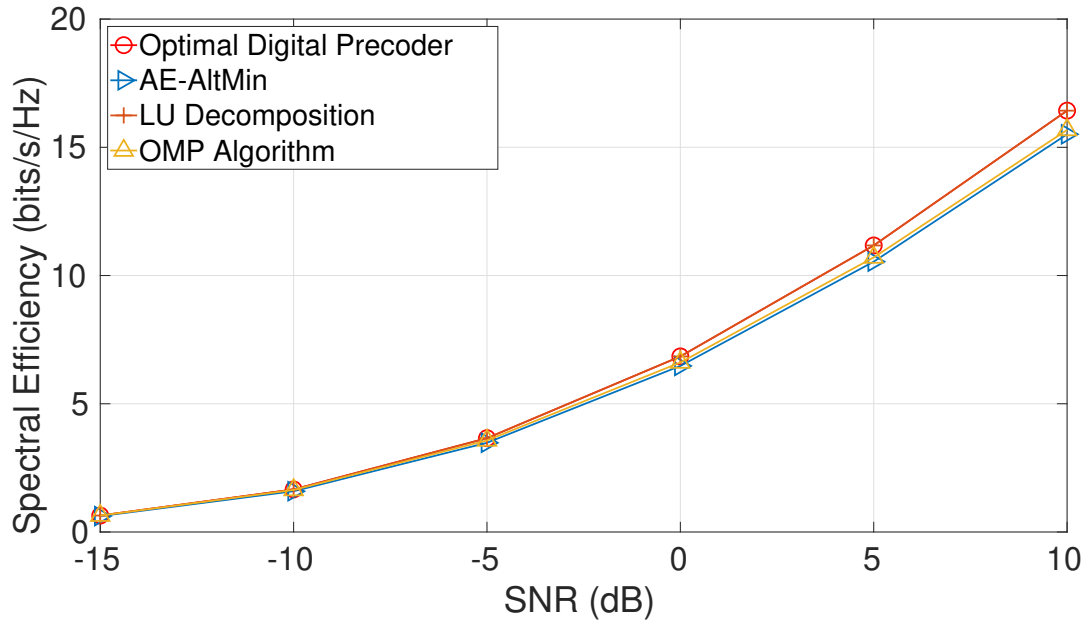


Figure 2.7: 16X4 MIMO system achievable spectral efficiency comparison for 5 user

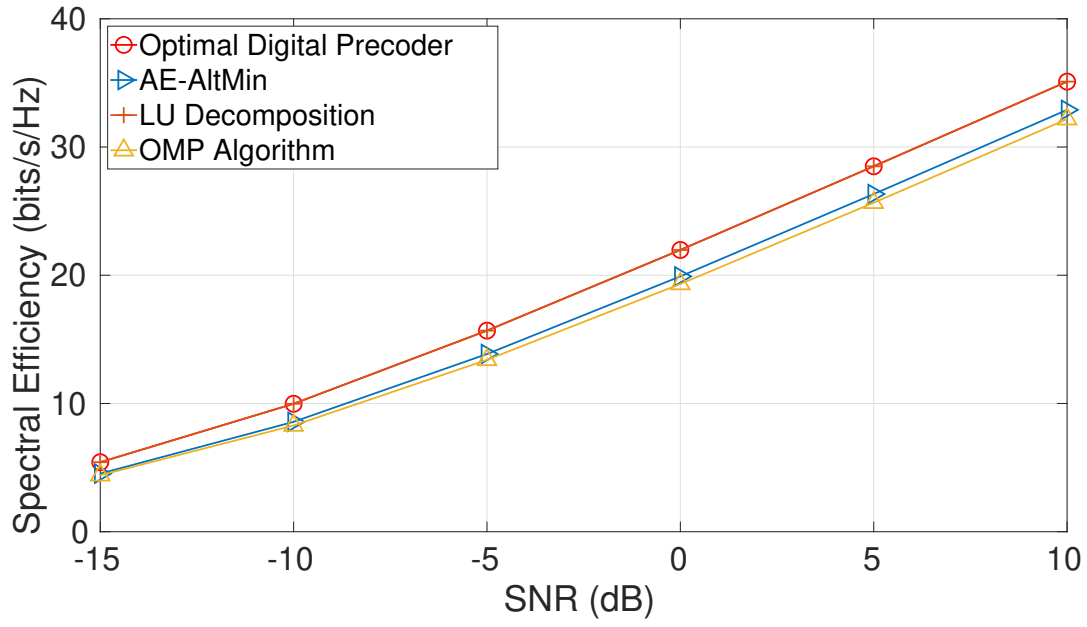


Figure 2.8: 64X16 MIMO system achievable spectral efficiency comparison for 5 user

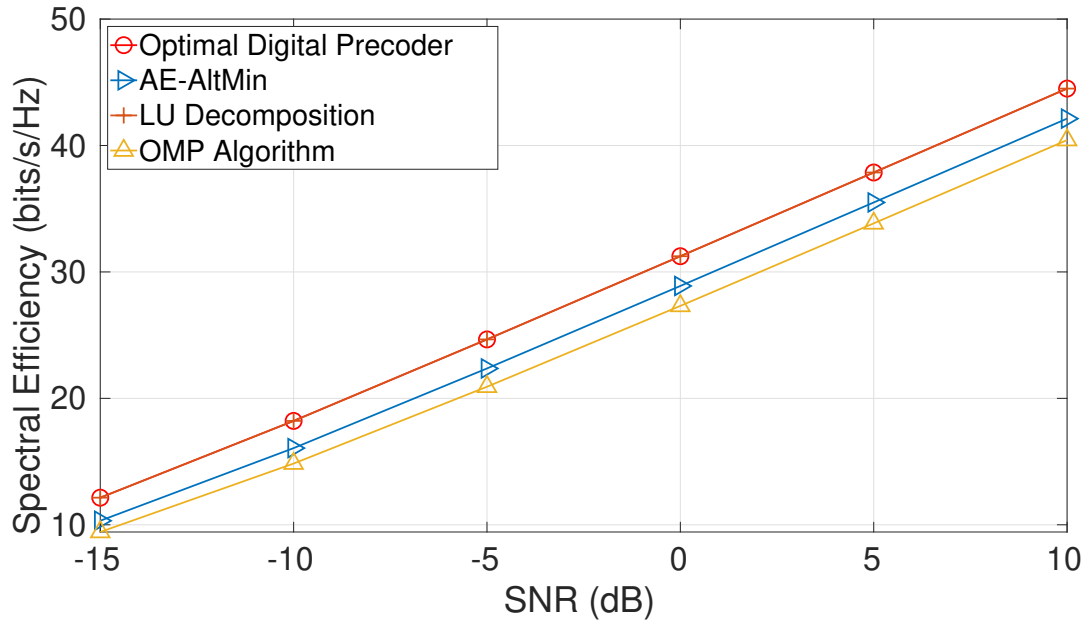


Figure 2.9: 144X36 MIMO system achievable spectral efficiency comparison for 5 user

2.2 Using Convex Optimization and Machine Learning

Beamforming has been one of the most important enabling techniques for millimeter wave (mmWave) communications and massive multiple-in-multiple-out (MIMO) systems. Due to the hardware limitation, fully digital beamforming has been proven to be difficult to achieve for commercial cellular communication systems. Consequently, the hybrid beamforming, as a combination of digital baseband precoders and analog RF phase shifters, has been intensively investigated in an attempt to achieve a performance close to the fully digital beamformers. In this section, we further step to develop a more flexible and feasible hybrid beamforming system that utilizes the machine learning techniques, to improve the achievable spectral efficiency. After using the traditional convex optimization techniques to optimize the baseband and phase shifter outputs, the results are then introduced to different machine learning approximation networks to approach the performance of fully digital beamforming. Simulation results show that the suggested two-step algorithm can attain almost the same efficiency as that can be achieved by fully digital architectures. The work in this section was published partially in [9].

2.2.1 Introduction

A new trend in designing beamforming systems was recently suggested in [12, 11], where deep learning techniques are adopted in a coordinated system of many base stations (BSs). Taking in consideration the new paradigm of network management schemes such as the Software Defined Radios (SRD) and the Software Defined Networks (SDN), these works assume multiple BSs that are serving the same user at any time [12] in a coordinated manner with a centralized system deployed locally or in the cloud to control the entire coordination process. Such an architecture makes the system more robust against blockage, enhances system coverage, and supports mobile users. Each of these coordinated BSs are connected to a centralized/cloud processing unit where the deep learning techniques are deployed and implemented. Beamforming in such systems is done in two stages, part of which is done within the BS itself while the rest is done by the central/cloud processing unit by using the model resulted from the machine learning/ deep learning training process.

In this section, we adopt a mixed methodology in designing the hybrid beamforming systems with the help of machine learning techniques. A single BS is assumed to serve a single user in an MIMO system where the beamforming system is built of digital baseband and analog phase shifters besides an exact radial basis function network (RBFN) for approximation. The suggested system achieves a higher spectral efficiency compared with the previously suggested systems, and helps to relax the hardware limitations of the traditionally suggested hybrid beamforming systems. In contrast to the existing works using deep learning [12, 11], our system is based on a single BS, thus substantially improves the feasibility of the proposed machine learning scheme.

2.2.2 Convex Optimization Using CVX

The cvx software from the Stanford university [32, 31] is used in our work to solve all Convex optimization problems. It is a modeling software that is used mainly to construct and solve convex optimization problems. It is available online free of charge for academic purposes and is compatible with Matlab. Once downloaded and installed, it can be called inside the Matlab to solve optimization problems after defining the objective functions and the constraints. CVX is implemented in Matlab environment and is successfully making Matlab as an optimization modeling tool where model specifications are constructed using common Matlab operations and functions. The default solver of the cvx uses the Semidefinite Quadratic Linear Programming (SDPT3) and it was used in our work without changing its default settings. Matlab codes can be mixed with CVX codes with high flexibility. For example, it is easy to compute an optimal trade-off curve by forming and solving a family of optimization problems by varying the constraints. As another example, CVX can be used as a component of a larger system that uses convex optimization, such as a branch and bound method, or an engineering design framework.

2.2.3 System Model

The system architecture, the received signal, and the channel model of this part are the same as the ones explained in section 2.1.1 and we suggest a two-step beamforming system as shown in Fig. 2.10.

In the suggested model, the results from the baseband and the phase shifters are first fed to a convex optimizer, and then the results are considered as the training data for the machine learning model. The resulted model from the training process is then used in the future to produce beamforming parameters that are similar to the fully digital beamforming system, with respect to the achievable spectral efficiency.

Both F_{opt} in the transmitter, and W_{opt} in the receiver can be calculated for the fully digital beamforming systems from the equations 2.11, 2.12, and 2.13. The second constraint is the power constraint of the transceiver. In other words, the problem is to minimize the difference between the results of the precoder and combiner and the optimal fully digital beamformer.

$$[U, S, V] = svd(H(:, :, k)) \quad (2.11)$$

$$F_{opt}(:, :, k) = V([1 : N_t], [1 : N_s]) \quad (2.12)$$

$$W_{opt}(:, :, k) = U([1 : N_r], [1 : N_s]) \quad (2.13)$$

where H is the channel matrix, and the *svd* is the singular Value Decomposition (SVD). Also the hybrid precoder design for multicarrier and multiuser systems using alternating minimization and double phase shifters (DPS), as shown in Fig. 2.2, can be expressed as:

$$\begin{aligned} \min_{F_{RF}, F_{BB}} \quad & \|F_{opt} - F_{RF}F_{BB}\|_f \\ \text{subject to} \quad & \|(F_{RF})_{i,j}\| \leq 2 \end{aligned} \quad (2.14)$$

which is a convex optimization problem (for both the precoder at the transmitter and the combiner at the receiver), and will be used as the basis for our two-step design [86].

To address the challenge of hardware limitation of the traditional beamforming architectures, a two-step hybrid beamforming is suggested, as shown in Fig. 2.10. In such a system, both the digital and analog parts of the hybrid precoder are first optimized using a convex optimizer (with the same assumptions as in [24, 86, 85]), where the goal is to achieve as close spectral efficiency as possible (with the hardware limitations) to the optimal fully digital precoder. The next step is to be even closer to the fully digital precoder, by using one of the machine learning approximation techniques, which is the Exact RBFN in our case [17]. Such functionality can be implemented onsite (within the same BS) with much less hardware and power issues than traditional solutions, or it can be implemented in a remote central (cloud) processing unit (as suggested in [12]).

Many approximation techniques have been suggested that are implemented using neural networks [57]. Some examples of such techniques include the simple linear regression [72], RBFN and exact RBFN networks [17], general regression neural network (GRNN) [46], RBFN with Bayesian Regularization [16], and multi-layer perceptron (MLP) [65]. After comparing the performance of these methods (as explained in the next section), the exact RBFN is selected for our work. One of the most important and fast approximation techniques is the exact RBFN that can be represented with radially symmetric hidden neurons [17]. RBFN networks are used to approximate functions. They have been proven to be faster and more accurate than many other standard feed-forward back-propagation networks. RBFN networks usually consist of 3 layers, namely the input layer, the hidden layer, and the output layer. The hidden layer usually consists of a large number of neurons, each of which has a parameter vector called a center. The output of the hidden layer can be expressed as:

$$O_k = \|A - C_k\| = \sqrt{\sum_{j=1}^T (A_j - C_{kj})^2} \quad (2.15)$$

where O_k is a function of the distance between the input vector and the stored center. The learning phase consists of using a clustering algorithm and a nearest neighbor heuristic to determine the C_k cluster centers. The weights from the hidden layer to the output layer are determined by using linear regression or a gradient descent algorithm [17]. Such networks can be trained for a specific time and with a moderate number of training samples (1000

samples in our case that has been generated from the same channel realization process in [86, 85]) to converge and give high accuracy results (as will be shown in the next section).

The results from the convex optimizer (i.e. F_{RFcvx} and F_{BBcvx} for precoder and W_{RFcvx} and W_{BBcvx} for the combiner) need to be converted to a $1 - D$ vector form to be used as inputs to the exact RBFN neural network. The optimal fully digital precoder and combiner parameters (i.e. F_{opt} and W_{opt} respectively) are used as the target output of the neural network. These parameters also need to be converted to a vector that includes both the real and imaginary parts of each parameter and then combined in the vector. After collecting a reasonable amount of training data (1000 samples in our case), these parameters are used to train the model. The resulted model is then used to produce the hybrid beamforming matrices (i.e. F_{RFopt} and F_{BBopt} in the transmitter and the corresponding W_{RFopt} and W_{BBopt} in the receiver) that have their product to be as close as possible to the F_{opt} and W_{opt} respectively. Training data can be collected offline before the operation of the system, or they can be accumulated while the system is idle or working normally. Also, these training data can be updated continuously, depending on the system operation condition and user mobility or density scenarios (assuming that we are working in a time varying environment scenario).

2.2.4 Simulation Results

As mentioned earlier, there are many approximation techniques that can be used in our second step design of the hybrid beamformer. To select one, we made several comparisons among them in terms of the training delay and the spectral efficiency resulted from each of them compared with the optimal fully digital one. The first comparison with respect to the training delay (in seconds) is summarized in Table 2.2.

The other comparison among these approximation methods was done by comparing the final spectral efficiency of each approximation technique with the fully digital precoder and the results in each case was very close with error margin in the order of 10^{-15} that is really difficult to distinguish, as shown in Fig. 2.11 for the case of 16X4 MIMO scenario:

Hence the exact RBFN was selected (as a good compromise among performance, delay, and architecture) to compare the performance of our suggested architecture with other

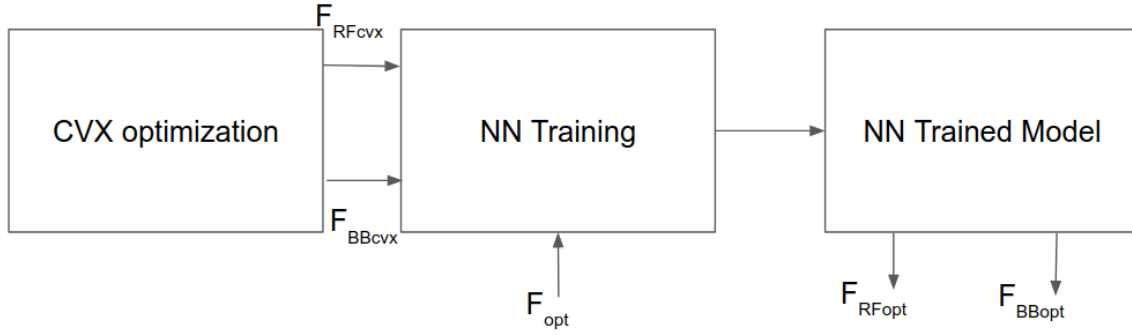


Figure 2.10: Suggested system structure in the Transmitter and the same is used in the receiver

Table 2.2: Approximation Techniques Comparison

Technique	16X4 MIMO	64X16 MIMO	144X36 MIMO
Linear Regression	8.4398	242	2500
Exact RBFN	0.55	0.6	2.3
RBFN	3.4	2.77	5.3
GRNN	0.3	0.4	0.5
RBFN with BR	22.61	222	1563
MLP	8.17	343	3300

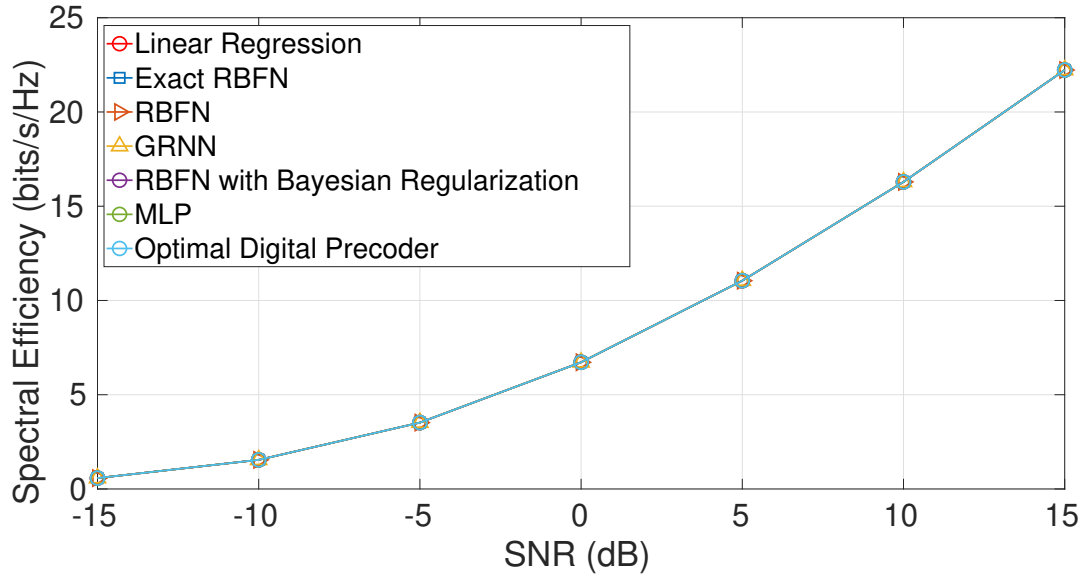


Figure 2.11: 16X4 MIMO system achievable spectral efficiency comparison among different approximation techniques and the fully digital precoder

methods. Despite the fact that the exact RBFN is not the fastest from the training perspective, it was selected because it is easier to build, and scales well with the larger MIMO systems that are expected in the 5G networks [29]. The first step to prove the validity of our idea was to implement the suggested architecture for a single user and compare the results with the previously suggested protocols in [86, 85, 24]. Fig. 2.12 shows the comparison of the achievable spectral efficiency of different systems. It is clear that our suggested system is achieving almost the same efficiency as the fully digital one.

By using another simple approximation technique (i.e. the linear regression), we obtain the results for the training, the validation, and the testing data for the 16X4 MIMO as shown in Figures 2.13, 2.14, 2.15, and 2.16.

Figures 2.17 and 2.18 are showing the 64X16 and 144X36 MIMO achievable spectral efficiencies (for our system compared with those from [86, 85] and [24] and the convex optimization architecture) respectively.

It is clear that, with larger MIMO systems, the trend is the same: the two-step precoder achieves almost the same performance as the fully digital one. In all the experiments, the exact-RBFN showed quick convergence after only 9- epochs and with delay as listed in table 2.2 The other interesting fact from the results is that the convex optimizer hybrid beamforming is getting closer and closer to the performance of (OMP algorithm) from [85] when larger and larger MIMO systems are used in the simulation.

Finally, the extension of the ML-aided Beamforming to multiple users (10 users in this case) and for several MIMO configurations is shown in figures 2.19, 2.20, and 2.21:

Both LU-decomposition and ML-aided beamforming for single user and 64X16 MIMO configuration are shown in figure 2.22:

2.3 Beamforming with DeepMIMO for mmWave Networks

The special characteristics of mmWave band have made the beamforming problem a challenging one because it depends on many environmental and operational factors. These

challenges made any model based architecture fit only special applications, working scenarios, and specific environment geometry. All these reasons have increased the need for more general machine learning based beamforming systems that can work in different environments and conditions. This increased the need for an extended adjustable dataset that can serve as a tool for any machine learning technique to build an efficient beamforming architecture. DeepMIMO dataset has been used in many architectures and designs and has proved its benefits and flexibility to fit in many cases. In this section, we extend the work in [12] where collaborative beamforming with many cooperating BSs is considered. First, we study the impact of UE's speed ranges on the beamforming performance, then, we optimize the parameters of the neural network architecture of the beamforming design, and finally, we suggest an optimal design that gives the best performance for as a small dataset as possible. Suggested architecture can achieve the same performance achieved before with up to 33% reduction in the dataset size used to train the system which provides huge reduction in the data collection and processing time.

2.3.1 System Model

The used system model is assumed to be the same as described in [12] in order to conduct a fair comparison when testing the UE speed effect on the performance and when optimizing the neural network architecture and parameters. The block diagram of the system is given in fig. 2.23:

Here we assume that each user is served by several cooperating base stations (4 BSs is assumed in our work) where they collect both the directional and omnidirectional channel information to build the beamforming weights matrices. Each Base Station (BS) here is reporting its collected channel information to a central (or cloud) processing unit where all the calculations for the beamforming is done. For the simulation purposes, the system is assumed to be deployed into a street environment as in the fig. 2.24 with the base stations (BS1, BS2, BS3, BS4) serving a moving user (walking, running, biking, or riding a car user) in the street in between these base stations.

The system is assumed to be frequency selective coordinated mmWave with the received signal at the subcarrier (k) after the precoding is expressed as:

$$\mathbf{y}_k = \sum_{n=1}^N \mathbf{h}_{k,n}^T \mathbf{x}_{k,n} + \mathbf{v}_k \quad (2.16)$$

where: $\mathbf{x}_{k,n}$ is the discrete time transmitted signal vector from the n^{th} BS at the k^{th} subcarrier, $\mathbf{h}_{k,n}$ is the channel vector between the user and the n^{th} BS at the k^{th} subcarrier, and \mathbf{v}_k is the received noise at the subcarrier k defined as a normal distribution with a zero mean and σ^2 variance. The channel model is expressed as:

$$\mathbf{h}_{k,n} = \sum_{d=0}^{D-1} h_{d,n} e^{-j2\pi kd/K} \quad (2.17)$$

where:

$$h_{d,n} = \sqrt{\frac{M}{\rho n}} \sum_{\ell=1}^L \alpha_{\ell} p(dT_s - \tau_{\ell}) \quad (2.18)$$

More details about these parameters can be found in [12]

2.3.2 Deep MIMO Dataset and Simulation process

The dataset used in this paper is collected using the DeepMIMO [11] tool available online with the features explained below. The number of base stations can be selected from a list of 18 base stations available in the original simulation environment [11]. In our experiments, we selected only (4) of these base stations with the names (BS1, BS2, BS3, and BS4) that are distributed as in fig. 2.24 and fixed on lamp posts on the sides of the road. The distance between BS1 and BS3 equals the distance between BS2 and BS4 and equals 100m. The distance between BS1 and BS2 (across the street) equals to the distance between BS3 and BS4 and equals to 40m. Each BS has a height of 6m from the ground level [11]. Each BS is assumed to have a uniform planar array (UPA) of antennas that are facing the street. The grid of the expected user locations starts from row number R550 and ends with the row number R1100 with each row having 181 users. The total number of expected users' locations in a uniform grid that is being collected for the full fingerprint is (99731) location. Each user location will be collected by the 4 BSs with each having 16 antenna elements and each UE with 4 antennas to have 16X4 MIMO structures. Also, for each user, 3 paths of

the signal between the user and each BS is collected (the LoS and the two strongest NLoS rays or the strongest 3 NLoS if there is blockage of the LoS path). First, the dataset is collected using MATLAB according to the simulation parameters explained above and listed in table 2.3 and the steps in [12]. After generating the dataset that will represent the inputs and outputs of the deep learning model, we use python to build, train, and test the deep learning model with different settings as we will see in the next section. To achieve that, we need Python 3.6 or later with Keras and Tensorflow libraries support. Finally, we used MATLAB again to process the deep learning outputs and generate the performance results and figures listed in the next section. More details about the simulation process are listed in the DeepMIMO official website [11].

The system is assumed to serve a mobile user using the unlicensed mmWave band of 60GHz frequency and focuses on vehicular applications in a street environment. The table 2.3 is listing all the parameters used in the system simulation.

Mobility Speed Effect

The first step in this work was to check the mobility speed effect on the performance of the system and we tried different speeds to check what would be the resulting spectral efficiency in (bits/sec/Hz). The fig. 2.25 shows that for different speeds (10, 50, and 100 mph), the deep learning network performance is almost the same and can still achieve a high system rate compared to the optimal genie-aided spectral efficiency. This means that the proposed network is stable for different mobility speeds and that it can be used for a wide range of mobile applications and scenarios.

DeepMIMO Neural Network Optimization

To optimize the network performance (i.e. to reduce the dataset required to achieve the best performance and the time required to train and use the model), we tried several optimizers and loss functions. Some of the tested optimizers include: ADAM, Ada Delta, Ada Grad, Ada Max, NADAM, and RMS prop. And it was clear that the optimizer (Nadam) could achieves the threshold (90% of the genie aided spectral efficiency) faster than all the others as

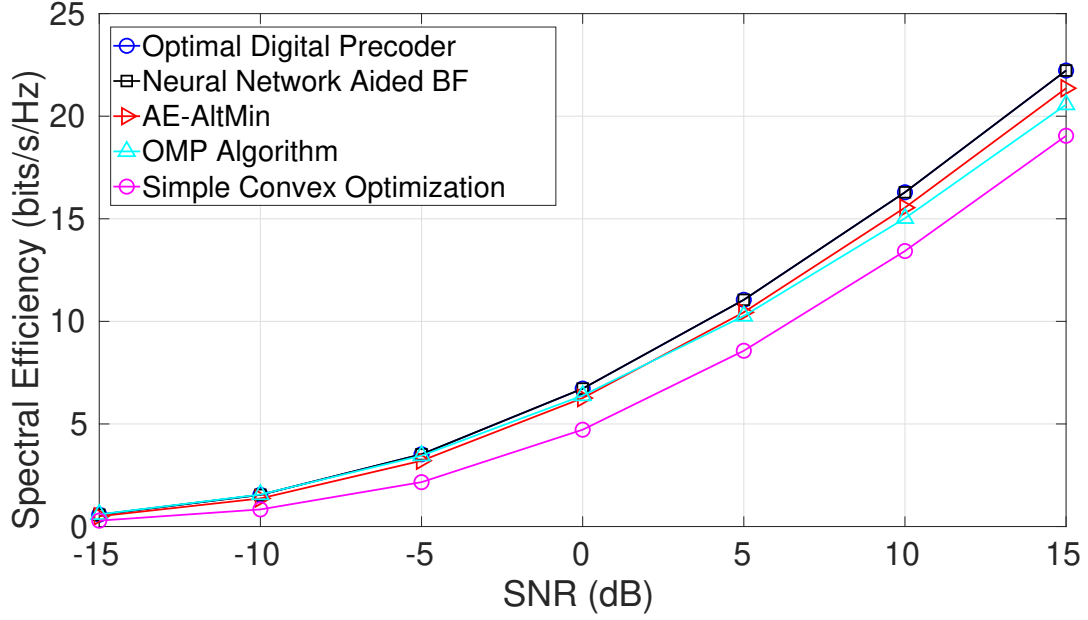


Figure 2.12: 16X4 MIMO system achievable spectral efficiency comparison

Table 2.3: Simulation Parameters

Parameters	Value
Number of Base Stations	4
Ray Tracing Building Material	ITU 60 GHz 3-layer dielectric material
Ray Tracing Ground Material	ITU 60 GHz single-layer dielectric
Ray Tracing Windows Material	ITU 60 GHz glass
BS height	6 meters
BS UPA dimensions	16X4 or 64 antenna elements
Tx power of BS	30dBm
UE height	2 meters
Tx power of UE	30dBm
Paths between each BS and UE	3
OFDM size (K)	1024
Bandwidth	1 GHz
Noise Figure	5dB
Operating System	Windows 10
PC features	Processor Intel Core i7 RAM 32GB

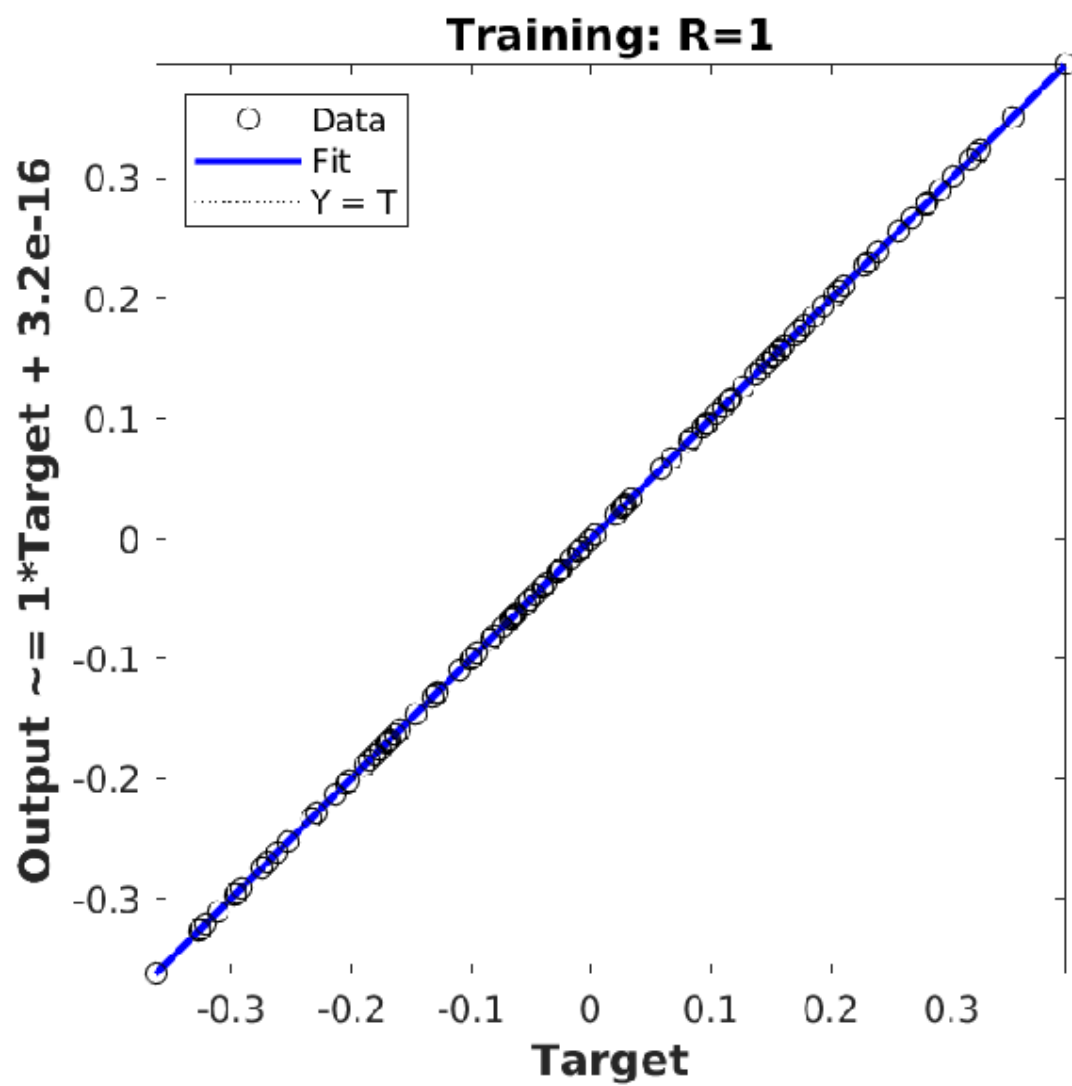


Figure 2.13: 16X4 MIMO linear regression results for the training data

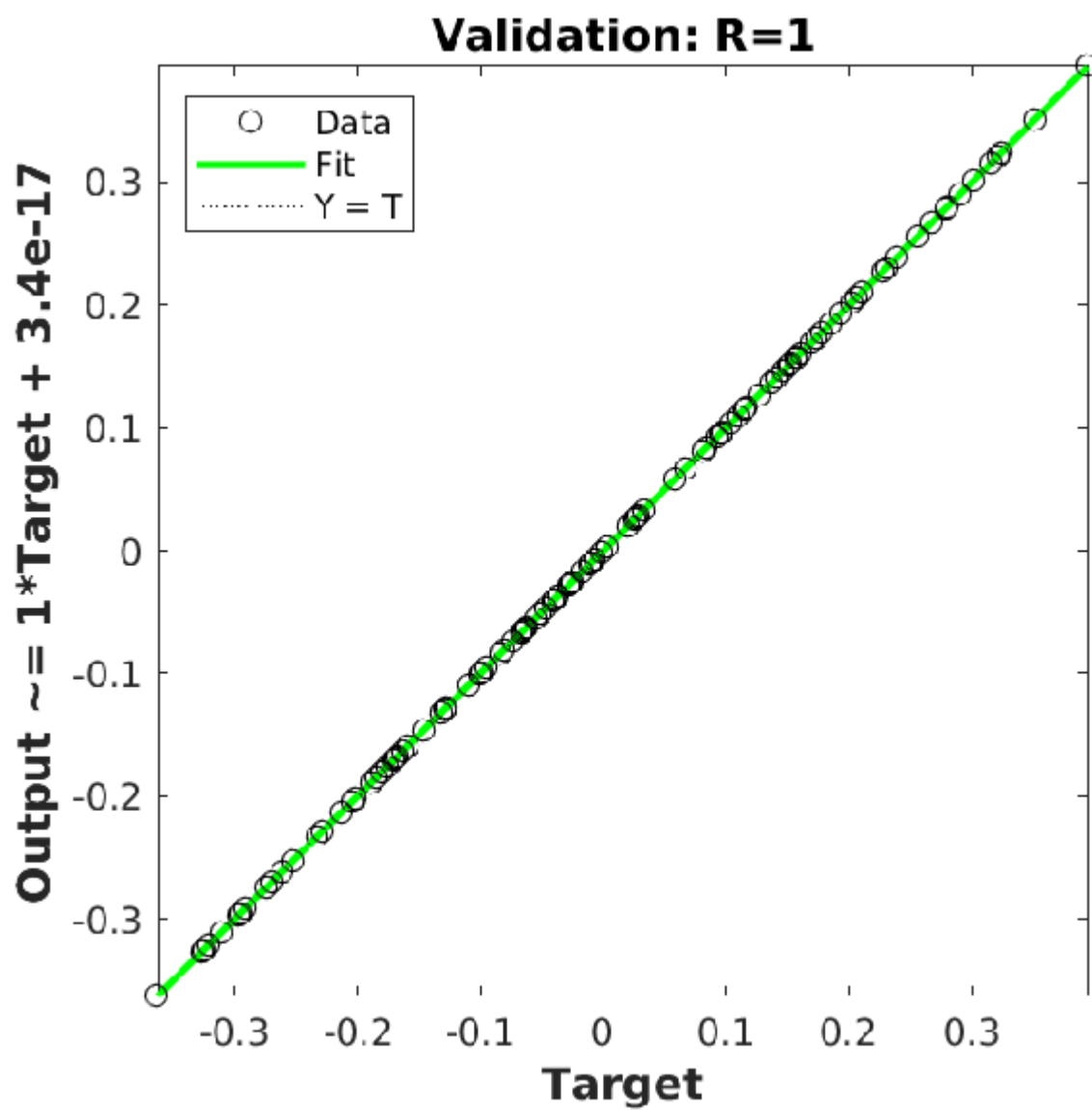


Figure 2.14: 16X4 MIMO linear regression results for the validation data

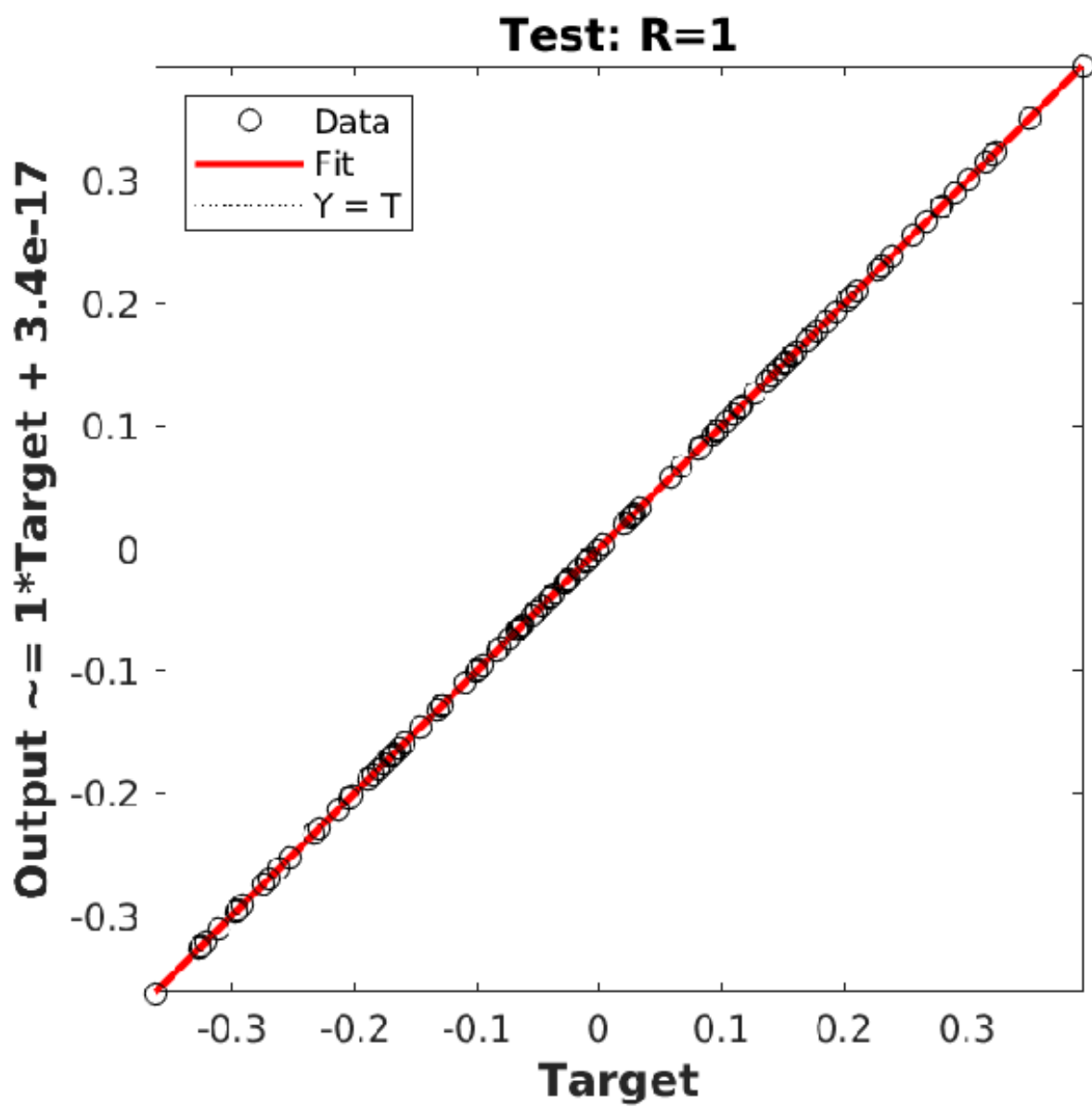


Figure 2.15: 16X4 MIMO linear regression results for the testing data

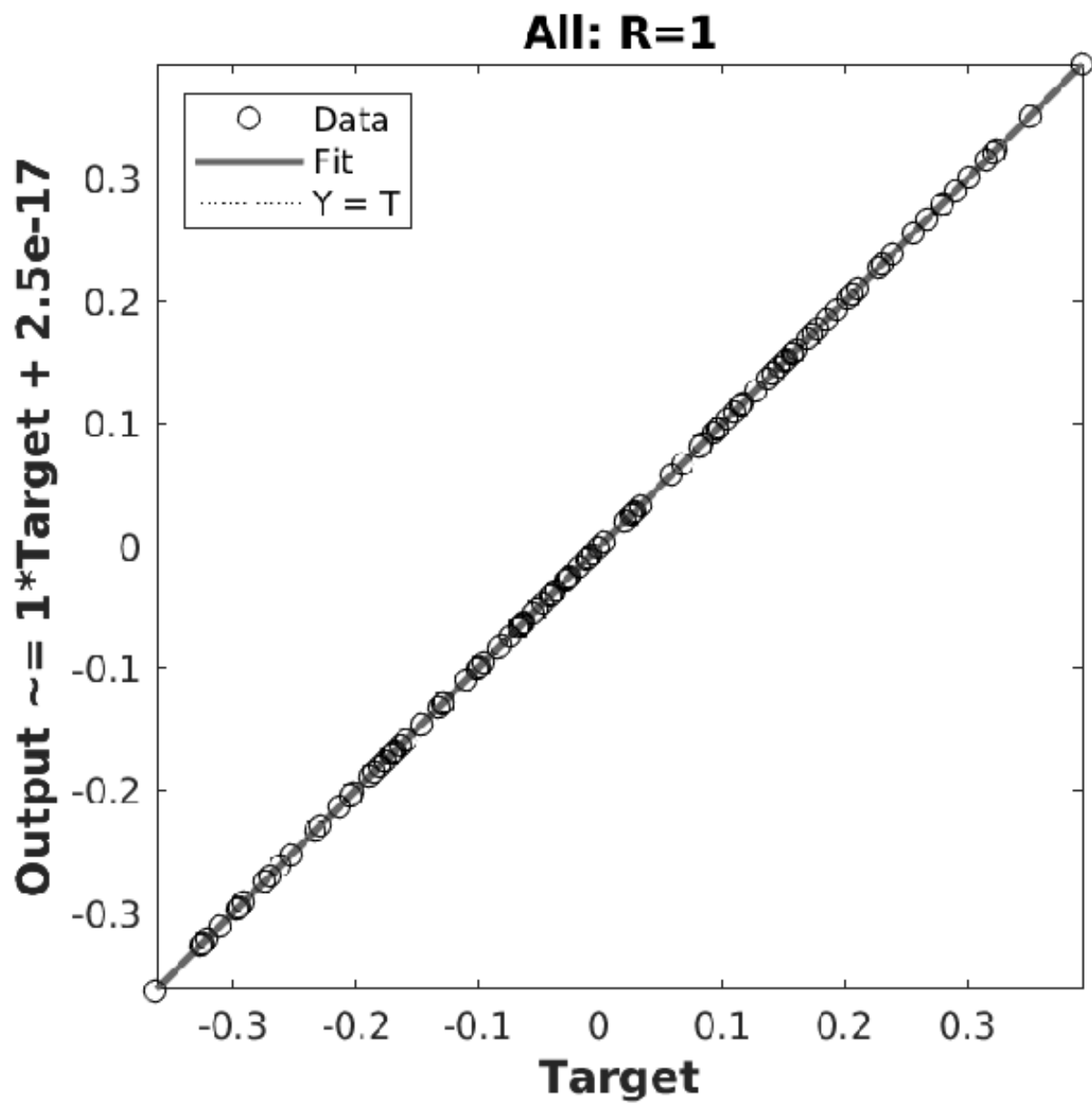


Figure 2.16: 16X4 MIMO linear regression results for all the data set

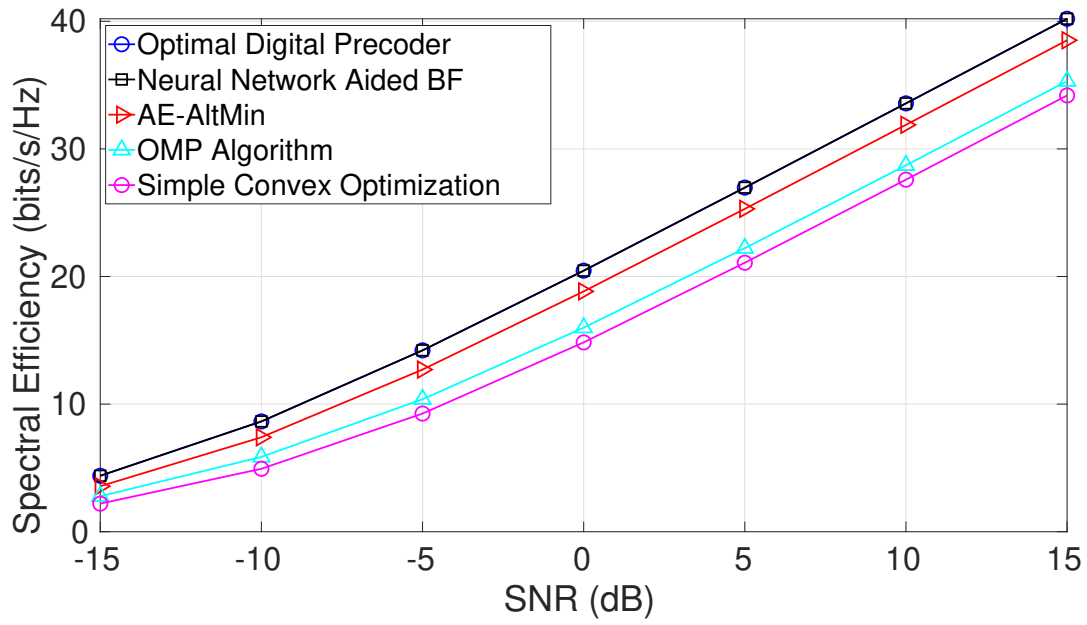


Figure 2.17: 64X16 MIMO System Achievable Spectral Efficiency Comparison

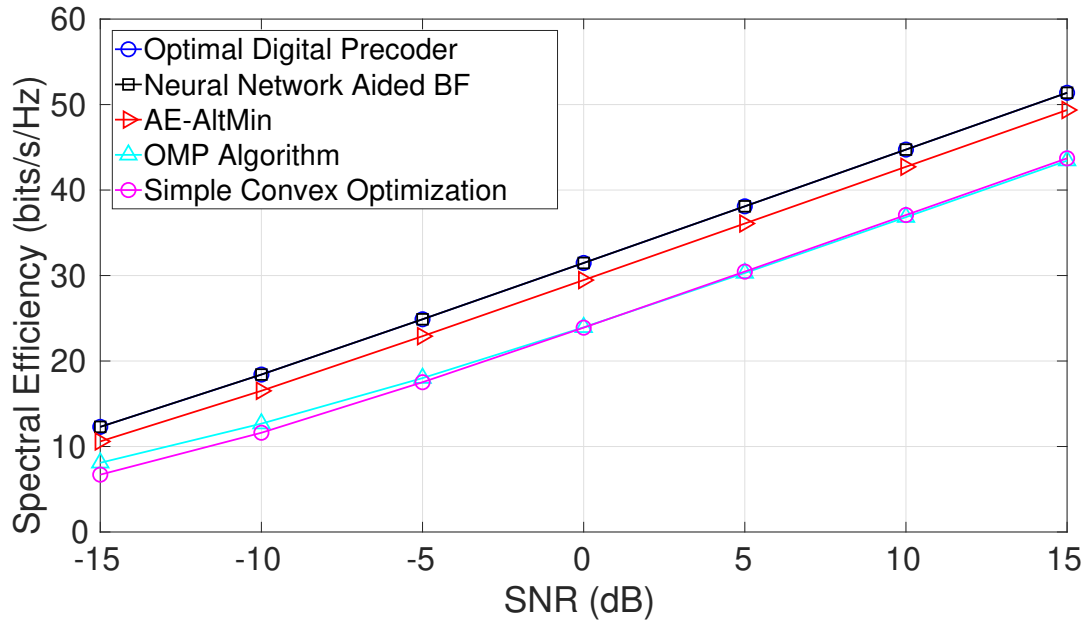


Figure 2.18: 144X36 MIMO System Achievable Spectral Efficiency Comparison

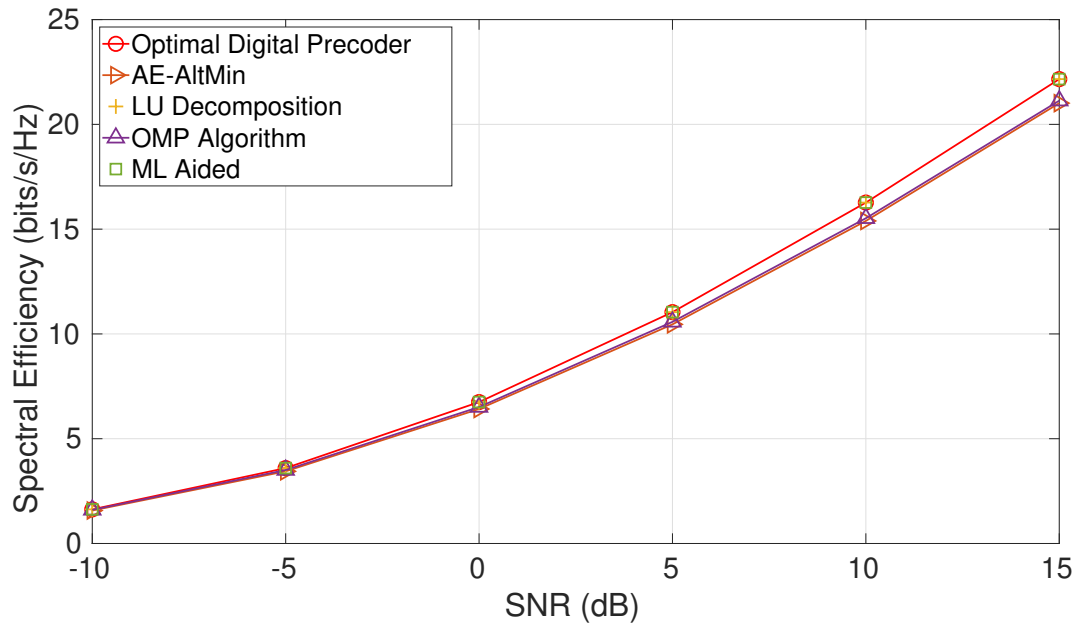


Figure 2.19: 16X4 MIMO System Achievable Spectral Efficiency Comparison for 10 users

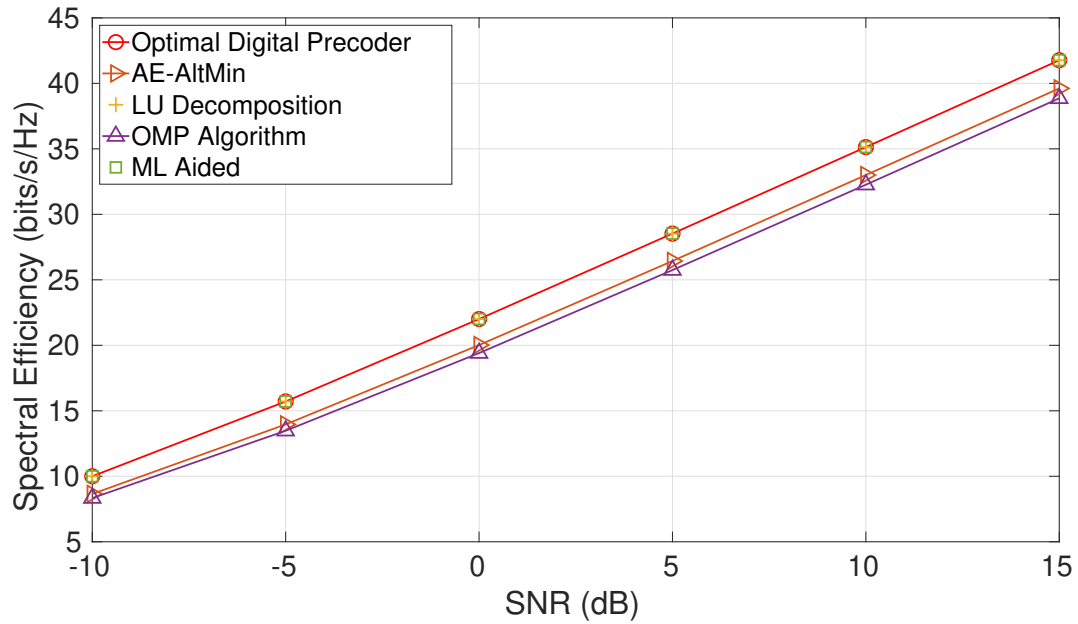


Figure 2.20: 64X16 MIMO System Achievable Spectral Efficiency Comparison for 10 users

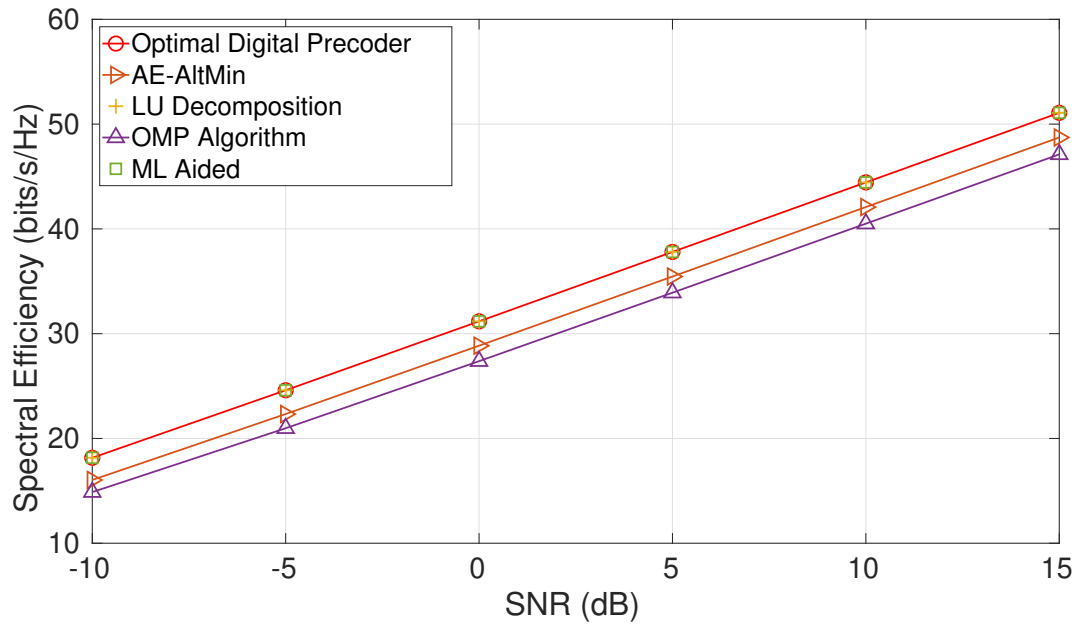


Figure 2.21: 144X36 MIMO System Achievable Spectral Efficiency Comparison for 10 users

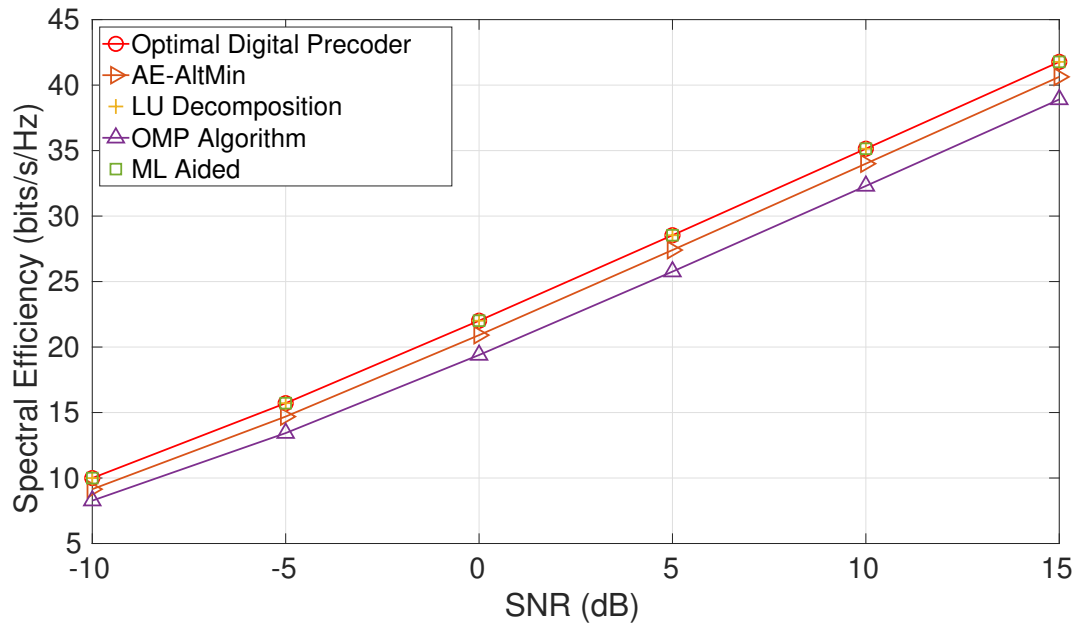


Figure 2.22: Both LU-decomp. and ML-aided for single user and 64X16 MIMO System Achievable Spectral Efficiency Comparison

shown in the fig. 2.26. So, it is considered as the chosen optimizer to build the beamforming neural network.

On the other hand, many loss functions were tried to select the best representative one for our design. We tried the Mean Squared error (MSE) loss function, the Mean Squared Logarithmic Error (MSLE), Poisson loss function, Mean Absolute Error (MAE), and the Mean absolute percentage error (MAPE) loss function all with the (Nadam) optimizer. It was clear that the (MSLE) achieves the best performance when combined with the (Nadam) optimizer, so they are selected to build the optimal deep neural network to produce the best model with the 33% reduction in the dataset size required and accelerate the training and operation of the collaborative beamforming system as in fig. 2.27:

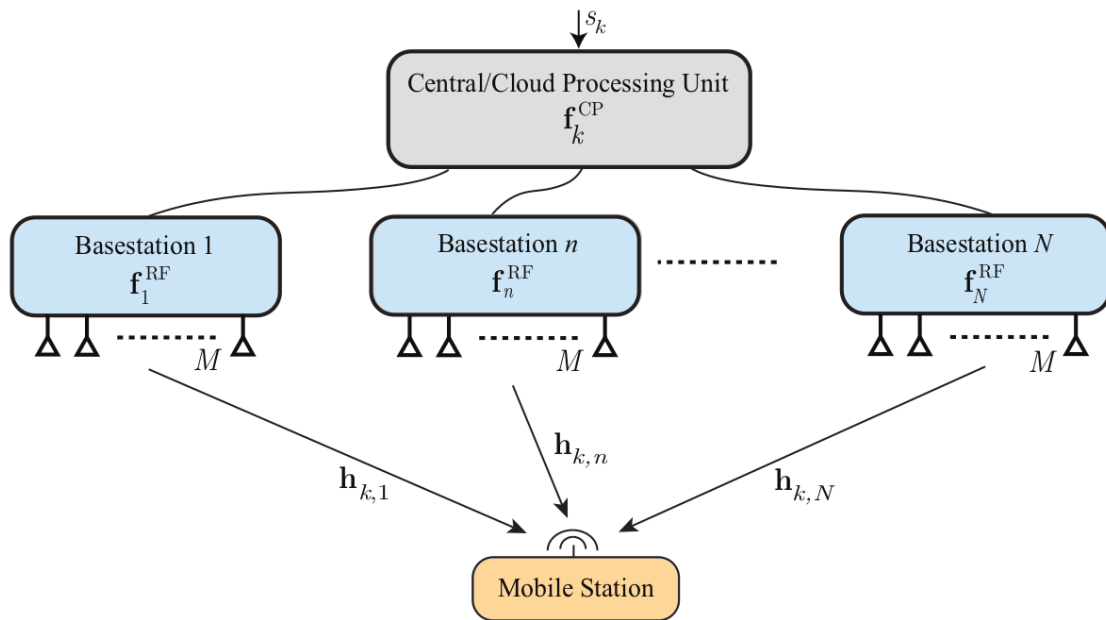


Figure 2.23: Coordinated Beamforming System Model

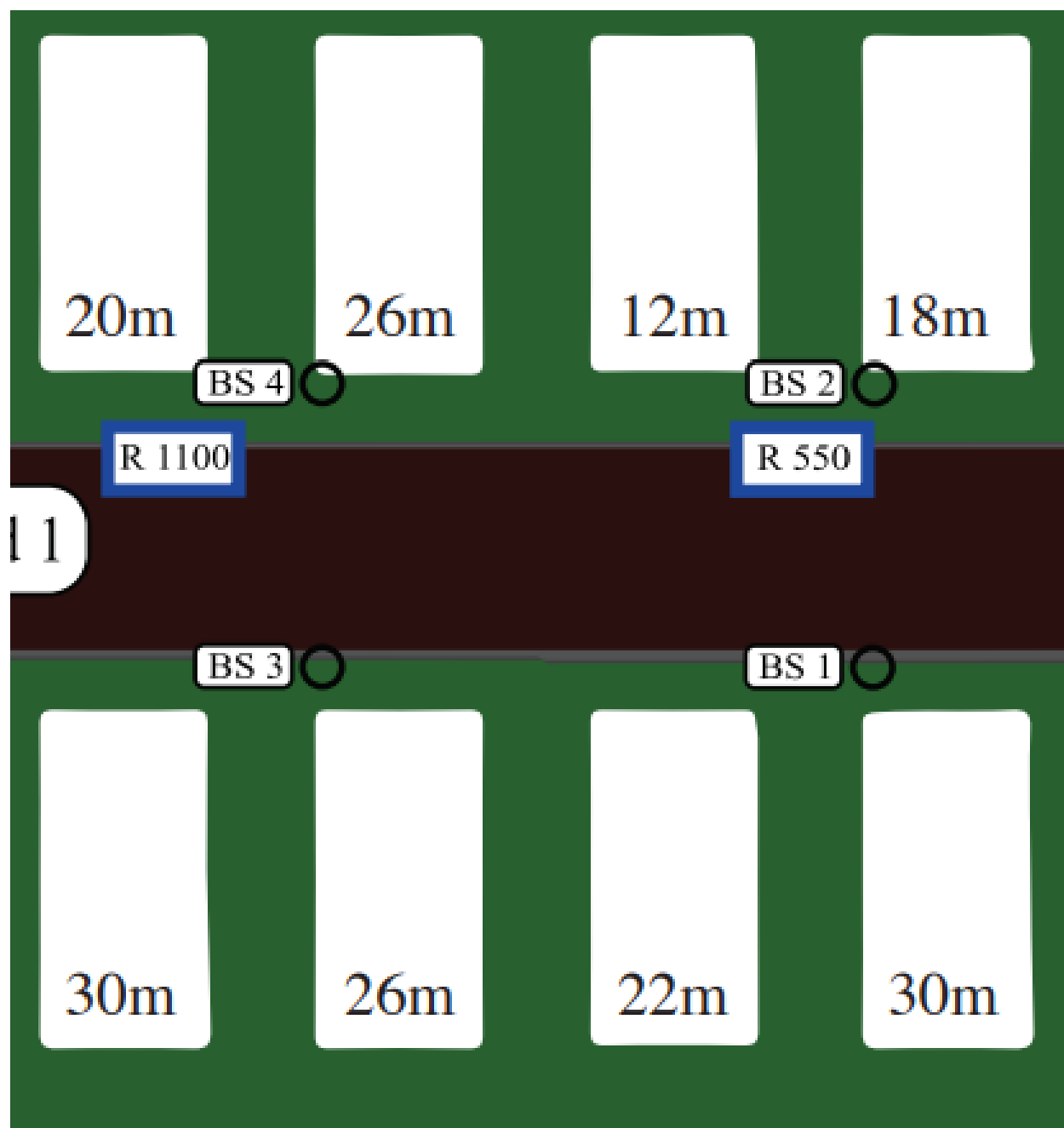


Figure 2.24: A top View of the street, buildings, and the Base stations distribution

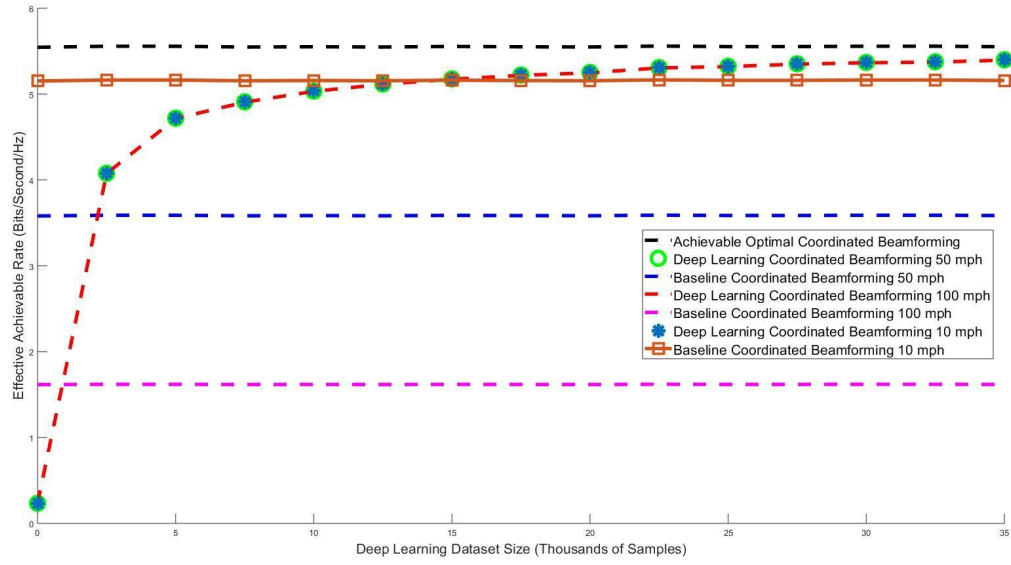


Figure 2.25: UE Mobility Speed Effect on the Achievable Spectral Efficiency

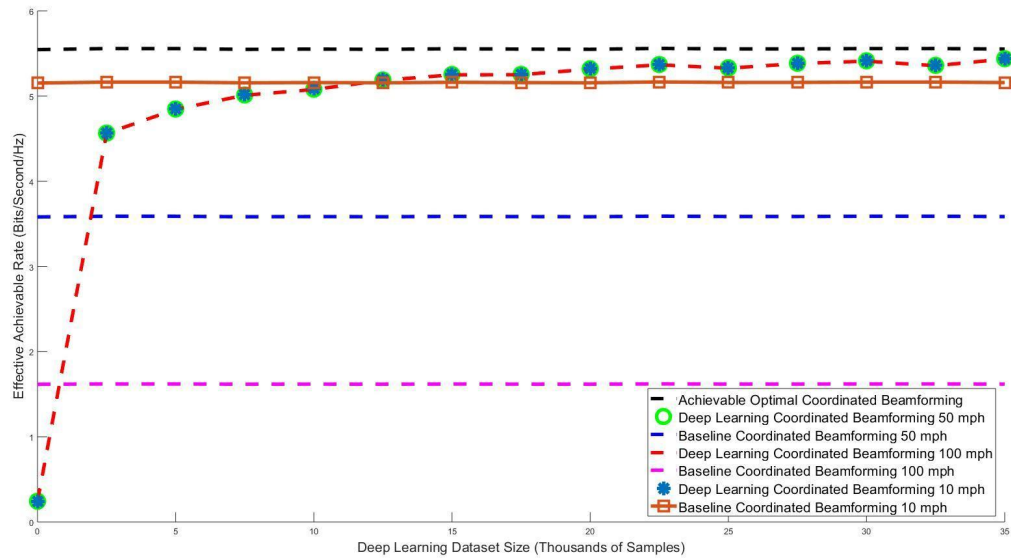


Figure 2.26: Achievable Spectral Efficiency with Nadam optimizer

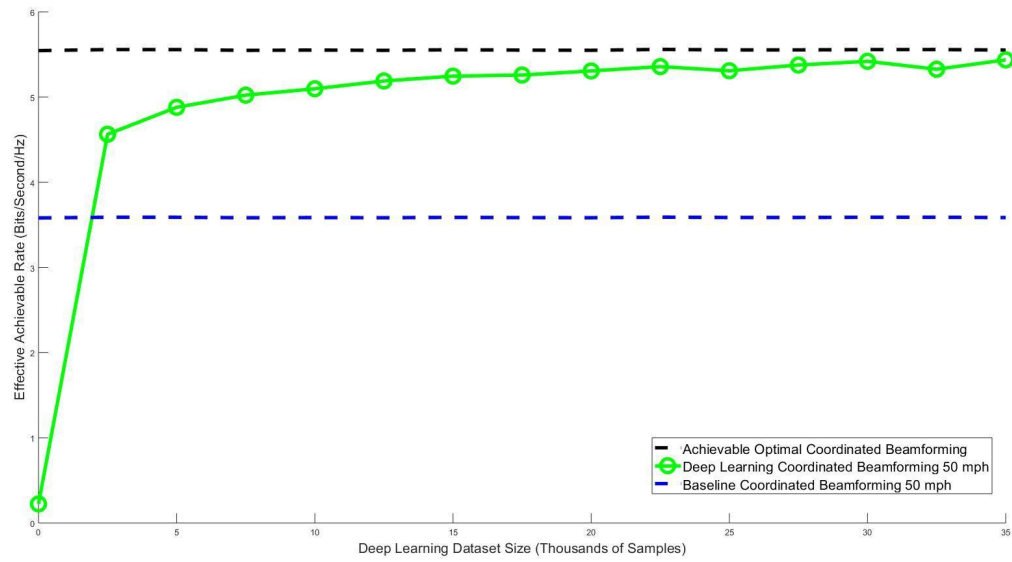


Figure 2.27: Achievable Spectral Efficiency with MSLE loss function

Chapter 3

Performance of Random Beamforming in Mobile mmWave Systems

Random Beamforming (RBF) as one of the most promising beamforming techniques especially for mmWave systems, has been proven to provide optimal performance for downlink MIMO systems in most of the cases. First, the user mobility and its effect on the system achievable capacity is studied and then some parameters of the system have been optimized. Some practical scenarios of mmWave broadcast downlink systems have been taken in consideration. Mathematical modeling and simulation results were derived and investigated to estimate the upper bound of the degradation in the overall system throughput that results from mobility of users in the small cells systems. Different possible factors that can affect the system throughput were taken in consideration. These parameters include the user location (within the cell area), the user direction of movement, movement speed range, and the beam width. Simulation results show that for all the typical mobility cases (walking, running, biking, and riding a car), the degradation in performance results from user mobility is too small for short frames and the Base Station (BS) will be able to deliver at least one message after each beamforming training period with high probability. To derive the best frame duration and beam width, the second part of this chapter is suggesting a framework to optimize the frame duration and the beam width for some mobility models with different outage probability thresholds (when the UE is moving out of the beam coverage area during transmission or reception). Convex optimization is used to derive the optimal

values as the outage probability has been proven to be monotonically increasing with both the frame duration and the beam width and the resulted optimal values are compatible with the standard for both walking and running users. See figure 3.1 for possible mobility scenario effect.

The contributions of this chapter include:

- Derive the mathematical expression for the performance degradation resulted from user mobility when using Random Beamforming (RBF) algorithm in mmWave small cells and Ultra Dense Networks (UDN) suggested for mmWave in 5G networks. Part of this work was published in [8].
- Extensive simulation was done to prove the theoretical results for different practical scenarios and the parameters used in the simulation are listed in tables 3.1 and 3.2. Part of these simulation results were also included in [8].
- Different system parameters (Frame duration and Beam width) were optimized for different mobility scenarios and practical systems scenarios. Some of these results were published in our work in [5].

3.1 System Model

In this section, the downlink broadcast mmWave MIMO system model and its assumptions are introduced and then we provide a brief introduction to the original random beamforming algorithm.

3.1.1 Downlink Broadcasting MIMO System that uses mmWave

For the typical static MIMO system suggested in [73], the Gaussian broadcast channel is assumed which consists of n user equipments (UEs) as receivers that are spread within the coverage area of the Base Station (BS) each is equipped with N antennas, and a base station (BS) that have M antennas as the transmitter. The system is assumed to satisfy a block fading channel model (i.e, the propagation matrix is constant during the coherence time T).

Other system assumptions include having more users than the number of antennas in the BS ($n \gg M$) at any time of the system operation. Also, we assume that each UE has no more antennas than the number of antennas in the BS or ($N \leq M$) which is the normal case in practice. Mathematically, the system is characterized by the equation 3.1:

$$\mathbf{y}_i(t) = \sqrt{\rho_i} \mathbf{H}_i \mathbf{s}(t) + \mathbf{w}_i(t) \quad i = 1, \dots, n, \quad (3.1)$$

where: $\mathbf{s}(t)$ is the M -vector of transmitted signal, $\mathbf{y}_i(t)$ is the N -vector of received signal by UE i , \mathbf{H}_i is the $N \times M$ channel matrix, \mathbf{w}_i is the N -vector of additive noise, and ρ_i is the signal-to-noise ratio (SNR) of the i -th user (averaged over the randomness of channel). We further assume that:

- (a) the total transmit power limitation is satisfying the relationship $E[\|\mathbf{s}\|^2] = M$; i.e, the average transmit power per antenna is a unit;
- (b) For each user in the coverage area, the averaged SNR is denoted by ρ .

3.1.2 System Throughput

It was stated in [78] that if the receiver (the UE) has full channel state information (CSI), then the capacity of the MIMO system can scale like $\min(M, N) \log \rho$. Whereas, if the receiver does not have the full CSI (which is the normal case especially with mmWave channel that is sparse in nature), then the capacity (or the achievable data rate) of the point-to-point (P2P) multiple antenna system will scale like $\min(M, N)(1 - \min(M, N)/T) \log \rho$. where T is the coherence time of the channel [35]. If $N=1$, the throughput is given by [73]:

$$R = E \left\{ \max_{P_1, \dots, P_n, \sum P_i = M_\rho} \log \det \left(1 + \sum_{i=1}^n \mathbf{H}_i^H P_i \mathbf{H}_i \right) \right\} \quad (3.2)$$

where M_ρ is the total average power. For a sufficiently large number of users, the sum rate capacity scales linearly with M , namely $(M \log \log n)$.

3.1.3 Random Beamforming

Directional transmission of mmWave communications is considered now a common sense to compensate for the high propagation loss of these high frequency bands. This means that the Base station needs to precisely align its transmission as a beam to the receiving UE all the time during the transmission. Traditional approach in doing so is by estimating the locations of UEs (e.g. using GPS or other localization techniques) and then aim the beam to the desired UE. However, the location information usually comes with a substantial overhead and the GPS information is usually having high error margin with respect to such highly sensitive applications. One of many alternative approaches, named the random beamforming [49], states that when the BS has messages to broadcast, it should form random beams in random directions. When there are many UEs in the coverage area of the BS, each beam will be pointed to at least one UE with a high probability; then the BS receives acknowledgement from the UE and transmits to this direction. Such a random beamforming approach avoids the overhead of location estimation and provides high accuracy. Moreover, as found in [49], *"RBF (random beamforming) achieves linear sum rate scaling w.r.t. the number of transmit antennas and, furthermore, yields optimal sum rate performance when the number of transmit antennas is large, if the number of users increases linearly w.r.t. the number of transmit antennas."* Based on that, RBF is promising better performance and high throughput for mmWave communication systems that use MIMO and have a large number of UEs. The detailed algorithm of random beamforming is given in Algorithm 2.

Algorithm 2 Random Beamforming for MIMO Systems using mmWave

- 1: BS constructs S random orthonormal beam vectors $\{u_1, \dots, u_S\}$.
 - 2: BS chooses a normalized direction θ randomly and transmits the beam x to it.
 - 3: **for** UEs receiving $\text{SNR} \geq$ a predefined threshold **do**
 - 4: UE sends the SINR to the BS
 - 5: BS sends data stream to the UE having the maximum received signal power using the beamforming vector x .
-

The throughput of the random beamforming scheme is approximately given by:

$$\begin{aligned}
R &\approx E \left\{ \sum_{m=1}^M \log(1 + \max_{1 \leq i \leq n} SINR_{i,m}) \right\} \\
&= ME \left\{ \log(1 + \max_{1 \leq i \leq n} SINR_{i,m}) \right\}.
\end{aligned} \tag{3.3}$$

Where $SINR_{i,m}$ is the Signal to Interference and Noise Ratio with the index m in which the SINR is maximized (i.e. the UE with largest SINR in the beam) [73].

3.2 Outage Probability Due to Mobility

In this section, we analyze the expected performance loss of the random beamforming algorithm that resulted from the mobility of UEs during the communication process.

3.2.1 Mobility Assumptions

The following assumptions are considered when analysing the performance degradation of the system explained in previous sections.

- A simplified channel model is assumed (Uniform Random Single Path (UR-SP)), where we consider only the strongest signal path between the BS and each UE (the LoS or the strongest NLoS).
- Number of antenna elements in each UE is less than that in the BS.
- There is a large number of UEs K in each cell during the system operation.
- The received signal by each UE k is described as follows:

$$y_k = \mathbf{h}_k^H \mathbf{x} + n_k, \quad k = 1, \dots, K. \tag{3.4}$$

where \mathbf{h}_k is the channel vector of the user k and \mathbf{x} is the vector representing the transmitted signal.

- We assume the following channel model:

$$\mathbf{h}_k = \alpha_k \sqrt{M} \mathbf{a}(\theta_k), \quad (3.5)$$

where α_k is the channel gain of user k , M is the number of antennas of BS, θ_k is the angle of the dominant path for user k , \mathbf{k} is the normalized direction of the single path for user k , and $\mathbf{a}(\cdot, \cdot)$ is the array steering vector. The channel power gain satisfies $E\{|| h_k ||^2\} = M$. Each user then reports back the average received power

$$|y_k|^2 = |\mathbf{h}_k^H \mathbf{x}|^2 + \frac{1}{N_s} \quad (3.6)$$

with N_s is the number of samples during the training period.

To sum it up, the performance degradation is analysed due to the UE mobility with the following factors being taken in consideration:

- The beam width, some realistic values are assumed.
- The direction of movement of each UE, assumed as a random gaussian variable.
- The speed of movement and its relationship to the coherence time.
- The distance between the BS and each UE within the beam coverage area and its corresponding Round Trip Time (RTT).

Figure 3.2 shows an example of the UEs distribution within any beam's area:

3.2.2 Degradation Analysis

Unlike the basic scenario, UE's can move while the RBF is going on. Such movement causes the derived optimal sum rate to degrade depending on many factors. When we have mobile UE, the UE may have moved to a different location and possibly different angle, when the BS sends out the signal. Therefore, the beam may miss the UE or may not be perfectly aligned to the UE. In the following analysis, we will quantify the above qualitative analysis on the performance degradation due to the UE mobility.

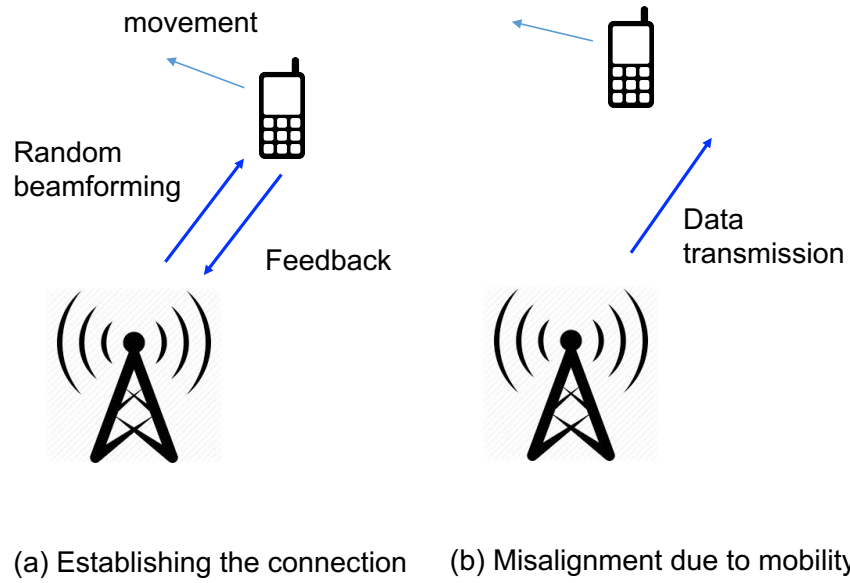


Figure 3.1: Possible Performance degradation resulted from mobility when using RBF.

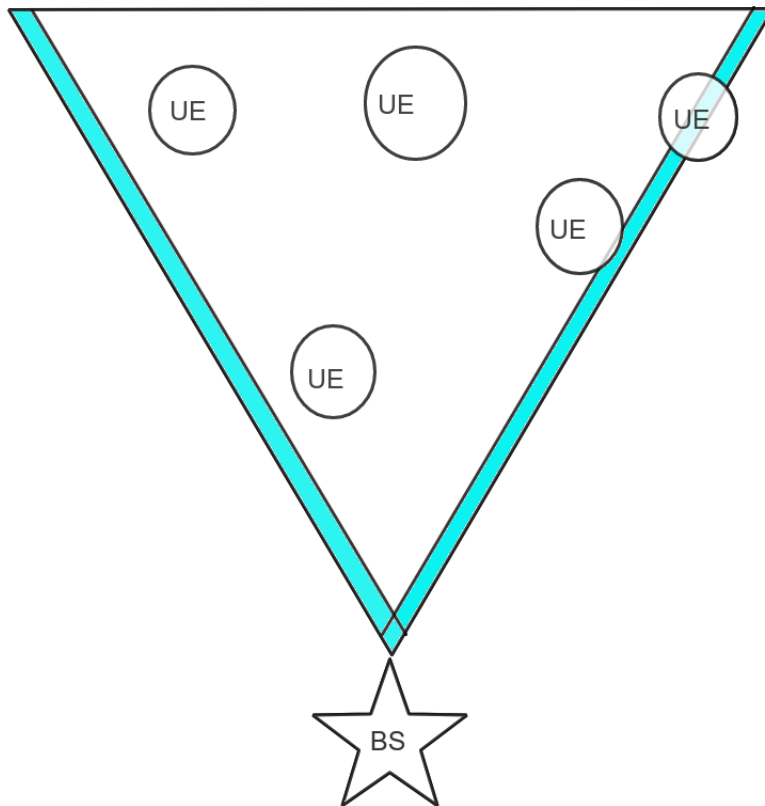


Figure 3.2: Beam Area with Side Borders.

Round Trip Time

Round trip time is the time interval between the moment when the UE sends the received SINR and the moment when the UE receives the data signal from the BS (after selecting the UE with the highest SINR). This time consists of the electromagnetic (EM) wave travel time, the processing time at the BS (e.g., decoding the packets fed back from the UEs, selecting the best UE, and preparing for the data transmission), and the frame duration time. The physical limit in our analysis is the propagation time. We neglect the processing time at the BS and assume it is too small compared with the propagation time. This means that the results of the performance degradation estimation are optimistic.

The EM traveling time is given by

$$T_{RTT} = \frac{2 * d}{c} + FD \quad (3.7)$$

where d is the distance between the BS and the UE, FD is the frame duration, and c is the speed of light. We multiply d by 2 because it is two way communications (RTT).

Edge Probability

The probability of the UE being on the edge of the beam is analysed first as shown in Fig. 3.2. The physical area of the BS beam has two narrow borders, where the UE may leave the beam if it was originally in it. The probability of the UE being on the edge is given by:

$$Pr(BeamEdge) = \frac{\text{Border Area}}{\text{Total Beam Area}} \quad (3.8)$$

where

$$\text{Border Area} = 2D_{\max}L_{BS}, \quad (3.9)$$

where $D_{\max} = v_{\max}T_{RTT}$ is the maximum distance that UE can move for different speed ranges, L_{BS} is the radius of the cell (namely the coverage distance of the BS), v_{\max} is the maximum speed of the user in each case, and

$$\text{Total Area} = \frac{1}{2}B_B B_H, \quad (3.10)$$

where B_B is the beam base which is given by

$$BeamBase = \frac{2B_H}{\tan \theta_B} \quad (3.11)$$

and B_H is the beam height, which is the same as L_{BS} , θ_B is the Beam angle, and θ_{BB} is the beam base angle which is given by

$$\theta_{BB} = \frac{\pi}{2} - \frac{\theta_B}{2} \quad (3.12)$$

Fig. 3.3 is showing the physical meanings of the above parameters:

Moving Away Probability

When the UE is within or close to any of the two edges of the beam, the probability of the UE moving out of the beam can be calculated as a Triangular distribution [45]. This kind of distribution is maximized when the UE is on the outside edge of the beam area and minimized when it is far away from it:

$$f(x \mid a, b, k) = \begin{cases} \frac{2(x-a)}{(k-a)(b-a)} & a \leq x \leq b. \\ \frac{2(k-x)}{(k-a)(k-b)} & b \leq x \leq k. \\ 0 & (x < a), (x > k). \end{cases} \quad (3.13)$$

where: a is the largest distance away from the beam edge where the UE can leave the beam coverage area with the lowest probability. $b = k$ is the peak location, which is when the user is on the outer border of the beam where the probability of leaving the beam is the highest, The distance between a and b is the D_{\max} which is the maximum distance any UE can move for any speed range during the RTT, and x is the random variable that expresses the random location of the user within the beam borders. Fig. 3.4 is showing the relationship between the UE location and the probability of leaving the beam coverage area:

Also, Fig. 3.5 shows the Triangular Distribution and the relationships among parameters in the equation 3.13:

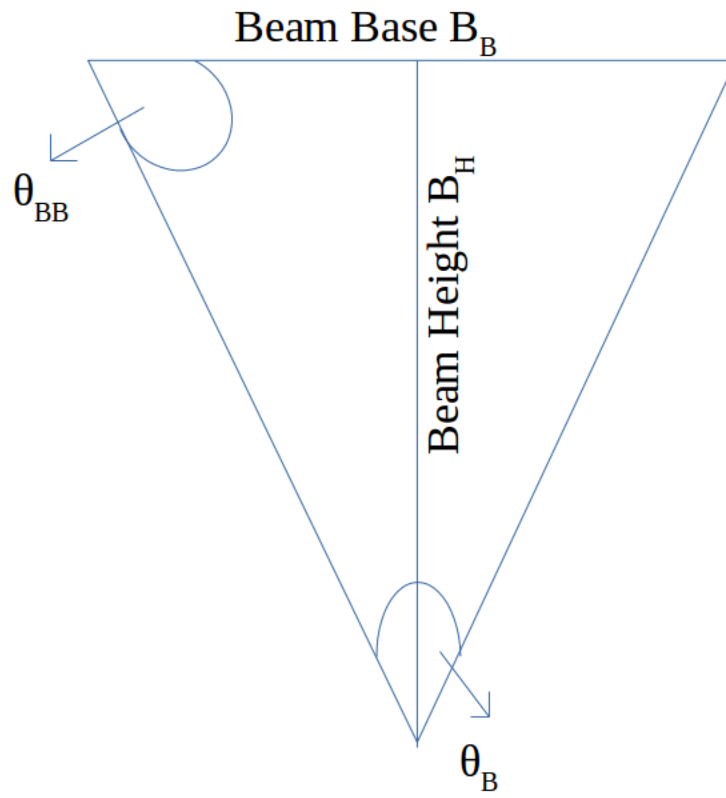


Figure 3.3: Beam Approximate Shape with the Edge Probability Calculation Parameters

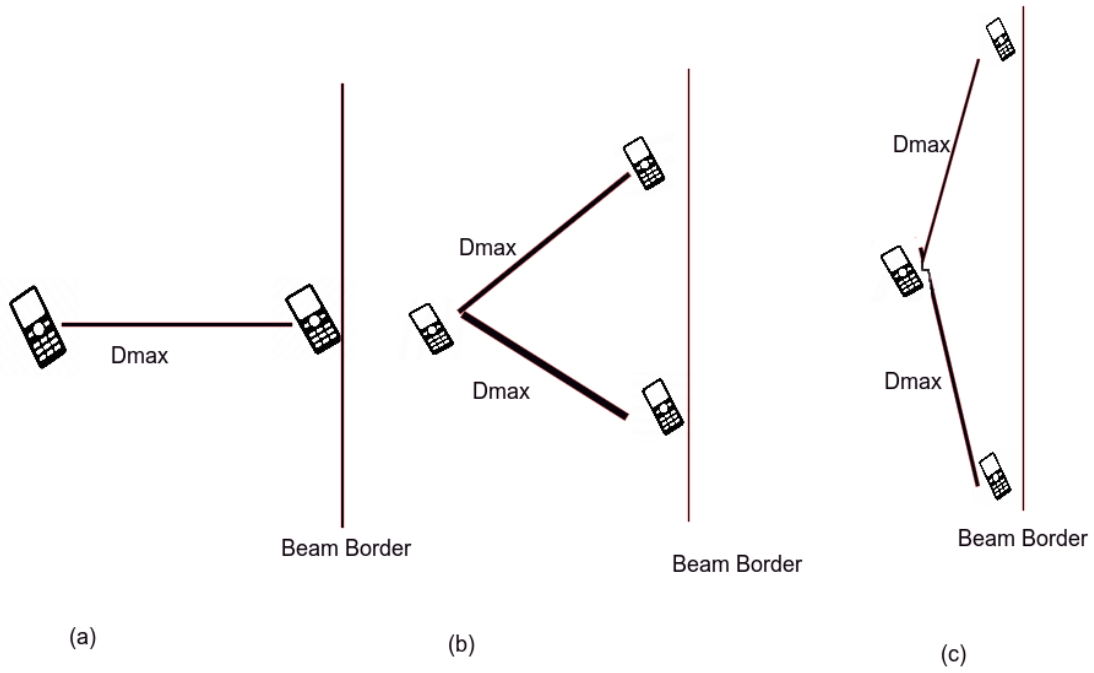


Figure 3.4: Relationship Between UE location and probability of leaving the Beam: (a) UE far enough from the Beam Border so that the probability of leaving the beam is too small. (b) UE is closer to the beam border which increases the probability of leaving the beam during the RTT. (c) UE is very close to the beam border, which increases the probability of leaving the beam even more.

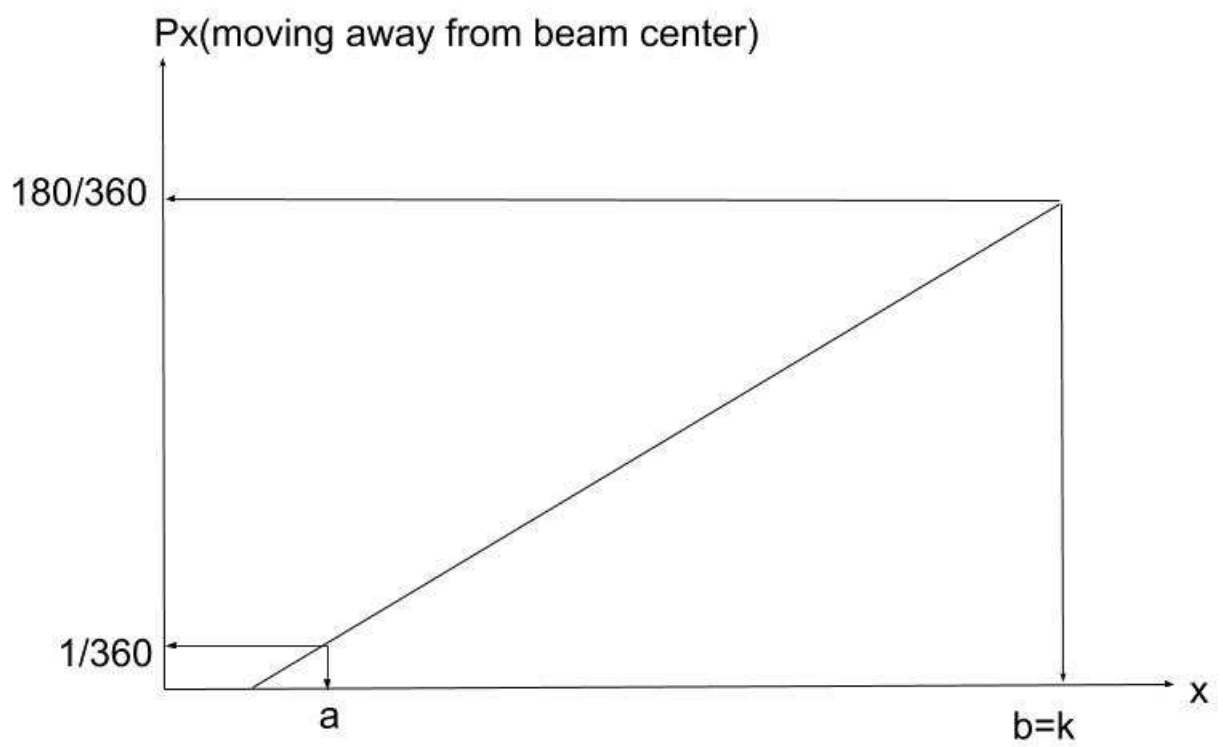


Figure 3.5: Assumed Triangular Distribution of the Beam Leaving Probability

Overall Mobility Effect

After analysing all the individual factors that affect the system throughput when the UE is in mobility status, here we put all of them together and show the cumulative effect for different beam widths (for different number of beams) and with the following assumptions:

- Random Beamforming for a MISO broadcast system with one BS and many UEs.
- Each BS has a Uniform Linear Array (ULA) of M antenna elements.
- The BS sector is covering 180 degrees with adjustable number of beams.
- Number of beams range from 10 to 120 (corresponds to 18°-1.5° as a beam angle (width)).
- Based on the number of beams, different triangles of beam coverage are created each time.
- We calculate the beam coverage total area and beam borders where there is a possibility that the user will leave the beam coverage area before the data arrives to it (as a result of mobility) which leads to throughput degradation.

Given the above assumptions, we obtain the following conclusion:

Theorem 3.1. *If the throughput of the MIMO downlink broadcast system with static UEs and BS is known (as calculated in [73]), then the average throughput degradation of the system with mobile users is given by:*

$$Th_D = \sum_{n=1}^N (Pr_n(OnBeamEdge) * Pr_n(AwayFromBeam)) \quad (3.14)$$

$$= \sum_{n=1}^N \left(\frac{2 * D_{max} * L_{BS}}{0.5 * \frac{2 * L_{BS}}{\tan(\frac{\pi - \theta}{2})}} \right) * f(E(x) | a, b, k). \quad (3.15)$$

$$= \sum_{n=1}^N 2 * Speed * RTT * \tan\left(\frac{180 - \theta}{2}\right) * f(E(x) | a, b, k) \quad (3.16)$$

where Th_D : is the average throughput degradation of the system.

$Pr_n(OnBeamEdge)$: is the probability that the user n is too close to the beam edge and can leave the beam coverage area once he/she moves away from the beam center.

$Pr_n(AwayFromBeamCenter)$ is the probability that the user (n) is moving out of the beam coverage. x is the user location within the beam borders and the expectation of (x) is expressed by the equation $E(x) = \int_{-\infty}^{\infty} x * f(x)dx$.

N is the number of users in the cell.

Speed is the Expectation of the speed of the UE, and the considered speed ranges are listed in table 3.1. RTT is the round trip time of the message between the BS and UE. θ is the beam angle. $F(x | a, b, k)$ is the triangular distribution from equation 3.16.

3.3 System Parameters Optimization

After studying the effect of mobility on the system's performance, we investigated the feasible system parameters (i.e. the frame duration and the beam width) and the best values for each of them for different system scenarios and practical applications.

3.3.1 Frame-Duration Optimization

Based on the results from the last section, we construct the following frame duration optimization problem as a convex optimization:

$$\begin{aligned}
& \text{maximize} && T_{RTT} \\
& \text{subject to} && Th_D \leq \Psi. \\
& \text{And} && d \leq 200.
\end{aligned} \tag{3.17}$$

where Ψ is the outage acceptable threshold for different applications, T_{RTT} is the round trip time from the equation 3.7 above, d is the distance between the BS and UE, and Th_D is outage expectation calculated in the equation 3.16 above.

3.3.2 Beam-Width Optimization

Next, we optimize the Beam width for any possible outage probability when random beamforming is used with mobile users. This is also a convex optimization and it is derived based on the equations mentioned above and the analysis results in [8]. This convex optimization problem can be expressed as:

$$\begin{aligned} & \text{Minimize} \quad \theta \\ & \text{subject to} \quad Th_D \leq \Psi. \\ & \text{And} \quad d \leq 200. \end{aligned} \tag{3.18}$$

where θ is the beam width that we minimize to reduce the competition among UEs in each beam for each time slot RBF and to increase the total number of Random Beams to serve a larger number of UEs in a shorter period of time.

3.4 Numerical Results

Mathematical modeling explained above with the parameters listed in table 3.1 are used in obtaining the results below.

The expected throughput degradation (%) resulted from the mobility of UE is shown in the figures 3.6 to 3.9. It has been observed that the probability of missing the UE decreases as the distance between the UE and BS increases. This makes sense as this reduces the RTT and the possible movement distance during this RTT. Also, we can see clearly that the larger the beam angle, the lower the probability of throughput degradation with mobility because this means more freedom to the users to move within the beam before getting out of it and cause the alignment miss .

The relationship between the average throughput degradation (outage probability) and the speed of movement is shown in Figures 3.10 to 3.13. We observe that the expected throughput degradation is linear with respect to the moving speed of the UE (i.e. the faster the UE, the more alignment misses we get which results in more degradation in the system throughput):

Table 3.1: Mathematical Derivation Parameters

Parameters	Specifications
Beam Angles (widths)	1.5, 2, 3, 4, 6, 9, and 18 Degrees
Speed Range for Walking	3-5 Km/h
Speed Range for Running	16-24 Km/h
Speed Range of Biking	15-40 Km/h
Speed Range of Car riding user	65-112 Km/h
Cell Radius (Beam Coverage Distance)	200 meters
Mobility Model	Random Way Point (RWP).
Number of Nodes (UEs)	1000.
Outage Threshold	1, 2, 5, 10, 15, 25, and 50%.

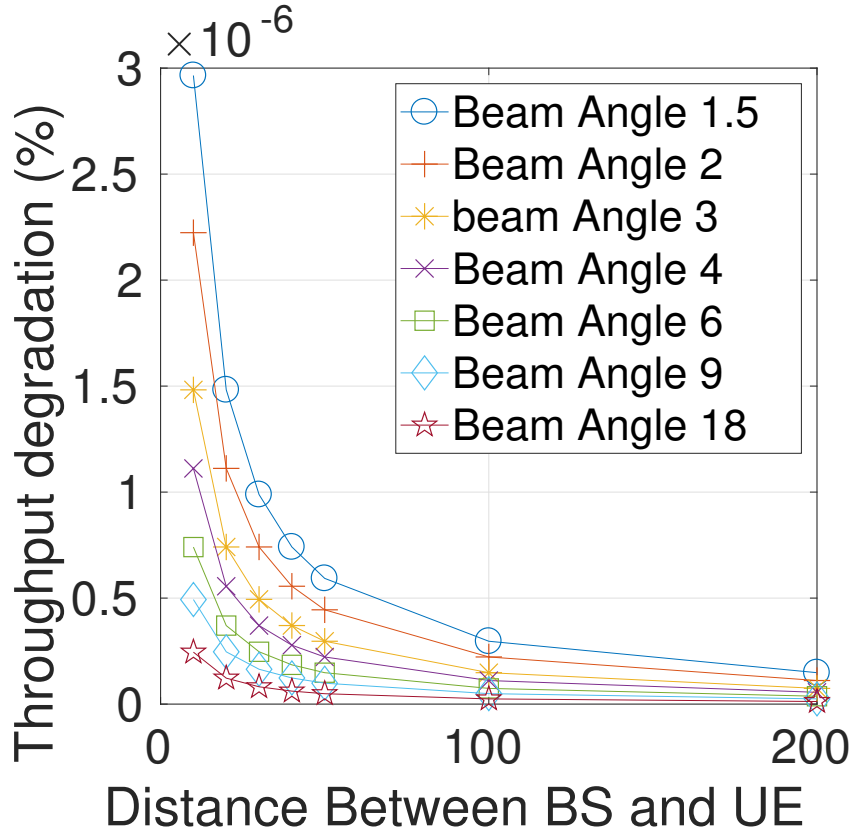


Figure 3.6: Probability of leaving the Beam Area for Walking Users for different beam angles

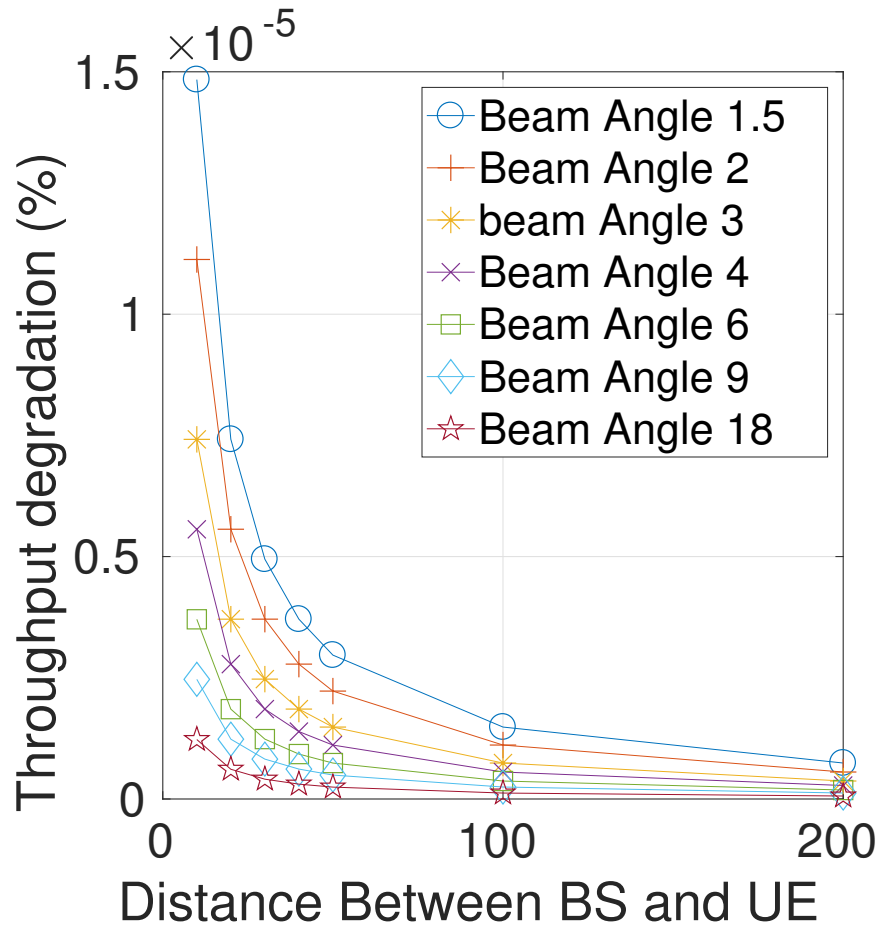


Figure 3.7: Probability of leaving the Beam Area for Running Users for different beam angles

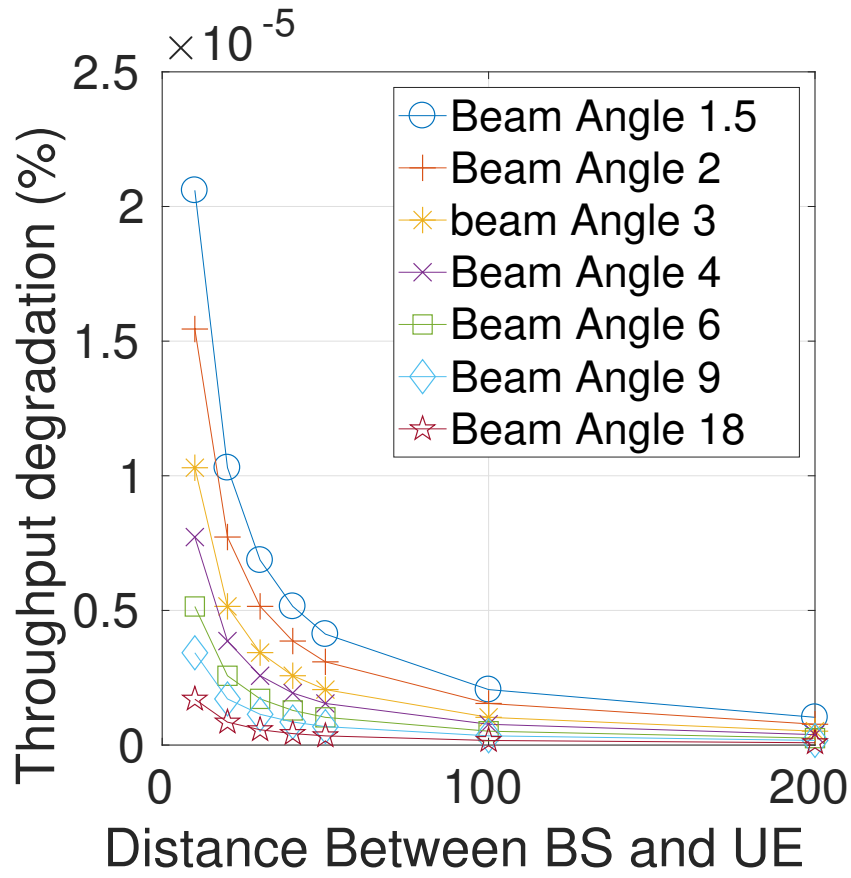


Figure 3.8: Probability of leaving the Beam Area for Biking Users for different beam angles

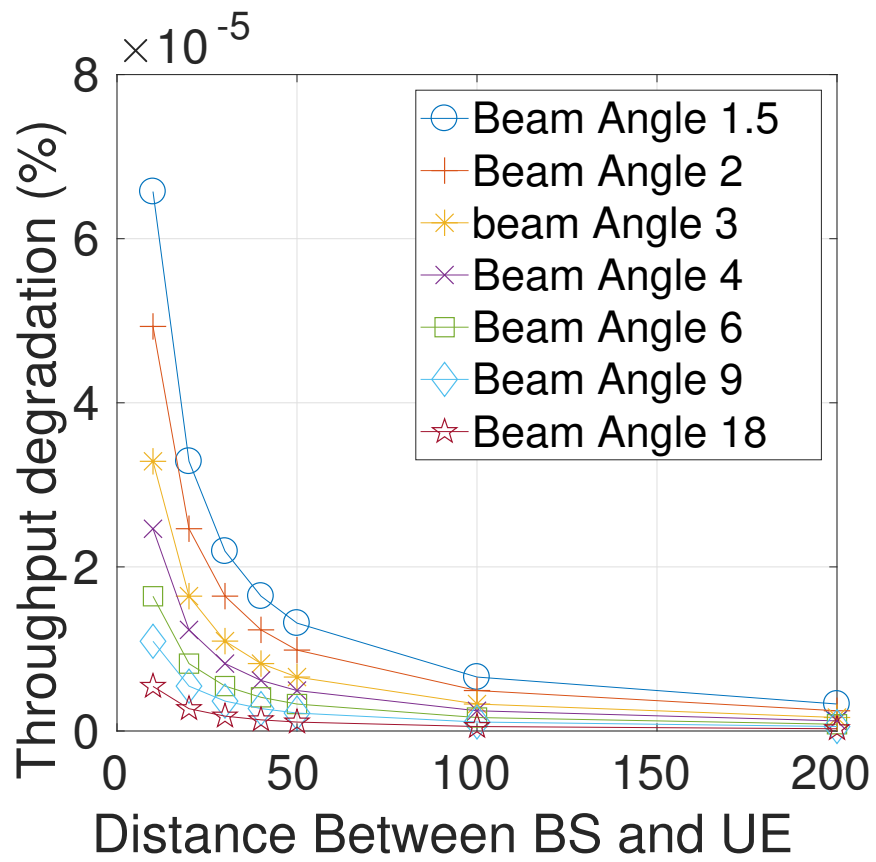


Figure 3.9: Probability of leaving the Beam Area for Users Riding a Car for different beam angles

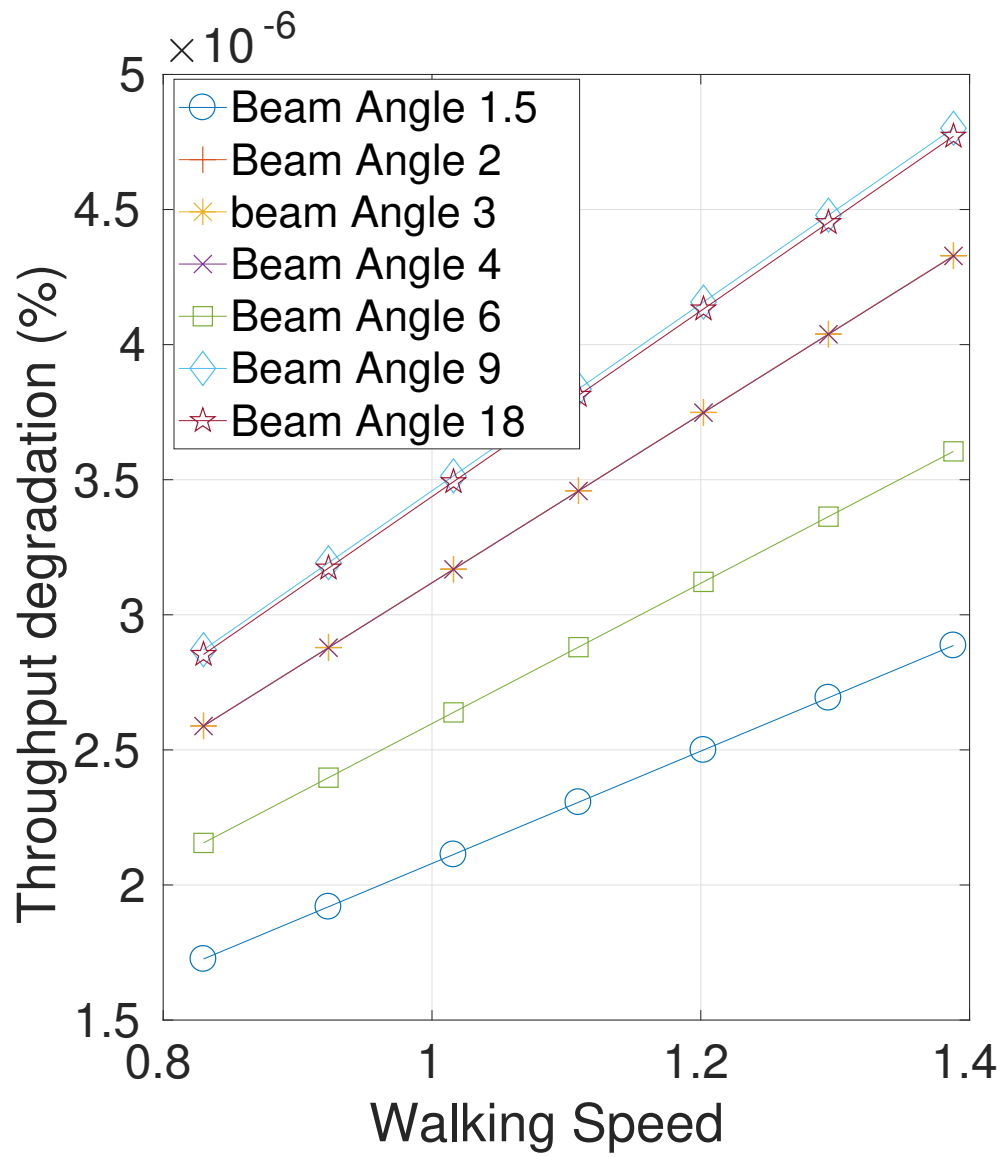


Figure 3.10: Expected Throughput Degradation for different Walking Speeds.

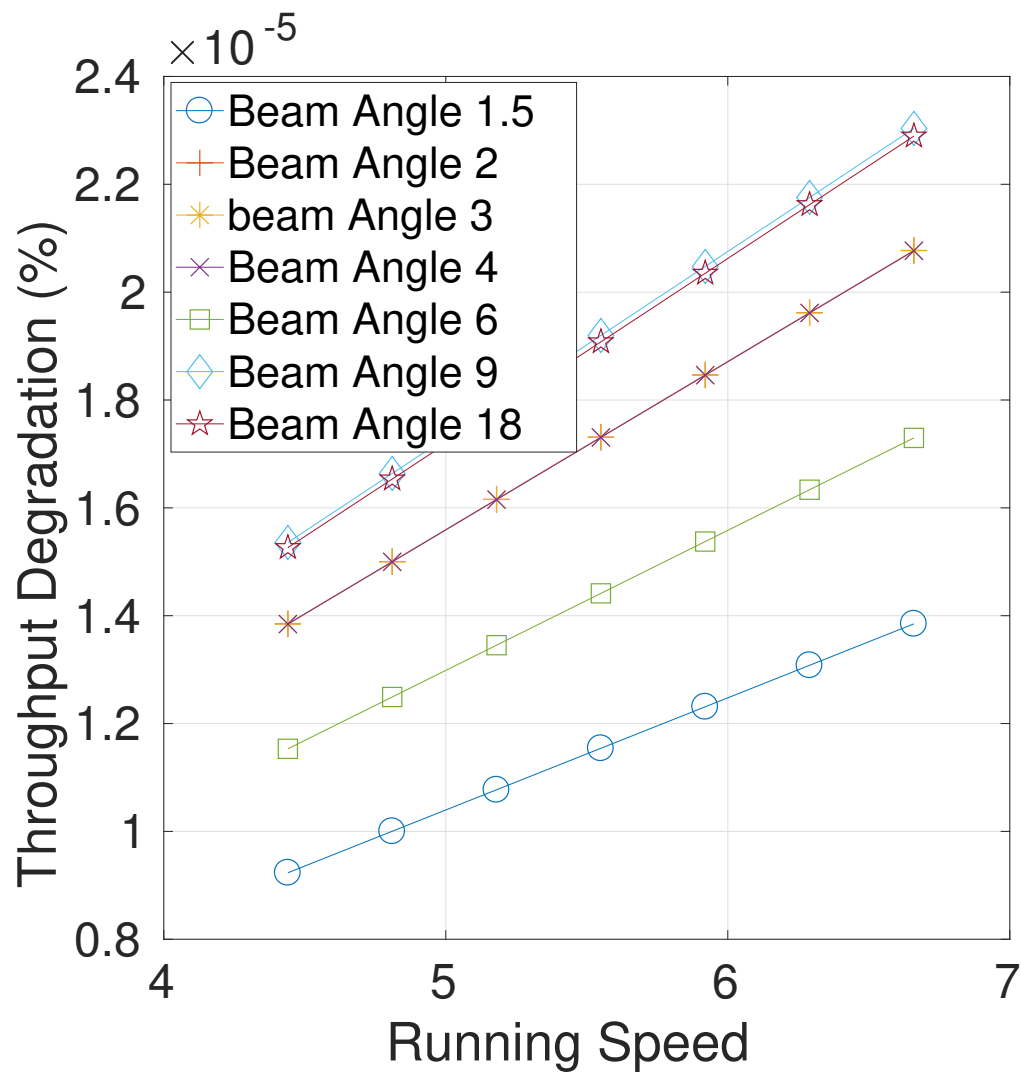


Figure 3.11: Expected Throughput Degradation for different Running Speeds.

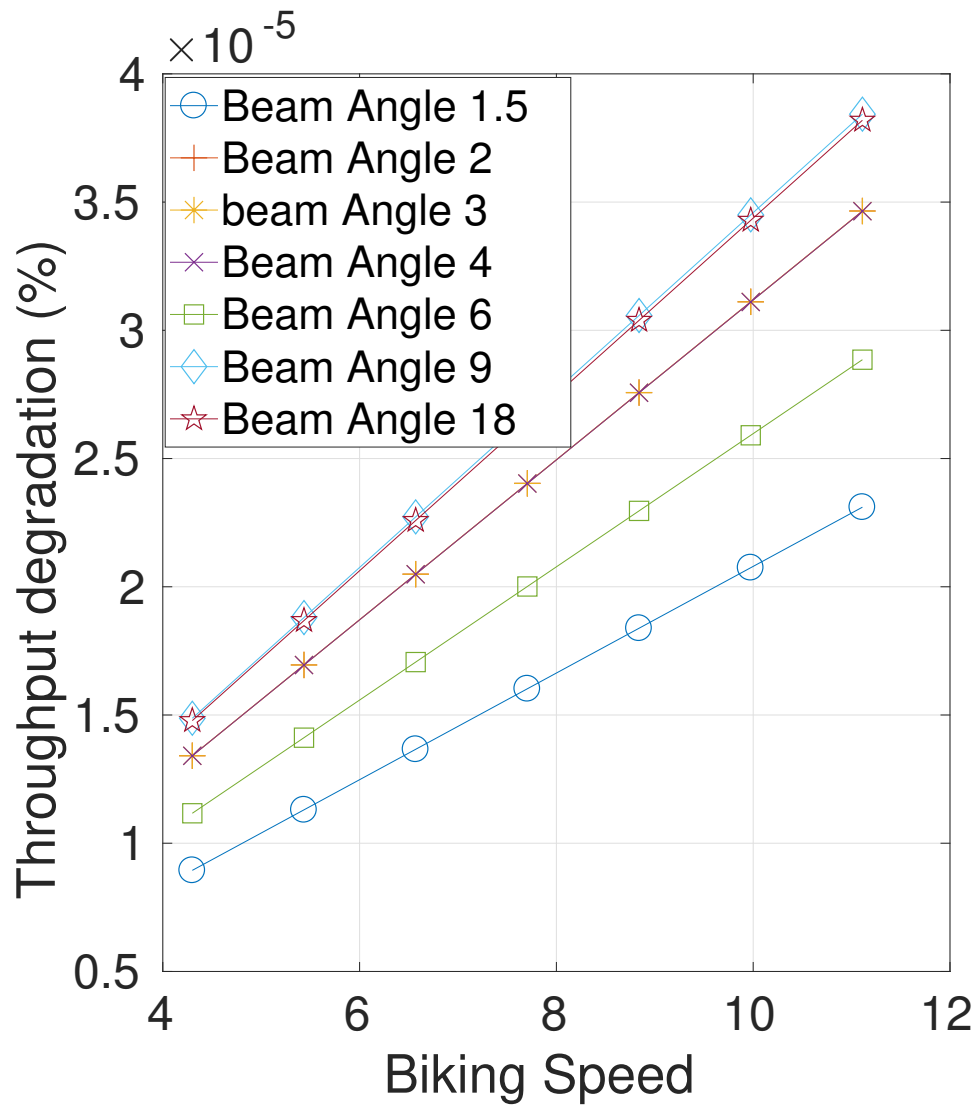


Figure 3.12: Expected Throughput Degradation for different Biking Speeds.

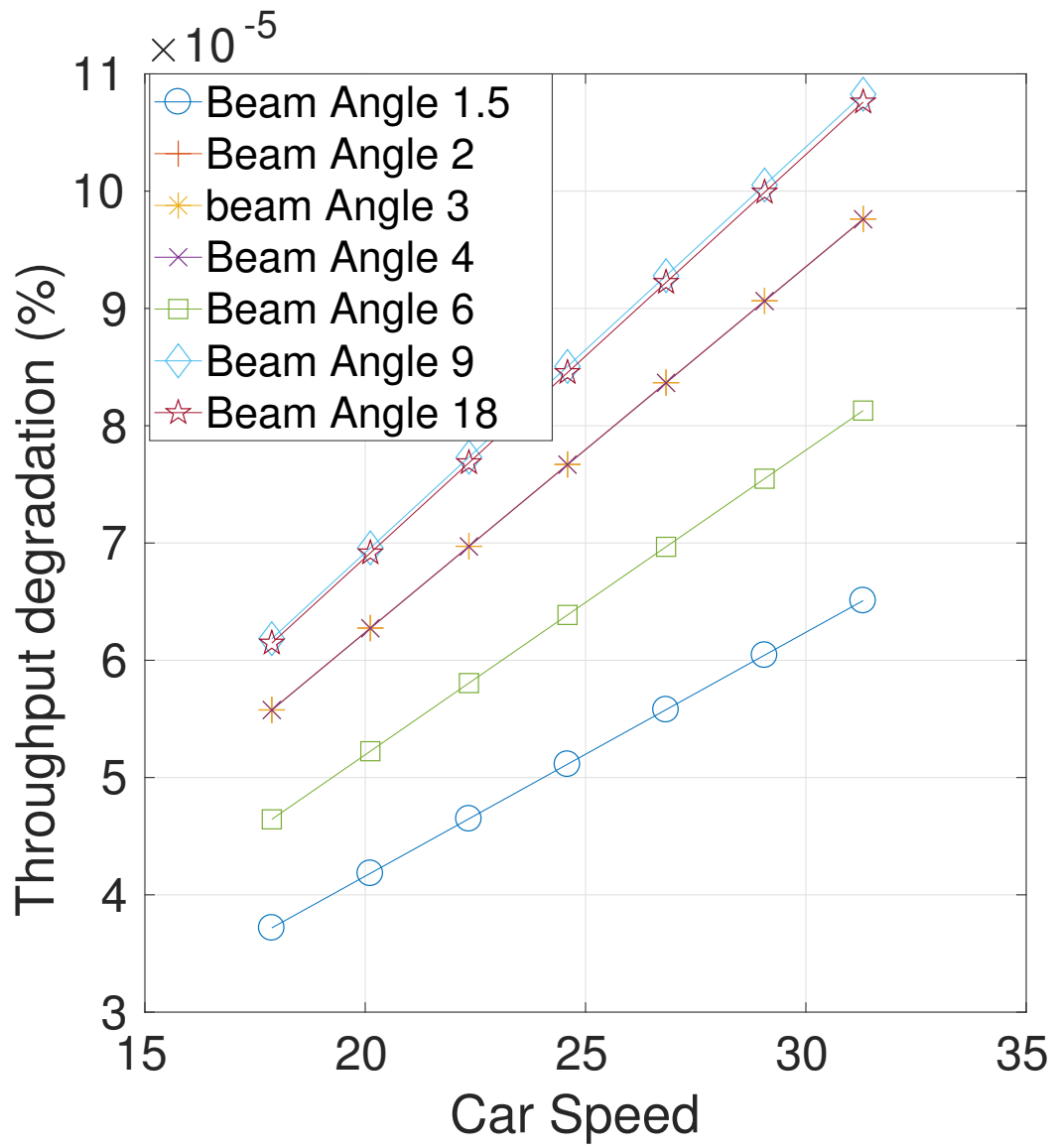


Figure 3.13: Expected Throughput Degradation for different Car Speeds.

To validate our mathematical modeling of this issue, we used one of the well known mobility models (the Random Waypoint (RWP) Mobility Model [41]) to calculate the real degradation in throughput for different scenarios and parameters that are summarized in the Table 3.2:

from the simulation of the mobility (using the random waypoint mobility model) of UE with different speeds, locations, directions, and different distances between the BS and UE, we got the results shown in Fig. 3.14 for different beam widths. As it can be seen clearly, these results are compatible with our mathematical analysis results where the probability of UE leaving the beam coverage area is about 3.5% in the worst case scenario:

As for the frame duration and beam width optimization, the optimization was performed using the convex optimization software called (cvx) from Stanford University described in [33] and with the same assumptions about it as mentioned in chapter 2. We use Convex optimization because it has been proven in [8] that the outage probability is a convex as it is monotonically increasing with respect to different frame durations and beam widths for the RBF. The results for frame duration optimization are shown in the figures 3.15 for walking speed and 3.16 for running speed users:

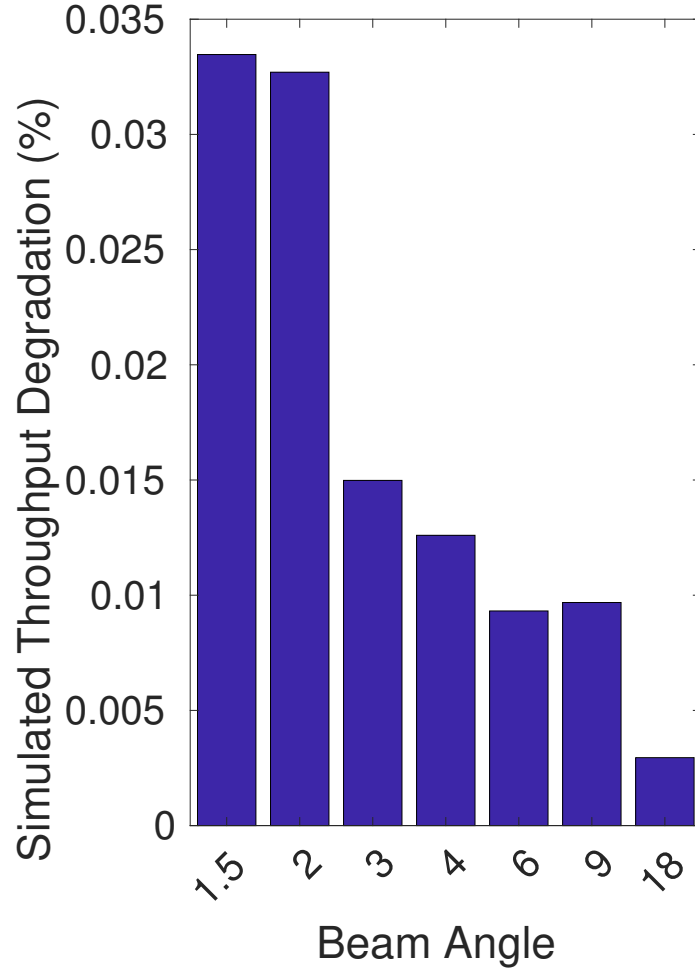
It is clear that RBF for mobile users cannot support large frames with lengths more than 10 msec without suffering from a large performance degradation. Here there should be a compromise between longer frames with a larger probability of retransmission or short frames with better delivery probability. This can be application dependant and decided prior to network configuration and operation. It is worth noting that the default frame duration suggested for 5G can be as short as (1 msec) for the single frame and can be (0.5 msec) for single subframe length [61].

The beam angle (for each RBF) optimization results for walking and running users are shown in figures 3.17 and 3.18:

These figures for walking and running users show the same trends as the optimal frame durations, where shorter frames seems to give less performance degradation and require narrower angles for each beam. Wider beams are required to ensure less degradation resulted from user mobility for each frame length. And the faster the user moves, the wider beam is required to ensure better performance. The other outcome from these results is that the

Table 3.2: Simulation Parameters

Parameters	Specifications
Mobility Model	Random Way Point (RWP).
Beam Angles	1.5, 2, 3, 4, 6, 9, and 18 Degrees.
Speed Range	0.2 - 31 m/s.
Pause Interval	[0 1] seconds.
Movement Interval	[2 6] seconds.
Direction Interval	[-180 180] Degrees.
Number of Nodes	1000.
Cell Radius (Beam Coverage Distance)	200 meters

**Figure 3.14:** Throughput Degradation Resulted from Simulated Mobility for Random Speeds, Directions, and Distances between BS and UE

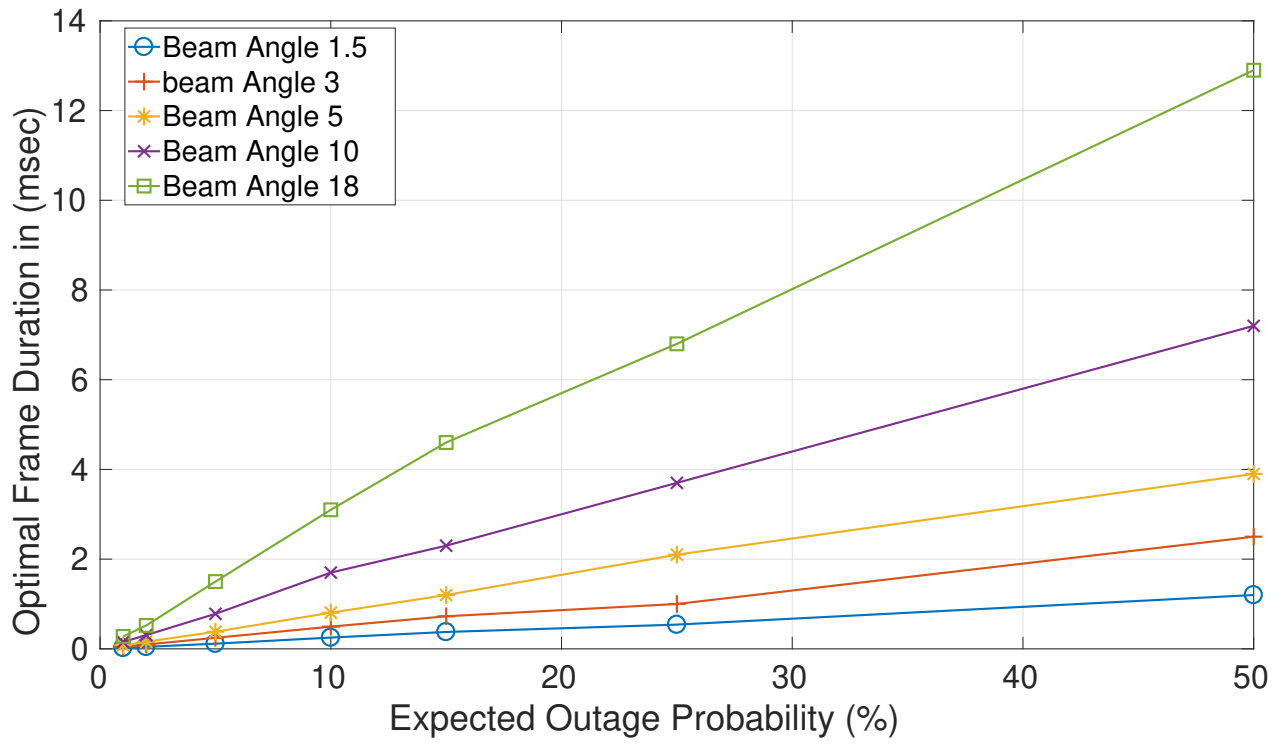


Figure 3.15: Optimal Frame Duration for Different Outage Probability Percentages with Walking Speed Range UEs

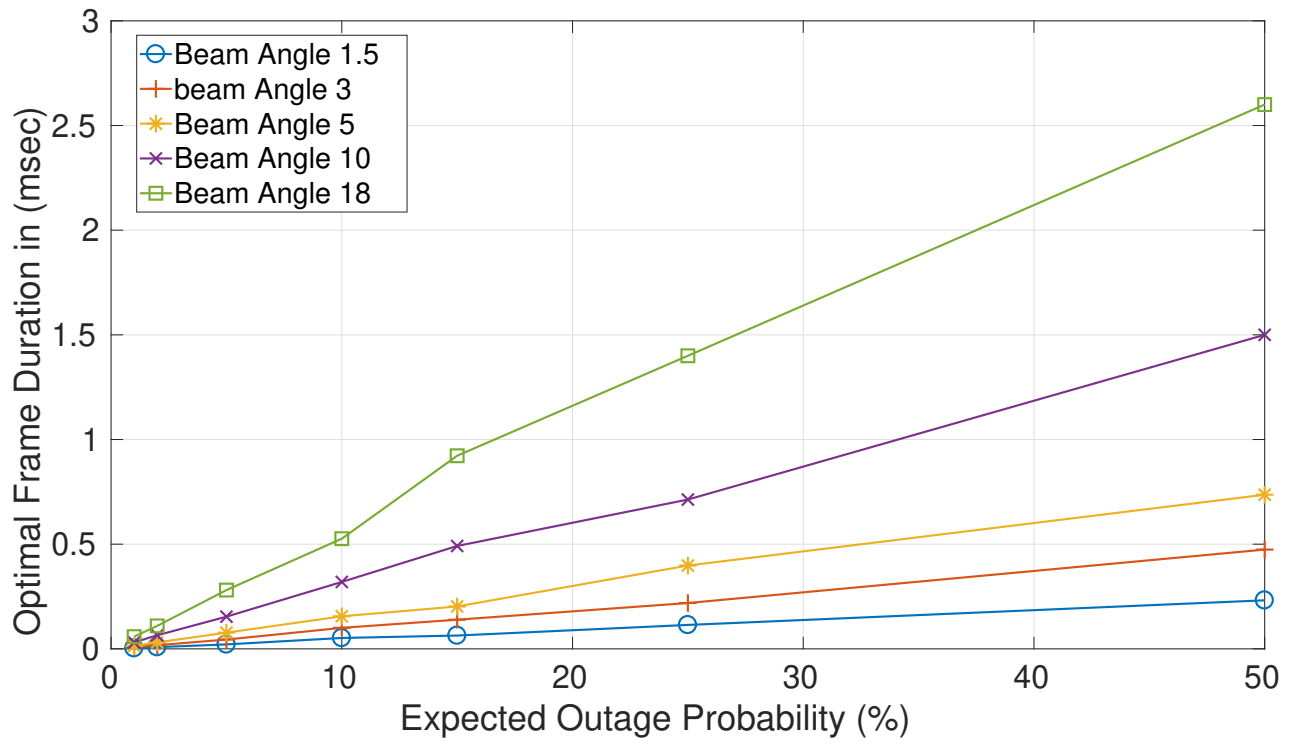


Figure 3.16: Optimal Frame Duration for Different Outage Probability Percentages with Running Speed Range UEs

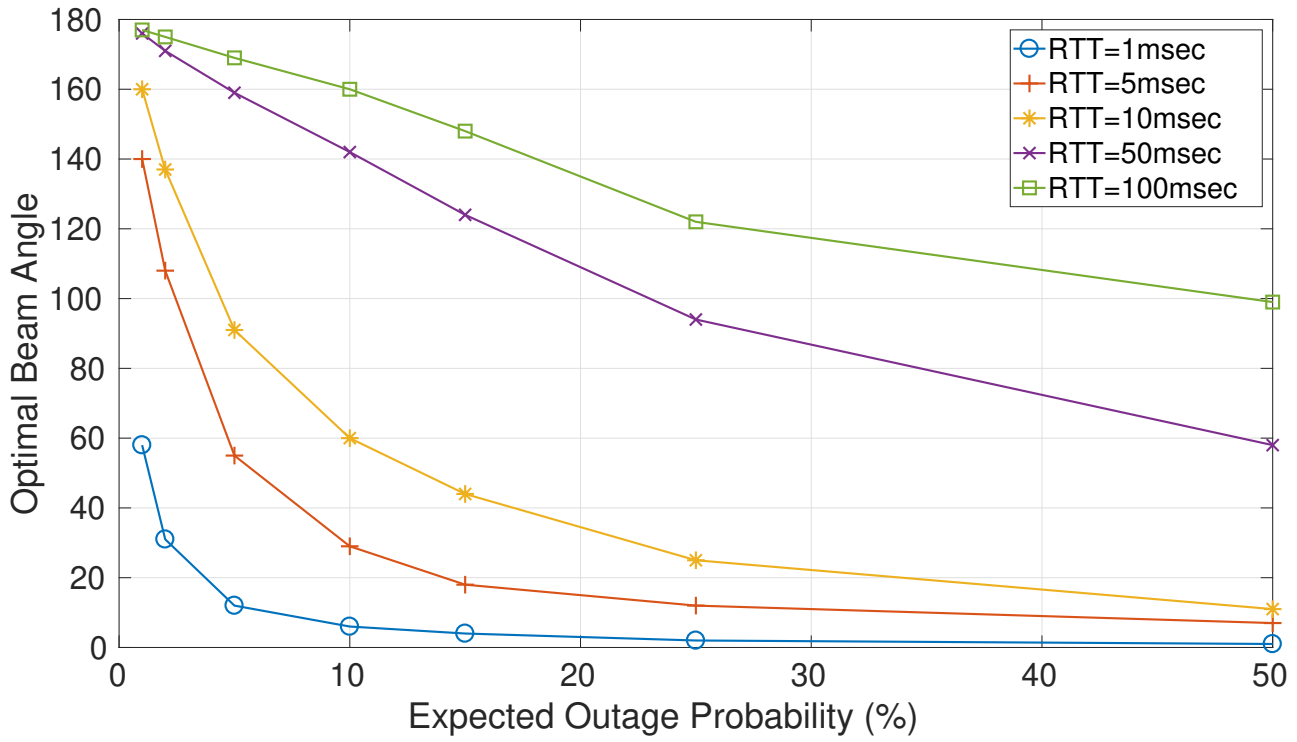


Figure 3.17: Optimal Beam Angle for Different Outage Probabilites with Walking UEs

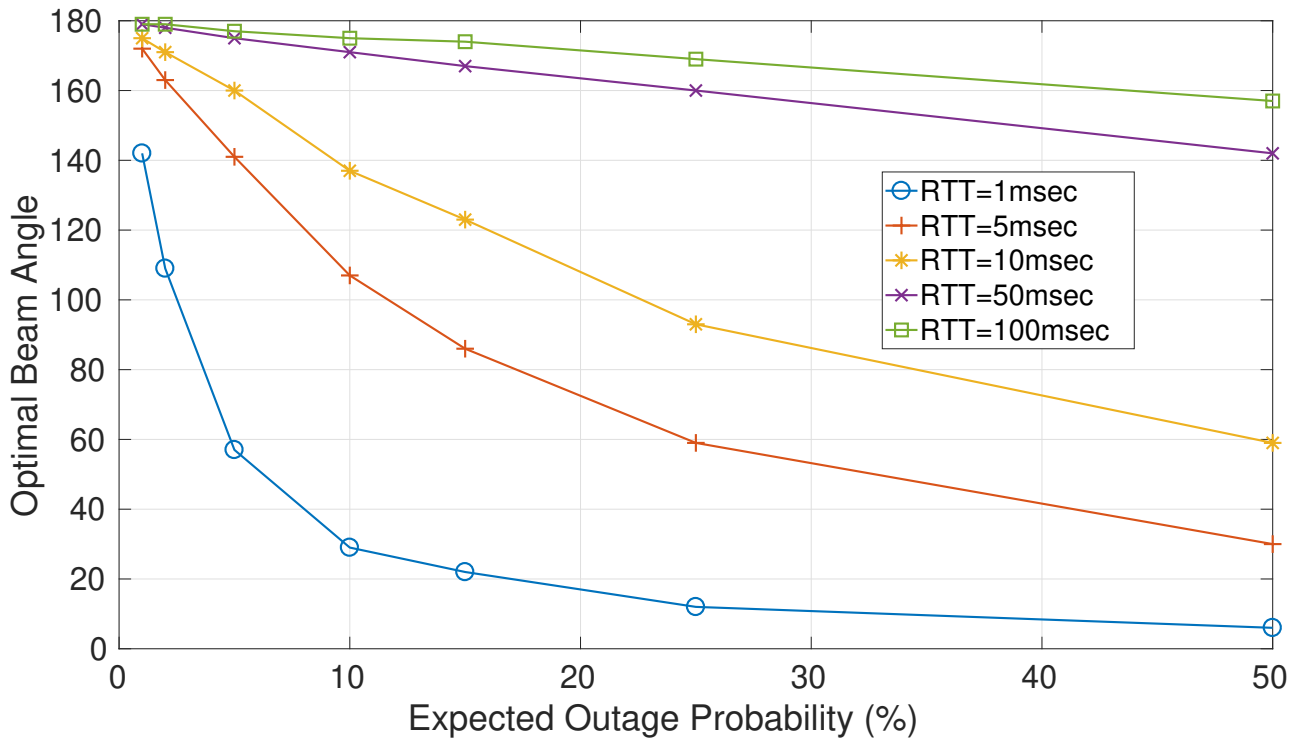


Figure 3.18: Optimal Beam Angle for Different Outage Probabilities with Running UEs

optimal conditions for RBF to work with is when the FD is ≤ 10 msec and the beamwidth $\theta \geq 60^\circ$.

Knowing that the frame duration can be as high as (10-100 msec) as in the 802.11ad [8] and as short as fractions of a millisecond [61], we got most of our optimal frame durations for different scenarios within this range. Also, having many suggestions for the beam angles ranging from too narrow as few degrees [8] up to few beams with large angles [13], the resulted optimal beams for each working scenario are all within this range. We did not list the results for faster moving UEs (bike and car riding) because it is obvious that supporting such speeds required more sophisticated beam alignment or tracking techniques as the ones suggested in [81] and [44].

Finally, in this chapter, the mobility effect on the performance of Random Beamforming (RBF) was studied. It seems that any beam angle (width) more than 3 degrees is giving acceptable throughput even with mobility. Random Beamforming got a linear sum rate as the number of the users increased linearly with the number of antennas in the BS (for static users). So, with the same assumption here, the throughput degradation is proportional to (1/distance) which means that the farther the UE, the less probable it will get out of the Beam coverage area because of its mobility. Throughput degradation is proportional to (1/beamwidth) which means that the wider the beam, the less probable the users will leave the beam as a result of their mobility. Even with mobility, BS can still deliver at least one message for the UE before it leaves the beam coverage area with a very high probability. Optimal system parameters for different practical scenarios such as the Frame Duration (FD) and the Beam width has been derived in this work as well.

Chapter 4

Routing Protocols in Mobile Ad-Hoc Networks Using Millimeter Wave

Self-Organized networks (SONs) have been studied for many years, and have attracted many researchers due to their substantial applications. Although the performance of such networks in the lower band networks (sub-6 GHz band frequencies) has been well studied, there are only sparse studies on SON in higher frequency bands, such as the mmWave band. mmWave frequencies have attracted many researchers in the past few years because of their unique features and are now considered as an important part of the next generation of wireless communications namely (5G). In the first part of this chapter, we study the performance of some well-known routing protocols in the case of mmWave Mobile Ad hoc Networks (MANET) using the ns-3 mmWave module that was developed recently. SONs are within the goals for the most recent release of the 3GPP New Radio (NR) standardization process (Release-16) for the 5G, which makes the study of the behavior of such frequency bands for these networks an important activity towards achieving such goal. Mathematical and simulation results show a great improvement in the routing protocols delivery rates and power consumption when using mmWave compared to the sub-6GHz band frequencies. The work in section 1 has been partially published in [6] whereas the work in section 2 of this chapter was partially published in [10].

4.1 MANET Routing Algorithm with mmWave

Mobile ad hoc networks consist of many User Equipment (UE) that are capable of transmitting and receiving directly from each other without the need for network infrastructure [55]. Each UE can be a transmitter, a relay, or a receiver node in any data transmission process, and each UE has a specific transmission range that depends on the transmission power, the frequency band used for transmission, the channel conditions, the propagation loss, and many other factors. As a comparative study, we first use Wi-Fi traditional frequency band within the IEEE 802.11 standard and then use the 28GHz mmWave band for the comparison purposes. The network is assumed to have (n) UEs at any time and there is a specific number of transmitters and receivers that are willing to exchange data packets at specific times during the network operation. Traditional Wi-Fi UE is assumed to use omnidirectional antennas with an equal gain in all directions, whereas the mmWave UE is equipped with directional antennas that can be directed in specific directions with larger gain within these directions. This directionality and antenna gain is the reason behind the different channel models and performance differences reported.

Many routing and data forwarding algorithms have been proposed for mobile ad hoc networks [3, 64, 20, 18]. Three of the most famous ones in the literature [64, 20, 18] are also the ones that we will compare their performance when using sub-6GHz frequencies vs. when using mmWave frequencies. Ad-Hoc On-demand Distance Vector (AODV) is a reactive routing protocol that floods the network with Route Request (RReq) packets when required [20]. AODV does not rely on periodic advertisements, which reduces the overhead and provides more bandwidth for users. Also, it is proven to be a loop-free routing protocol even in the case of mobility and repairing broken links. It scales well with the large numbers of mobile nodes that are cooperating to form an ad hoc networks. It is expected that using mmWave frequencies with directional antennas with such protocol would improve the overall performance as it will reduce interference (due to directional narrow beams communications) and the large gain the directional antennas can provide towards the relay nodes or the final destinations.

Destination-Sequenced Distance-Vector (DSDV), on the other hand is a proactive (table driven) routing protocol that is a destination based protocol with no need for a global view of the network topology [64]. Considering each mobile host as a specialized router, this protocol periodically advertises its view of the network topology to other hosts in the network. With such a mechanism, it can modify the Routing Information Protocol (RIP) [38] to be suitable for dynamic and self-starting networks (such as the MANET). Again, using mmWaves with directional antennas and large directed gains can improve such protocol performance due to fewer interference effects and better received SNR at any relay or destination nodes within the transmission range of the mmWave devices.

Finally, Optimized Link State Routing protocol (OLSR) is another table-driven routing protocol for mobile ad hoc networks that exchanges periodic messages to maintain the network topology information at each node [18]. OLSR is an optimized protocol over a pure link state protocol because it compares the size of data sent in each message to reduce the number of retransmissions while flooding the entire network with these messages. It uses multipoint relays technique to efficiently flood the network. Again, using mmWaves with such protocol is expected to improve the performance due to the reduction of interference among all these message flooding processes and improving the received SNR due to the antenna gain and directionality.

We have studied some channel models suggested by 3GPP in [1], and their impact on the performance of some well-known MANET routing protocols [64, 20, 18]. To understand the difference in performance between traditional Wi-Fi MANET and the networks that use mmWave, we need first to clarify the following:

- Wi-Fi devices broadcast wireless signals in all directions and cover larger distances (up to several miles), whereas mmWave devices only transmit narrow beams in specific directions and cover shorter distances (up to few hundred meters for the Ultra-Dense Networks (UDN) [29]).
- Path Propagation loss for Wi-Fi signals is determined by Friis equation as follows (assuming no transmission antenna gain (G_t) or reception antenna gain (G_r) i.e. G_t and $G_r = 0dB$):

$$L = \frac{4\pi df}{c^2} \quad (4.1)$$

$$PL(dB) = 20\log(f) + 20\log(d) - 147.56dB \quad (4.2)$$

Where:

L : is the path loss.

d : is the distance between the transmitter and receiver.

f : is the used frequency.

c : is the speed of light ($3 * 10^8$ m/sec) [27].

If we use the same path loss for mmWave UE and take the Tx gain and Rx gain in consideration (which ranges between 14-17 dB as suggested in [40], then the equation will be:

$$PL(dB) = 20\log(f) + 20\log(d) - 147.56dB - 17dB - 17dB. \quad (4.3)$$

Which clearly reduces the path loss to a large extent. Many other path loss models for mmwaves have been proposed in the literature recently. According to 3GPP in [50], assuming rural Line of Sight (LoS) path between any two nodes in the MANET, the path loss can be defined as:

$$PL(dB) = 20\log(40\pi df/3) + \min(0.03h^{1.72}, 10)\log(d) - \min(0.044h^{1.72}, 14.77) + 0.002\log(h)d. \quad (4.4)$$

Where:

$PL(dB)$: is the path loss in dB.

d : is the distance between transmitter node and receiver node.

f : is the used carrier frequency.

h : is the height if the Tx node.

The other path loss model of mmWave signals was suggested in [77] and has been proven to match the high fitness of the Line of Sight (LoS) and the Non-Line of Sight (NLoS) environments is the one-parameter close-in (CI) model described below:

$$\mathbf{PL}^{CI}(f, d)[dB] = \mathbf{FSPL}(\mathbf{f}, \mathbf{1m})[dB] + 10n \log_{10}(d) + \mathbf{X}_{\sigma}^{CI}. \quad (4.5)$$

where n denotes the single model parameter, the path loss exponent (PLE), with $10n$ describing the path loss in dB in terms of decades of distances beginning at $1m$, d is the separation distance between the transmitter and receiver nodes, X_{σ}^{CI} is the Shadow Fading (SF) standard deviation describing large-scale signal fluctuations about the mean path loss over distance, and $FSPL(f, 1m)$ denotes the free space path loss in dB at the transmitter-receiver separation distance of $1m$ at the carrier frequency f . Also, the free space path loss (FSPL) can be described as:

$$\mathbf{FSPL}(\mathbf{f}, \mathbf{1m})[dB] = 20 \log_{10}\left(\frac{4\pi f}{c}\right). \quad (4.6)$$

where c is the speed of light.

It is clearly proven now that there is no one model that is capable of describing the mmWave channel in different environments and that the transmission scenario conditions need to be taken into consideration when trying to talk about such channel models[1, 50]. The following figure show some of the propagation path loss for different frequencies and distances according to some of the previously described models:

The figure 4.1 shows clearly that the devices that use mmWave frequencies are suffering more severe path loss than the traditional Wi-Fi devices if we don't take the directional antenna gain in consideration. While this is only true for omnidirectional antennas, using beamforming and directional antennas has been proven to have much less path loss than that of equivalent Wi-Fi devices for short distances [50]. These facts suggest that the UEs in MANET that use Wi-Fi frequencies are tended to transmit messages to farther nodes which means more propagation loss (and more probability of errors in messages and reduction in delivery ratio), whereas the UEs with mmWave are tend to transmit messages to closer nodes and with narrow beams with high directional gains which means less propagation

losses (and better delivery rates). the reduced propagation loss of UE's with mmwave means better received Signal to Noise (SNR) which leads directly to better delivery ratio as we will see in the next section.

Finally, to examine the superiority of some traditional routing protocols in MANET when using mmWave over their performance when using the sub-6GHz band, we will use a network with specific features and network scenarios and compare these scenarios with respect to:

- Different channel models for Wi-Fi and mmWave signals.
- Different Data rates.
- Different packet sizes.
- Different Tx power.
- Different Routing Protocols.

4.1.1 Performance Evaluation Metrics

The metrics used to compare the MANET routing algorithms with sub-6GHz band and the ones with mmWave are listed below:

- Number of Delivered Packets: total number of delivered packets to all destinations per each simulation second.
- Packet Delivery Ratio (PDR): Which is defined as the number of packets received divided by the number of packets sent each second.

$$PDR = \frac{Packets_{received}}{Packets_{sent}} \quad (4.7)$$

- Average Delivery Ratio: Which is the mean of all the Packet Delivery Rates for the entire network operation lifetime.

4.1.2 mmWave Frequencies in the NS3 Simulator

The well known network simulator (NS3) has been used for simulating different types of networks for many years [68]. Until recently, all the simulation that was possible with this simulator was for the traditional sub-6GHz frequency bands. Few years ago, the wireless community started showing great interest in mmWave frequencies and it became obvious that it will be part of the future generations of wireless communications (as it is already now) which urged many research groups to start developing all different kinds of platforms, testbeds, simulators, and measurements to understand it better. The wireless communications research group from the New York University has developed the first open-source millimeter wave module that can be used to evaluate cross-layer and end-to-end performance of 5G mmWave networks. The simulator is built using some of the original modules from the the widely-used ns3 platform which implements a wide range of protocols in C++ [53]. The fig. 4.2 shows some features of the newly suggested simulator with the original components from the ns3:

4.1.3 Performance Evaluation

The goal of this work is to analyze the feasibility of routing protocols in mmWave MANETs, and then compare its performance with the traditional routing protocols in MANET for different network settings. In this section, we show a comparison of three of the most famous routing algorithms in the MANET networks and these are: Destination-Sequenced Distance Vector (DSDV) [64], Ad hoc On-demand Distance Vector (AODV) [20], and Optimized Link State Routing (OLSR) [18] under a typical random waypoint mobility model [26]. The newly proposed module for mmWave in (ns-3) [26] is used for simulation as it provides different channel models for mmWave that are derived from many measurement campaigns done in different places and with different environmental conditions recently. This module that was explained in [26] and [23] with more details focuses on the modeling of the customizable channel, physical and medium access control (MAC) layers of millimeter wave systems and was utilized throughout the simulation steps explained in the next sections.

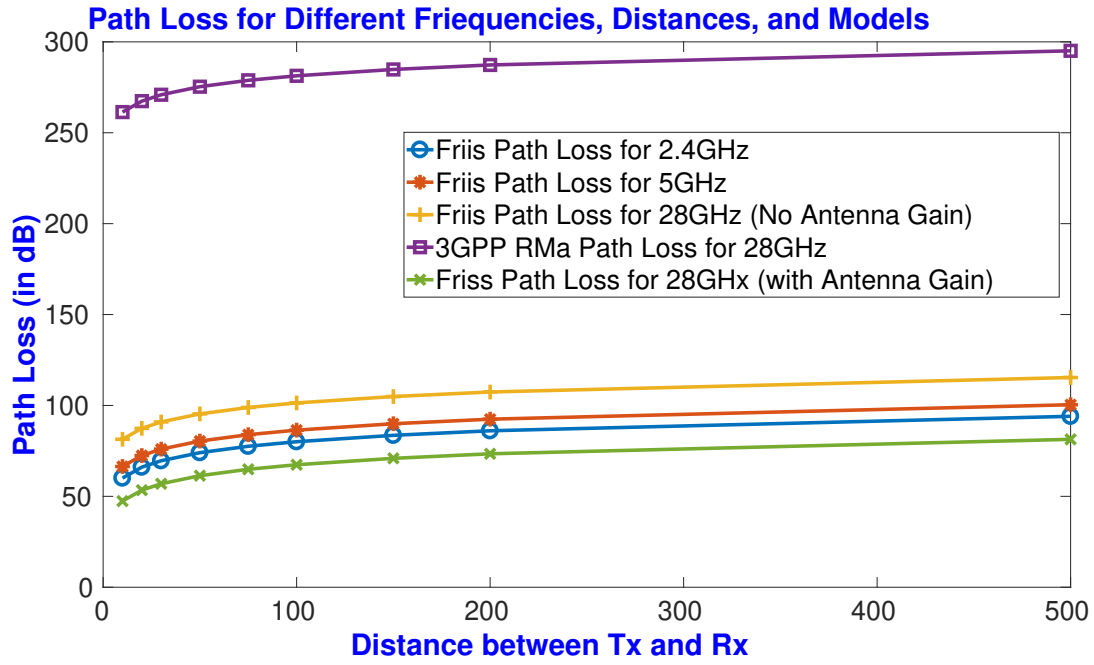


Figure 4.1: Path Loss Comparison for different Channel models and Distances

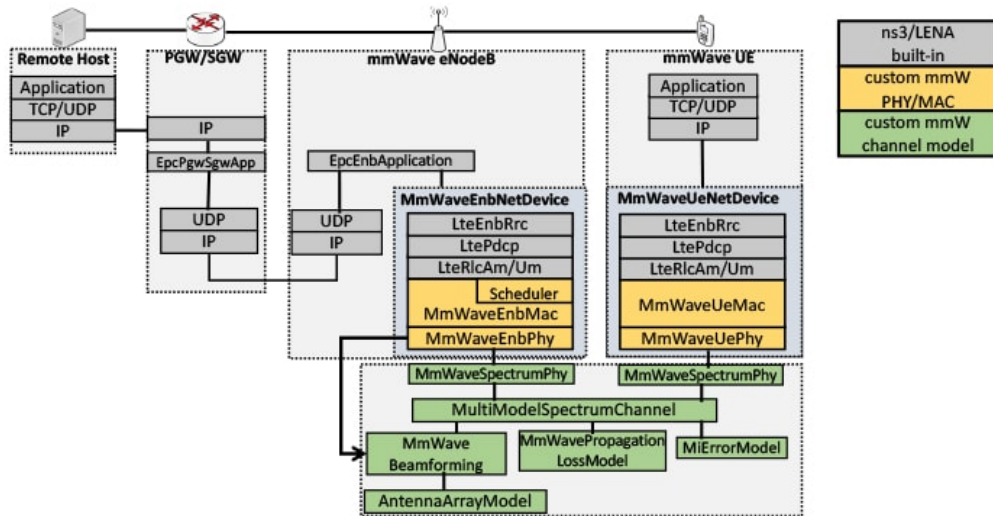


Figure 4.2: mmWave modules in the ns3 Simulator

The comparison is performed first among these protocols in the traditional Wi-Fi frequency range; then we evaluate the same algorithms' performance under different mmWave channel models for the used devices such as the Urban Macro-cells (UMa) and Rural Macro-cell (RMa) as suggested in [1]. The basic simulation scenario in the ns3 runs for 200 simulated seconds, where the first 50 seconds are used for start-up time. The number of UE nodes is 50, and the nodes are moving according to Random Way point Mobility Model with a speed of 20 m/s and no pause time within a 300x1500 m region. The Wi-Fi (which is the basic type of communications in this scenario that we intend to change to higher frequencies) is in ad-hoc mode with a 2 Mb/s rate (802.11b) and a Friis loss model (for Wi-Fi) and 3GPP propagation path loss (for mmWave). The transmit power is set to 7.5, 10, 20, and 40 dBm. In this scenario, there are 10 source/sink data pairs sending UDP data at an application rate of 2.048 and 4.96 Kb/s each. This is done at a rate of 4 64-byte and 128-byte packets per second. Application data is set to start at a random time between the 50 and 51 seconds (of the simulation time) and continues till the end of the simulation.

Details of simulation scenario parameters are listed in table 4.1:

Some performance comparisons between the traditional Wi-Fi MANET and mmWave MANET are shown in figures 4.3, 4.4, and 4.5.

Figure 4.3 shows the number of received packets each second using AODV, DSDV, and OLSR and it is clear that OLSR is better than the other protocols most of the time for the scenario mentioned above.

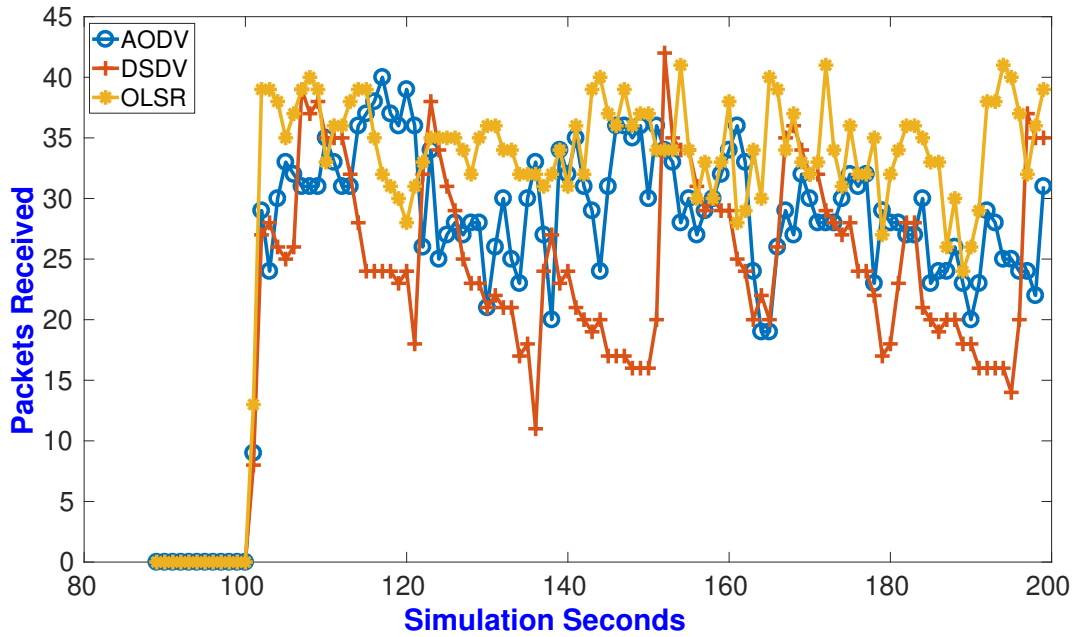
Figure 4.4, on the other hand, shows the number of received packets by the same routing protocols when using mmWave frequencies and it is clear that these protocols show more stability and better delivery ratio when used with mmWave than with the traditional sub-6GHz frequencies.

Figure 4.5 is showing a comparison of the average packet delivery ratio between different routing protocols with mmWave versus the same protocols with traditional sub-6GHz frequency bands.

The same performance comparisons that were done in figures 4.3, 4.4, and 4.5 are repeated for the mmWave MANET routing protocols under the UMa channel model in the Figures 4.6 and 4.7.

Table 4.1: Simulation Scenario Parameters

Parameters	Specifications
OS	Linux Ubuntu 16.04 LTS
Network Simulator	ns-3.27
Simulation Time	200 Seconds
Simulation Area	1500 m X 300 m
Number of Wireless Nodes	50
Speed of Mobile nodes	20 m/s
Mobility Model	Random Way Point
Data Rate	2Mbps and 4Mbps
Tx Power	7.5, 10, 20, 40 dBm
Number of Tx nodes	10
Number of RX nodes	10

**Figure 4.3:** Packets Received for Different Wi-Fi MANET Routing Protocols

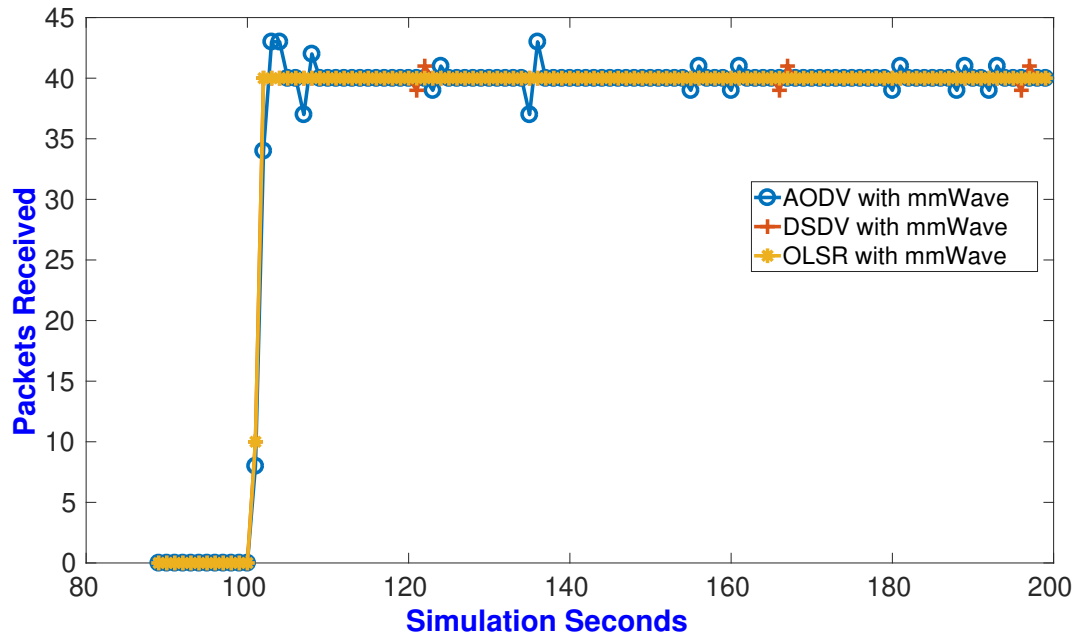


Figure 4.4: Packets Received for different mmWave MANET (with RMa Channel Model) Routing Protocols

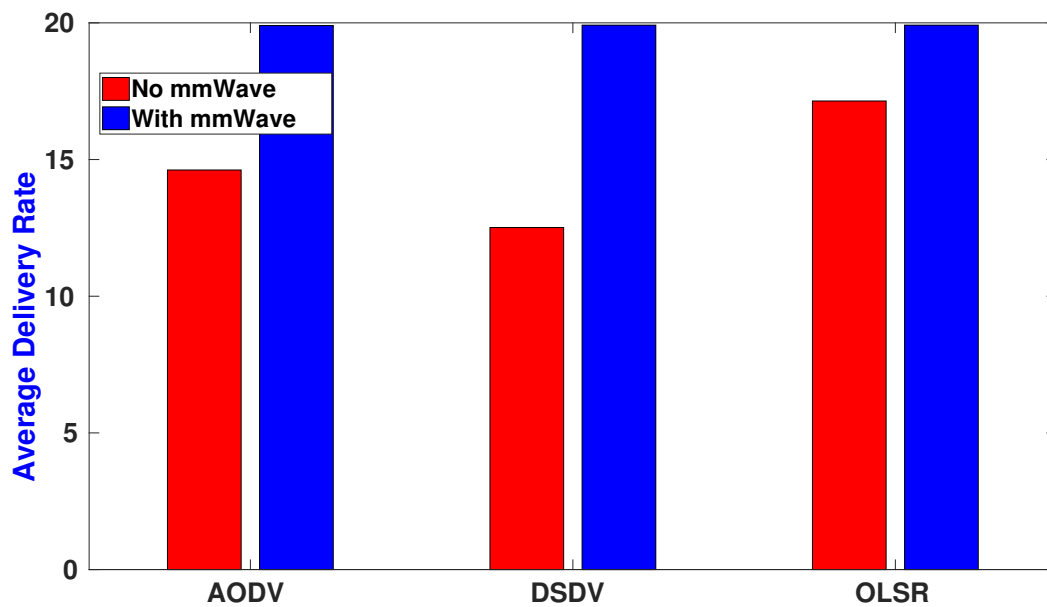


Figure 4.5: Average Delivery Ratio for both Wi-Fi MANET and mmWave MANET (with RMa Channel Model) Routing Protocols

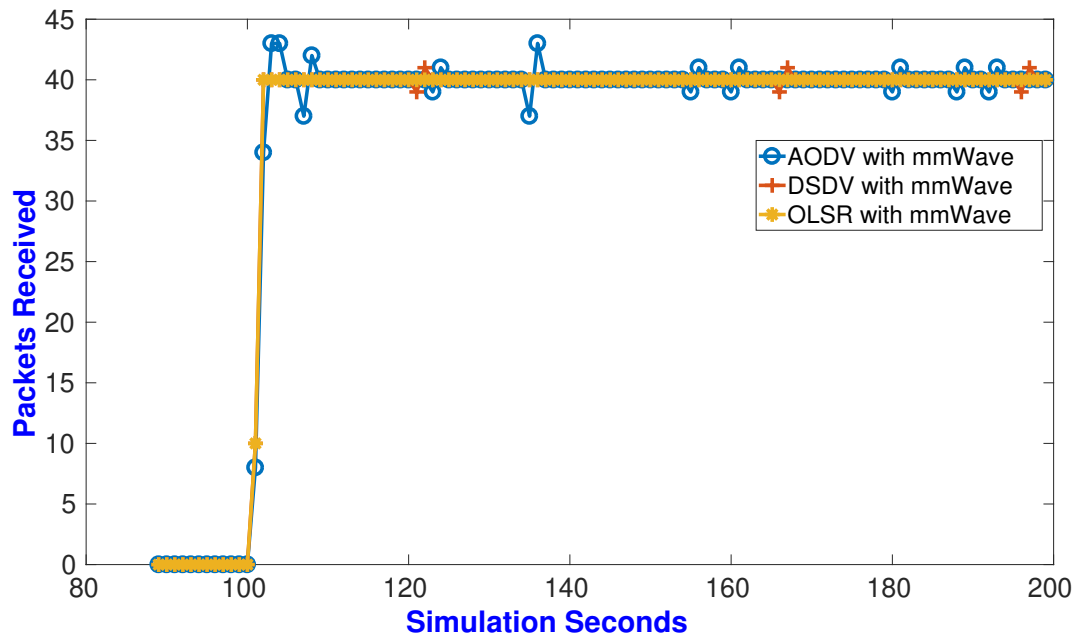


Figure 4.6: Packets Received for different mmWave MANET (with UMA Channel Model) Routing Protocols

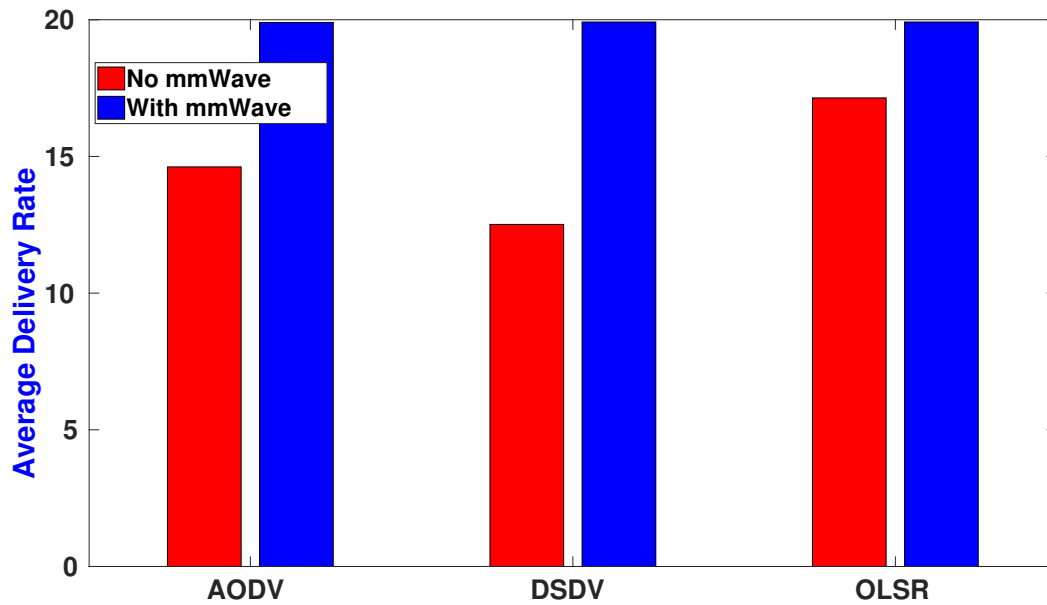


Figure 4.7: Average reception rate for different routing protocols for mmWave UMa channel

Now, we change the data rate and packet size of the messages and repeat the comparison in figures 4.8, 4.9, and 4.10 to calculate the average delivery rate of the received packets:

As can be seen, the delivery ratio and the number of delivered packets during the work of the network in the simulator are much better and more stable for the mmWaves rural and urban channels than the normal Wi-Fi channels. This shows the huge potential for the mmWave in the short-range communications as it is planned in the Ultra Dense Networks (UDN) [29]. More investigations need to be done in this field to unveil the properties and limitations of the mmWave in the MANET field. Also, besides the delivery rate and propagations loss, the effect of large bandwidth (that mmWave brings as a feature) on the network performance and battery-driven devices lifetime (especially in the disastrous regions) must be studied as well.

The final step in our investigation for the mmWave in MANET, is the effect of transmission power on the delivery ratio. It is well known that for broadcast wireless channels, increasing the power would reduce the effect of path loss because of interference and attenuation, but for the directional beams of mmWave, less power should be enough to perform the same. According to the recent FCC regulations in [40], the highest UE Effective Isotropic Radiated Power (EIRP) is 43dBm (almost 20 watts). So, we studied the effect of increasing the Tx power of the UE's on the delivery rate of the data packets for different routing protocols in ad-hoc networks and the results are shown in figure 4.11. The results are ,as expected, showing that mmWaves are doing better than traditional Wi-Fi frequencies even with less Tx power:

For the Tx power effect on the MANET routing protocols performance, we can see that increasing the power helped in increasing the delivery ratio of the Wi-Fi MANET routing protocols, whereas it did not help in the case of mmWave as the delivery ratio was almost constant, but it is still better than that of the Wi-Fi networks. This can be explained by taking in consideration that mmWave devices with the help of beamforming utilize the power better than the Wi-Fi devices and concentrate the Tx power in a narrow beam to reduce the path loss. This means that the mmWave devices can prolong the network lifetime as they provide energy efficiency and reduce the power consumption compared with the Wi-Fi devices to cover the same area and provide even better performance.

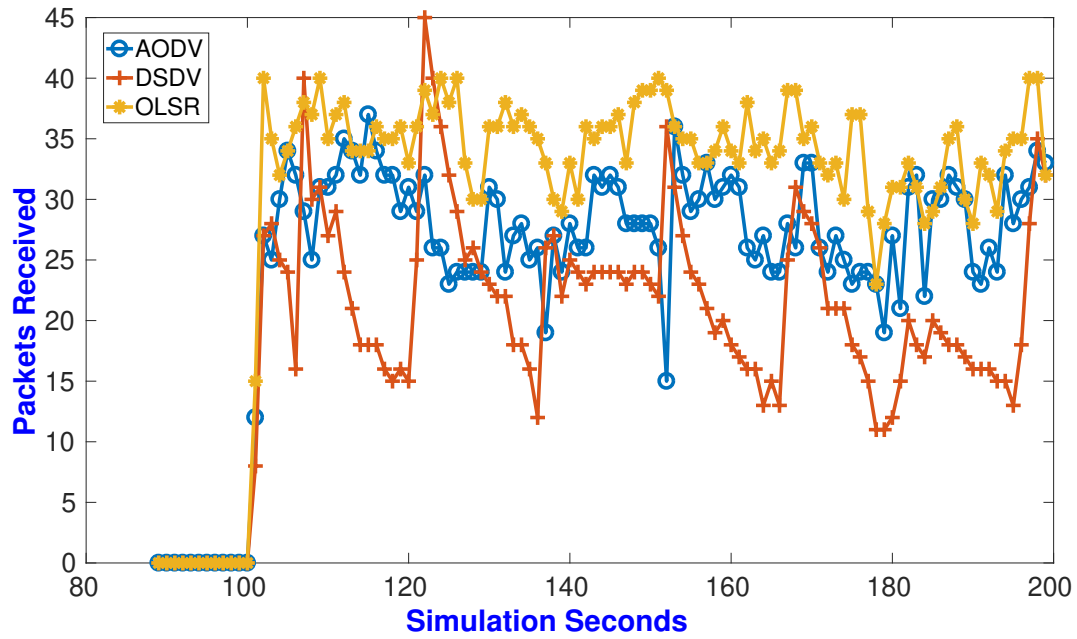


Figure 4.8: Packets Received for Different Wi-Fi MANET Routing Protocols with 4kbps transfer rate and 128 Byte packet size

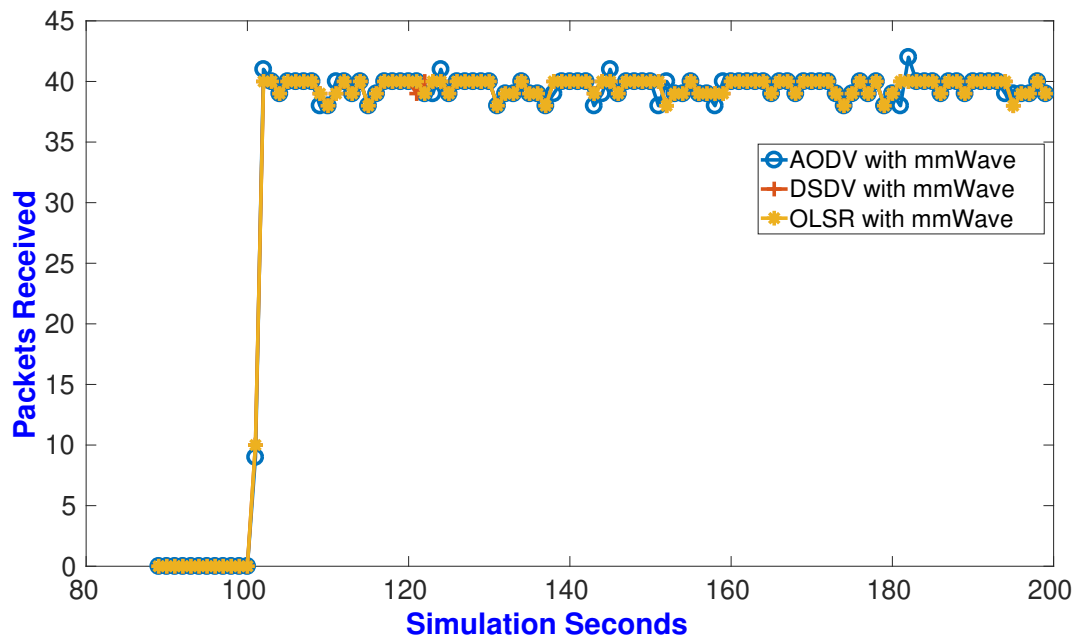


Figure 4.9: Packets Received for different mmWave MANET (with UMa Channel Model) Routing Protocols with 4kbps transfer rate and 128 Byte packet size

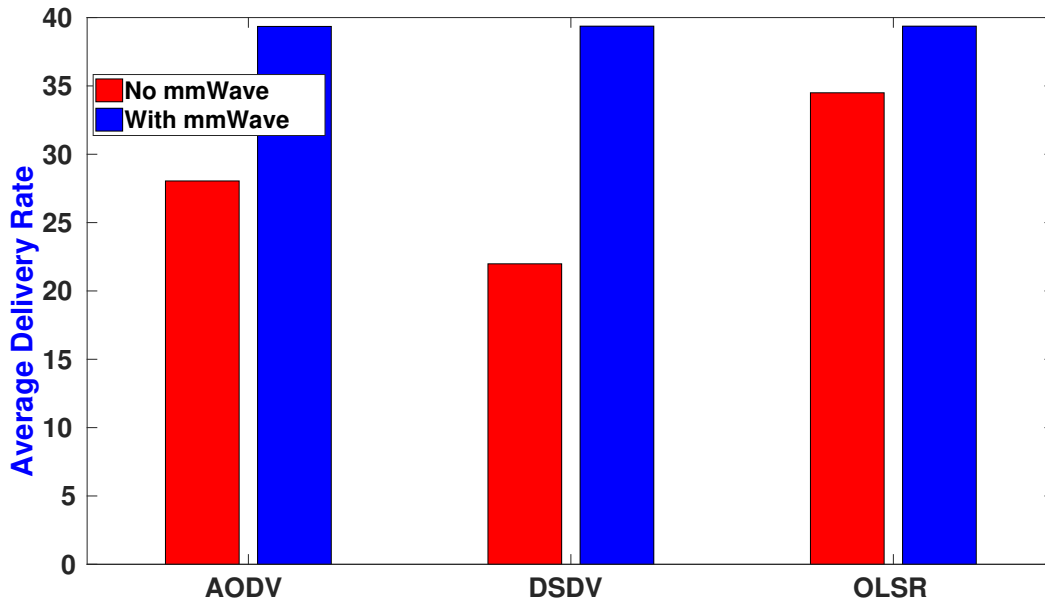


Figure 4.10: Average Delivery Ratio for both Wi-Fi MANET and mmWave MANET (with UMa Channel Model) Routing Protocols with 4kbps transfer rate and 128 Byte packet size

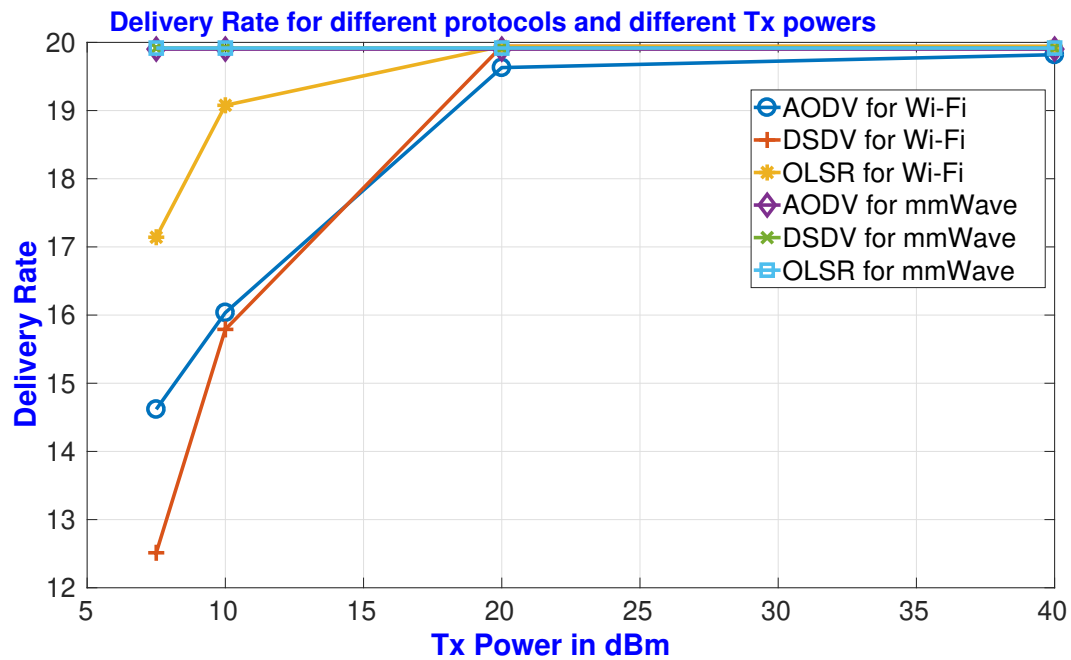


Figure 4.11: Tx Power of each UE and its Effect on the Delivery Ratio

4.2 Opportunistic Routing Protocol For Ad-Hoc Networks Using mmWave and Random Beamforming

In this section, we suggest a new routing protocol for mobile ad-hoc networks that uses mmWave by utilizing its directional antennas, limited transmission range, and the random beamforming technique. The main goal of the proposed protocol is to increase the network throughput, reduce the delay, and mitigate the effect of the interference of concurrent communicating nodes. Mathematical analysis of the network per hop achievable throughput, expected interference, and average delay per hop has been carried out. Multiple realistic simulation scenarios have been conducted to confirm the analytical results and prove the advantages of the proposed protocol.

4.2.1 Introduction

Mobile Ad-hoc Networks (MANETs) as a special type of Self-Organized Networks (SONs) have been studied for many years because of their advantages in both infrastructure and infrastructureless environments. Some of their applications include communications in battle fields, communications among disastrous relief workers, communications among wireless Virtual Reality (VR) and Augmented Reality (AR) devices, and in the congested areas like stadiums and campuses. Tradeoff between the transmission range and the throughput has always been an issue when designing routing and forwarding protocols for the traditional sub-6GHz frequency band networks. Increasing the transmission power of each node in the MANET would increase the transmission range. This will reduce the total number of hops from source to destination; however, it will increase the interference with other ongoing transmissions among other nodes. On the other hand, reducing the transmission power will reduce the transmission range and the interference with other communicating nodes, whereas it would increase the total number of hops from source to destination which incurs more delay, less energy efficiency especially for battery driven mobile nodes, and more error probability.

To solve such a problem, many routing and forwarding protocols were suggested to use directional antennas, instead of the traditional omnidirectional ones, which both increase the transmission range and reduce the interference with other communicating nodes [58, 59]. With this solution comes a new challenge, because using directional antennas means that some nodes might suffer deafness to incoming transmissions from unlucky directions. Also, selecting the optimal relay set (the set of candidate nodes to forward the data packets between the source and destination in a multi-hop network) has been a substantial challenge, as it depends on many factors such as the network node density, antenna beam width, randomness in the Signal to Interference plus Noise Ratio (SINR), the Channel State Information (CSI), and many other factors.

Directional antennas have been suggested for data routing and forwarding in MANET since early 2000s in the work of [58] and in the Directional Medium Access Control (D-MAC) in [59], in order to provide a good combination of less interference and more transmission range. Since then, many researches have been done to explore the potential of directional antennas in the mobile ad hoc networks and wireless sensor networks (WSN) [34]. Most of the work (until recently) was focused on traditional sub-6 GHz frequency band and was not on the mmWave band. Some recent works started to study mmWave in MANET such as the work in [15] where they took advantage of the directional antennas to suggest some routing and distributed directional medium access control (DDMAC) protocols for mobile ad hoc networks. More recent works on the mmWave performance and the maximum achievable throughput in the ad hoc networks have been done in [79], where they use stochastic geometry to derive the throughput for one way and two way communications.

In this section, a promising beamforming technique named Random Beamforming (RBF) [49], which is opportunistic in nature, is utilized as the way to select the relay nodes in a new opportunistic routing protocol for mobile ad hoc networks that are working with mmWave frequencies and using directional antennas. Such an opportunistic protocol is capable of solving the problems of selecting the best relay nodes of data from the source to the destination, while reducing the interference with other ongoing transmissions and the end to end delay incurred in the transmission. The performance of the suggested protocol

is derived mathematically and proved with different simulation tools and realistic MANET scenarios.

4.2.2 System Model

We consider random multi-hop wireless networks that consist of user equipments (UEs) that use mmWave frequency band (28GHz in our case). The nodes are uniformly and randomly distributed and moving according to a certain mobility model (Random Way Point (RWP) for example [14]). In this model of mobility the movement of each node is done as follows: Each node begins by pausing for a fixed number of seconds. The node then selects a random destination in the simulation area and a random speed between 0 and some defined maximum speed. The node moves to this destination and again pauses for a fixed period before another random location and speed. This behaviour is repeated for the length of the simulation [14]. Each node is assumed to be aware of its location and the location of the packet destination. Random beamforming is used for selecting the relays for the multi-hop data forwarding. Many beamforming and beamsteering techniques have been suggested for mmWave communications due to their highly directional transmissions, where the BS needs to precisely align its beam to the receiving UE as in [49]. One approach that we use here, coined random beamforming [49] is modified and summarized as follows: any node in the network with data to send tries to form random beams assuming that there are many nearby UEs; the beam will be pointed to a UE with a large probability; then the beamforming node will receive an acknowledgment from the UE and transmit to this direction. Such a random beamforming approach avoids the overhead of location estimation. The details of the modified algorithm of random beamforming is given in Algorithm 3.

Algorithm 3 Single Round of RBF for mmWave Systems

- 1: The Tx UE constructs S random orthonormal beam vectors $\{u_1, \dots, u_S\}$.
 - 2: The Tx UE chooses a normalized direction θ of the intended destination and transmits the beam x to it.
 - 3: **for** Other UEs receiving $\text{SNR} \geq \text{predefined threshold}$ **do**
 - 4: The Tx UE receives the feedback from these UEs
 - 5: The Tx UE sends data packets with the beamforming vector x to the UE that reported the maximum received signal power.
-

With the use of random beamforming, we can make sure that exactly one intermediate node will always be selected to forward the data. Other nodes within the beam area will receive the data packets, and discover that it is destined for other nodes (the one with the largest SINR in the beam area). They will discard the data packets, back-off for a specific time, and send no further data packets in that beam during the back-off time. This will eliminate the contention for acting as the relay nodes. For a normal static MIMO system [73], the network is assumed to have n user equipments (UEs) as receivers of each random beam. Each UE is equipped with N antennas and the system is assumed to satisfy a block fading channel model (i.e, the propagation matrix is constant during the coherence time T). Mathematically, the system is characterized by:

$$\mathbf{y}_i(t) = \sqrt{\rho_i} \mathbf{H}_i \mathbf{s}(t) + \mathbf{w}_i(t) \quad i = 1, \dots, n, \quad (4.8)$$

where $\mathbf{s}(t)$ is the N -vector of transmitted signal, $\mathbf{y}_i(t)$ is the N -vector of received signal by receiving UEs after each beamforming i , \mathbf{H}_i is the $N \times N$ channel matrix, \mathbf{w}_i is the N -vector of additive noise, and ρ_i is the signal-to-noise ratio (SNR) of the i -th user (averaged over the randomness of channel).

We assume that the path loss of the mmWave signal is the one-parameter close-in (CI) model described in [77]. This path loss can be described as:

$$\mathbf{PL}^{CI}(f, d)[dB] = \mathbf{FSPL}(\mathbf{f}, \mathbf{1m})[dB] + 10n \log_{10}(d) + \mathbf{X}_{\sigma}^{CI}. \quad (4.9)$$

where n denotes the single model parameter, the path loss exponent (PLE), with $10n$ describing path loss in dB in terms of decades of distances beginning at $1m$, d is the separation distance between the transmitter and receiver nodes, and $FSPL(f, 1m)$ denotes the free space path loss in dB at the transmitter-receiver separation distance of $1m$ at the carrier frequency f . Also, free space path loss (FSPL) can be described as:

$$\mathbf{FSPL}(\mathbf{f}, \mathbf{1m})[dB] = 20 \log_{10}\left(\frac{4\pi f}{c}\right). \quad (4.10)$$

where c is the speed of light.

4.2.3 Opportunistic Routing in MANET Using mmWave

After the initial deployment of the nodes in an ad-hoc network, some nodes will have data to send. Nodes are assumed to have knowledge of their position and the position (coordinates) of the destination nodes. Also, each node should be able to perform random beamforming with different (adjustable) beamwidths (open angles). Random Beamforming originally is an opportunistic technique, that we utilize here as the way of selecting relay nodes in a multihop ad hoc network. The resulting routing protocol is opportunistic as well, as it depends on the Random Beamforming in finding the best relay node along the multihop path from source to destination. Practically, it is not possible to control the node density in the network, and as we already assumed an adjustable beamwidth, we can see the tradeoffs between the beam width and node density as follows.

Let ρ denotes the UE density per unit area (ex. UE/m^2), and θ is the beam angle. We need to set the beam angle, such that the probability of always having nodes in the beam coverage area is maximized, and meanwhile it reduces the number of participating UEs in each random beamforming process to the minimum. To do so, we need to assume some realistic expectations of node density and try to figure out the best beam angle to achieve the goals above. 5G networks are supposed to serve as much as 10^6 UE per km^2 or up to one UE/m^2 . Depending on the applications and scenarios, having such a huge density in an ad-hoc network is rare. So, we will assume some node densities less than that and see what is the best beam angle for each density.

Ultra-Dense Networks (UDN) consist of mmWave devices are suggested to work well within $200m$ or less transmission range [29], and we assume that this is the typical transmission range of each UE in our network. Now, to calculate the area of each beam, we use the following equation:

$$BeamArea = \frac{d^2}{2} \left(\frac{\pi}{180} (\theta - \sin(\theta)) \right) \quad (4.11)$$

where d is the transmission range of each UE using mmWave, and θ is the beam angle (beam width). Fig. 4.12 shows the relationship between beam angle and expected number of nodes per beam.

From Fig. 4.12, it is safe to say that we can start with small beam angle (beamwidth) to perform the random beamforming to select the relay node (with the highest SINR). Then we can increase the angle in the unusual case of having no UEs in the beam range, or the existing UEs are too far such that the SINR is less than a pre-defined threshold. The network is assumed to be a dense network with many cooperative users that are willing to participate in any data forwarding process anytime they are selected as relays (using the RBF). So, our opportunistic routing protocol can be described in terms of sender algorithm 4 and the receiver behavior after that:

Algorithm 4 Sender Node Algorithm

```

1: Begin:
2: A node has a data packet for transmission;
3: Perform random beamforming in the direction of the destination with small angle (ex.
   between 1-10 degrees).
4: if Receive feedback from nodes in that direction then
5:   if More than one node with received SINR  $\geq$  threshold then
6:     Choose the one with the largest SINR and send data to it
7:     Go to End
8:   else if One node with received SINR  $\geq$  threshold then
9:     Send data to it
10:    Go to End
11:  else
12:    Increase Beam Angle and go to line-3
13: else
14:   Increase Beam Angle and go to line-3
15: End

```

The other nodes in the network that have no data to sent will be listening all the time using omnidirectional antennas. When receiving pilot data (the beamforming message) from specific directions, they calculate the received SINR and send back the calculated SINR, as well as the beam index, to the sending nodes. Once a node is selected as a relay (or the final destination), the node will receive the data packets and decide what to do with it depending on its location in the network. If packets are destined to them, then they will consume it. Otherwise, they will keep forwarding it to the final destination using the location information of themselves and the ones in the packet header about the destination location. Meanwhile, the mobile nodes would always change their locations, Previous work in [58, 15, 34] assumed

no or low mobility. Although some studies have been done on the mobility effect on the system performance [8], We will assume the same about mobility for fair comparison with these protocols in [58, 15, 34]. Eventhough, mobility of the devices participating in the suggested routing protocol only have a limited effect on the overall expected performance as it was proved in [8]. Finally, one can ask about how the mmWave devices power consumption is compared to that of the devices using traditional sub-6GHz bands, and the answer to this question has been reported in [6].

4.2.4 Performance Evaluation

To the best of our knowledge, the proposed protocol is the the first opportunistic routing protocol that uses mmWave with the goal of maximizing end to end throughput, minimizing the delay, and mitigating the interference effect on the overall system performance. So, to evaluate its performance, we compared its per hop performance with some well known previously developed protocols using the list of parameters in the Table 4.2. The same comparison of performance can be generalized for the end to end performance evaluation.

Using the Random Beamforming (RBF) for selecting the relay nodes promises to reduce the interference from other transmitting nodes because RBF is only using one relay and a backoff timer to prevent other nodes from transmitting during the current transmission. Also, better acheivable per hop throughput is realized because of the one relay node selection. Finally, the expected overall delay (per hop per packet) is reduced in our protocol due to the simpler MAC scheme we use. The performance of our suggested protocol is evaluated based on the expected interference, achievable throughput, and the delay of delivering data packets per hop and from end to end as in the following sections:

4.2.5 Interference Analysis

Assuming that at any time of the network operation, we have a total of n UEs with node density ρ (UE/m^2), the beam area as described in Eq (4.11), each node transmits with a probability (α); then the number of transmitting nodes in the beam is given by $\rho\alpha \times BeamArea$. Our contention prevention scheme assures that, whenever a node is selected as

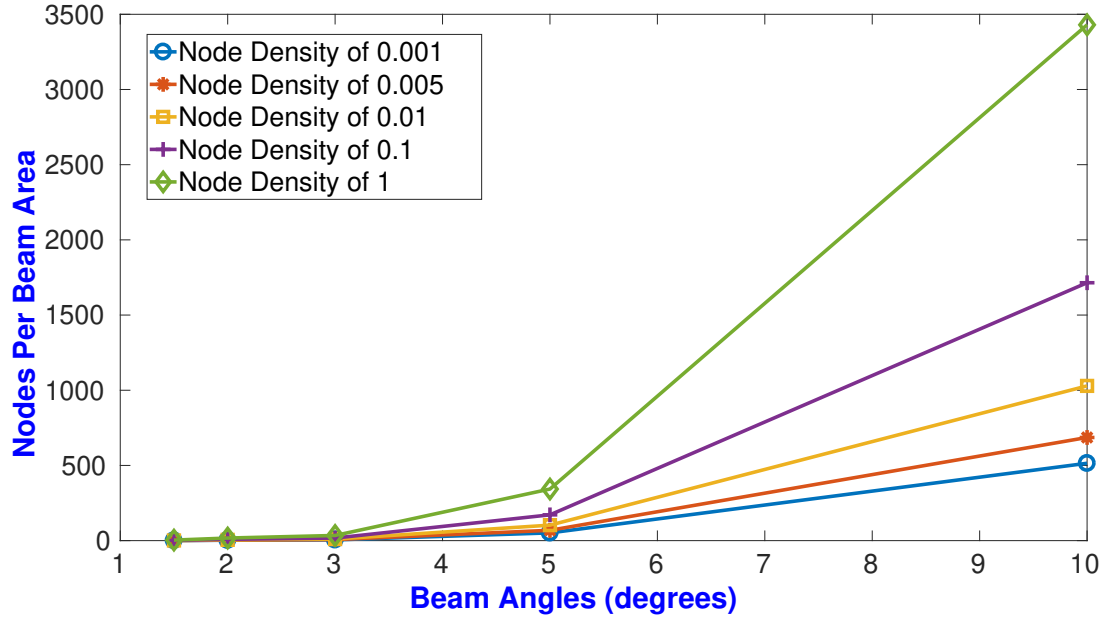


Figure 4.12: Expected number of nodes per beam for different beam angles and node densities

Table 4.2: Performance Evaluation Parameters

Parameter	Value
Beam Angle	1-180 degrees
Transmission Range	200 meters
Node Density	0.001-1 $nodes/m^2$
Bandwidth (W)	1000 MHz
Transmission Power	1 Watt
Noise (N_0)	-117 dB
G_o	20 dB
A	40.4 dB
α	2.17
h_0	Gamma
Transceiver Efficiency η	0.09842
T_{Ack}	3.709μ second
T_{DCTS}	4μ second
T_{DIFS}	34μ second
T_{DRTS}	4.5366μ second
T_{SIFS}	2.5μ second
$T_{processing}$	10μ second
Max Buffer size	50 Packets

a relay, other nodes that lost in the competition will *backoff* for a specific time (proportional to the propagation time of the packet and the expected hop distance), see Eq (4.12):

$$backoffTime = \frac{AvgD}{c} + PD \quad (4.12)$$

Where, *BackoffTime* is the time the lost nodes will refrain transmitting or receiving any packets. *AvgD* is the expected per hop distance (will be derived shortly). *c* is the speed of light. And *PD* is the packet duration which is fixed for any network type and application.

Using such strategy would prevent the collision among the transmitting nodes in the beam to a large extent and eliminate the need for clock synchronization among the nodes in the network. But, interference is still possible in the following situations:

- Other nodes outside the beam want to send data to nodes within the beam during the current transmission, see Fig. 4.13.
- Other nodes within the beam want to transmit at the same time as transmitters or relays.
- The backoff time is not sufficient because of a large packet, the need for retransmission or any other reason.

In all of these cases, interference may still occur with the following probability:

$$P(Interference) = (P_1 + P_2)P_3, \quad (4.13)$$

where P_1 is the probability of a node outside the beam wanting to send a packet to a node inside the beam during the current transmission, P_2 is the probability of concurrent transmission of other node within the beam during the current transmission, and P_3 is the probability that the backoff timer is not enough.

Obviously P_1 can be expressed as follows:

$$P_1 = P(dist(Rx1, Rx2) \leq BeamBase) \quad (4.14)$$

where $P(dist(Rx1, Rx2) \leq BeamBase)$ is the probability of another node outside the beam sending to a node within the beam during the current transmission, $Rx1$ is the destination node for the current transmission, $Rx2$ is the destination for the outsider node that is within the beam area, and $BeamBase$ is the length of the beam base arc. P_2 can be expressed as:

$$P_2 = (\rho\alpha \times BeamArea) \quad (4.15)$$

as explained earlier. Finally both P_1 and P_2 are only affecting the current transmission if the backoff time (P_3) is not enough. It is obvious that P_3 is proportional to the transmission distance per hop, namely $P_3 \propto \text{hop distance}$ or $P_3 = constant * HopDistance$, because the farther the receiving node, the more probable that the transmission will fail and needs retransmission, or the more probable it will take longer time than the (backoff) time.

This interference can be minimized by minimizing the beamwidth, such that there will be as few nodes in each beam as possible which would minimize the contention for transmission and the interference with other transmissions happening at the same time. The other strategy to minimize interference is to force the node working at the current time slice as a transmitter or an intermediate relay to ignore any incoming pilot from other UE to compete for being relay to other transmissions while having data to send or acting like a relay, which means that it will not compete with other nodes in vicinity for other transmissions than the one it is involved in during the current time slot.

4.2.6 Expected Per-Hop Throughput

To calculate the per-hop throughput we assume that the transmission range of each node is $r(\theta)$, and the transmission power of all nodes is the same (to simplify calculations). Knowing the transmission range of each node and the assumption of dense ad-hoc network allows us to calculate the average distance per each hop as following [82]:

$$AvgD = \frac{2r(\theta)}{3} \quad (4.16)$$

Knowing the average distance between any two nodes in the network (which is also the expected hop distance), the transmission power of each UE, the transmission and reception

antenna gains (range between 14-17 dB for UEs in the 5G networks as suggested in [40]), and the path loss of mmWaves, we can calculate the expected throughput per hop as follows [79]:

$$Throughput_{per-hop} = \eta W \log_2 \left(1 + \frac{P_t G_0 h_0 A Avg D^{-\alpha}}{N + I} \right) \quad (4.17)$$

where W is the signal bandwidth, η is the transceiver efficiency constant, P_t is the transmitted power by each UE, G_0 is the antenna gain corresponding to both main beams aligned, h_0 is the fading power at the main beam, A is the path loss intercept, $Avg D$ is the average hop distance, α is the path loss exponent, and N is the noise power. I is the Interference power with the expected probability (the cross correlation) analysed in the previous section and calculated as in [15].

Fig. 4.14 shows the comparison of the achievable throughput per hop (in Mbps) for different hop distances and different conditions. It is shown by extensive simulation that the theoretical throughput (without taking the interference effects in consideration) is comparable to that for indoor or Urban Microcells (UMi) environments because of the benefits of using directional antennas and the mmWave frequencies. The derived interference expression (from the previous section) is also showing the same trend as the other previously reported results. It is clear that increasing the transmission distance (per hop) means reducing the maximum achievable throughput because of the severe path loss of mmWave which again can be utilized in dense networks to reduce interference with other concurrent transmissions. Also, the achievable throughput of our protocol is shown to be comparable to that is achieved with no interference taken in consideration.

4.2.7 Average Delay Per Hop

Beside the propagation delay of packets between each transmitter and receiver nodes, our protocol has other delay source that is resulted from the random beamforming process for each transmission. So, the total delay per hop would be:

$$T = T_{beamforming} + T_{data}. \quad (4.18)$$

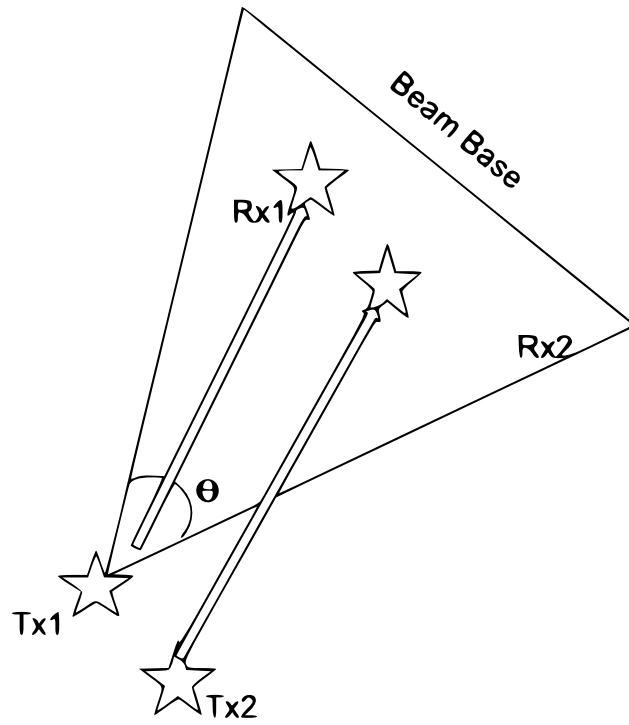


Figure 4.13: An illustration of possible Interference

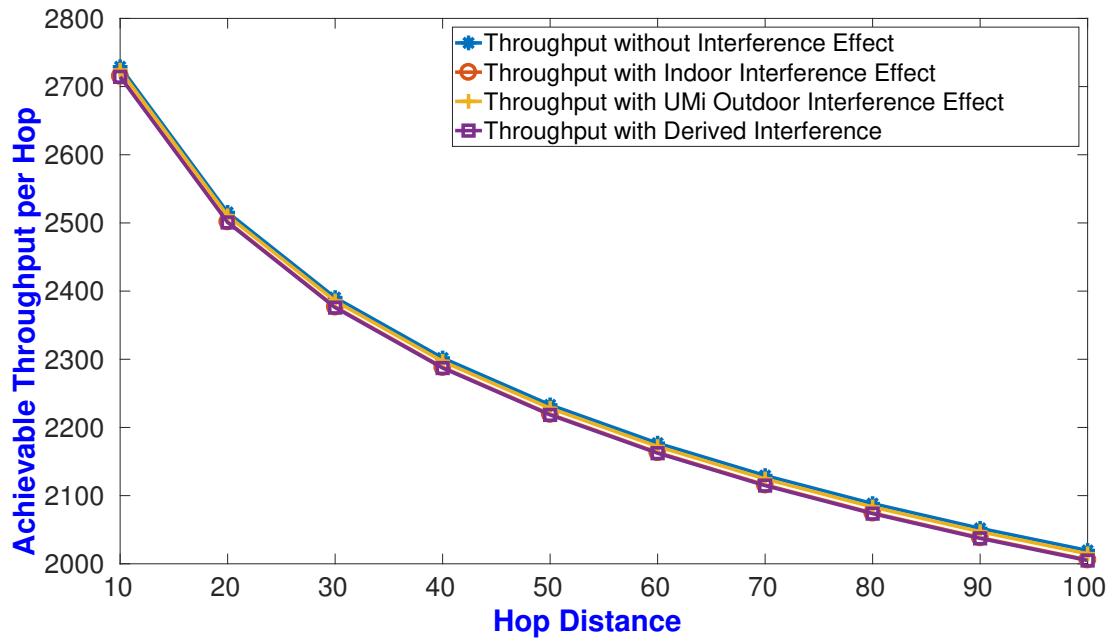


Figure 4.14: Achievable Throughput per Hop (in Mbps) for Different Hop Distances

where $T_{beamforming}$ is the time duration of the beamforming process, and T_{data} is the time spent sending the data (frame duration). It is clear that this delay is less than that produced by the protocols in [15, 34]. In [15], the delay includes the time to transmit the packet and the overhead of the Directional MAC (D-MAC) and that includes the time to transmit the Directional Ready To Send (DRTS), Directional Clear To Send (DCTS), the Acknowledgement (ACK), three Short Inter-Frame Space (SIFS), and one Distributed Coordination Function Inter-Frame Space (DIFS) [15]. On the other hand, the delay involved in each packet transmission in [34] includes the time to transmit the packet and the protocol timer that need to be expired before any node can send any packet [34]. Average delay per each hop of our suggested protocol compared to those expected from [15, 34] is shown in the Fig. 4.15 for different hop distances:

4.2.8 End to End Performance

To expand our performance analysis beyond single hop, we performed the following simulation scenarios:

- First, we deployed the network with different numbers of nodes and dimensions of the area (50 nodes in a 500 m X 500 m, 100 nodes in 1000m X 1000m, and 1000 nodes in 1000X1000m area) with random locations for the nodes each time.
- Then after specifying the number of nodes, the area dimensions, and the transmission range of each node, we select transmitter and receiver nodes arbitrary.
- Then we calculate the path between the Tx and Rx nodes based on our suggested algorithm.
- Using the derived equations and the simulation parameters mentioned in the Table 4.2, we calculate the end to end delay and throughput for each scenario.

By assuming that the end to end throughput can not be more than the achievable throughput per the longest hop, we got the results shown in 4.16 and 4.17:

And we can see that the expected end to end throughput and delay is better than those achieved in the perviously suggested protocols as they take advantage of the random

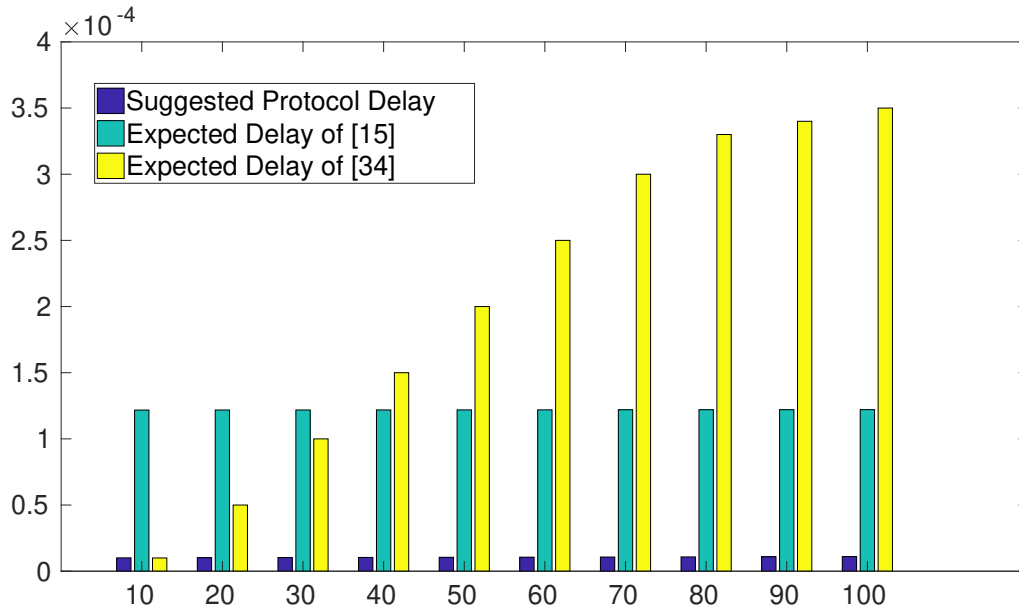


Figure 4.15: Average Delay (in seconds) per Hop for Different Hop distances (in meters)

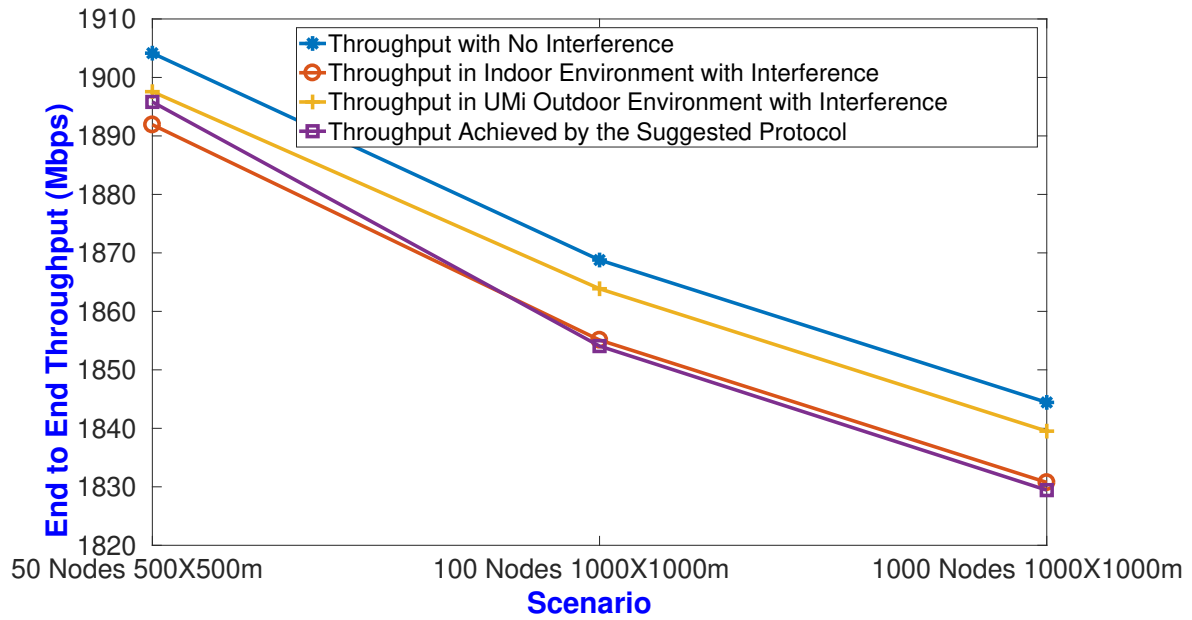


Figure 4.16: End to End Throughput (in Mbps) for Different Simulation Scenarios

beamforming opportunistic nature, the huge available bandwidth for mmWave frequencies (several GHz), and the narrow beams with less interference and competition among transmitting and relay nodes.

4.2.9 Conclusions

In the first part of this chapter, we studied the feasibility of some well-known routing protocols for mobile ad-hoc networks with mmWave frequency bands and showed how utilizing mmWave frequencies can increase the network efficiency and delivery ratio. Several parameters of the network have been adjusted and in each case the MANET with mmWave was shown to be better than the Wi-Fi counterpart. Simulation using mmWave module of the ns-3 simulator was used to confirm the results. Further investigation of the utilization of mmWave frequencies in different types of Self-Organized Networks (SON) by utilizing the unique features the mmWave frequencies offer for such networks is part of our future work.

In the second part of this chapter, a new opportunistic routing protocol for mobile ad hoc networks that uses mmWave has been proposed. Mathematical performance analysis and extensive simulation have been conducted and proved the feasibility and superiority of the proposed protocol compared with other routing protocols in terms of interference mitigation, achievable throughput improvement, and the average delay reduction. The same protocol can be generalized for many applications like routing information among backhaul links, and vehicular networks that uses mmWave frequencies. The investigation of such generalization for different environments and working scenarios can be an interesting direction for future work.

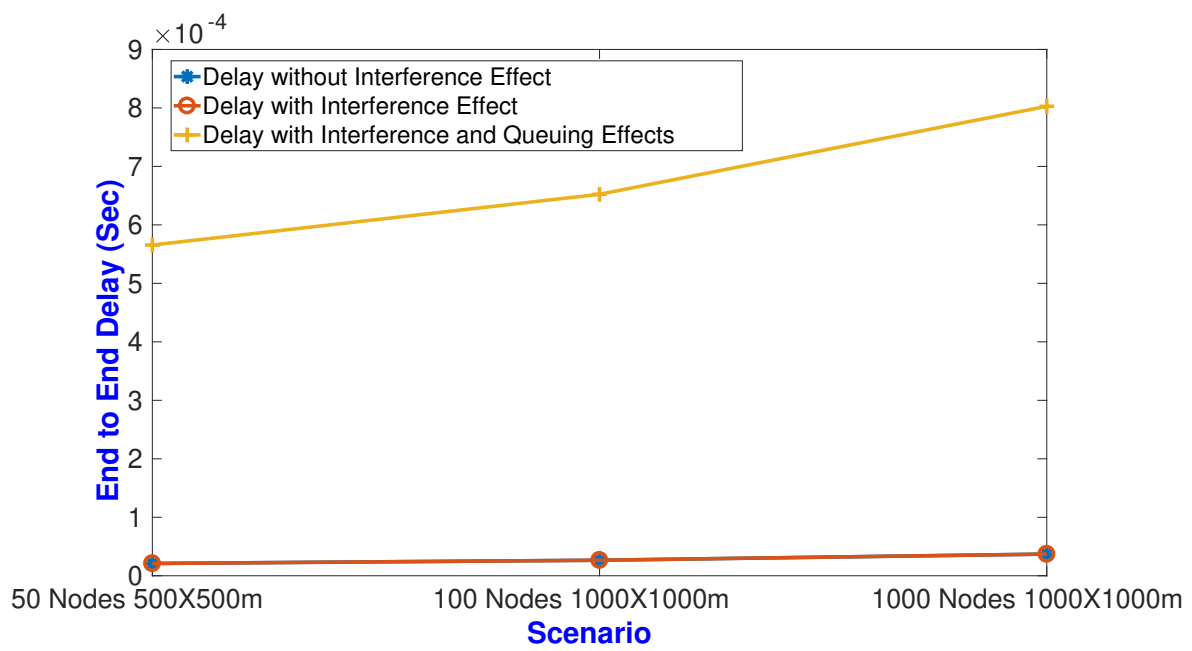


Figure 4.17: End to End Delay (in seconds) for Different Simulation Scenarios

Bibliography

- [1] 3gpp (2017). Tr 38.900, study on channel model for frequency spectrum above 6 ghz, v14.2.0. Technical report. [1](#), [3](#), [78](#), [80](#), [84](#)
- [2] Abbasbandy, S., Ezzati, R., and Jafarian, A. (2006). Lu decomposition method for solving fuzzy system of linear equations. *Applied Mathematics and Computation*, 172(1):633–643. [17](#)
- [3] Abins, A. A. and Duraipandian, N. (2015). Survey on opportunistic routing protocols in wireless networks. *American-Eurasian Journal of Scientific Research*, 10(3):148–153. [11](#), [77](#)
- [4] Ahmed, H. A., Salah, H., Robert, J., and Heuberger, A. (2016). Time aware closed form frame slotted aloha frame length optimization. In *2016 IEEE Wireless Communications and Networking Conference*, pages 1–5. IEEE. [8](#), [9](#)
- [5] Aljumaily, M. and Li, H. (2019a). A framework to optimize the frame duration and the beam angle for random beamforming of mmwave mobile networks. In *Proceedings of the International Conference on Information and Communication Technology*, pages 1–6. ACM. [2](#), [8](#), [48](#)
- [6] Aljumaily, M. S. (2018). Routing protocols performance in mobile ad-hoc networks using millimeter wave. *arXiv preprint arXiv:1808.03168*. [2](#), [76](#), [97](#)
- [7] Aljumaily, M. S. (2019). Hybrid beamforming in massive-mimo mmwave systems using lu decomposition. In *2019 IEEE 90th Vehicular Technology Conference (VTC2019-Fall)*, pages 1–5. IEEE. [1](#), [13](#)
- [8] Aljumaily, M. S. and Li, H. (2018). Throughput degradation due to mobility in millimeter wave communication systems using random beamforming. In *2018 IEEE 88th Vehicular Technology Conference (VTC-Fall)*, pages 1–5. IEEE. [2](#), [8](#), [9](#), [48](#), [61](#), [70](#), [75](#), [97](#)
- [9] Aljumaily, M. S. and Li, H. (2019b). Machine learning aided hybrid beamforming in massive-mimo millimeter wave systems. In *2019 IEEE International Symposium on Dynamic Spectrum Access Networks (DySPAN)*, pages 1–6. IEEE. [1](#), [24](#)

- [10] Aljumaily, M. S. and Li, H. (2019c). Opportunistic routing protocol for ad-hoc networks using mmwave and random beamforming. In *2019 IEEE 90th Vehicular Technology Conference (VTC2019-Fall)*, pages 1–6. IEEE. [2](#), [12](#), [76](#)
- [11] Alkhateeb, A. (2019). Deepmimo: A generic deep learning dataset for millimeter wave and massive mimo applications. *arXiv preprint arXiv:1902.06435*. [1](#), [24](#), [25](#), [32](#), [33](#)
- [12] Alkhateeb, A., Alex, S., Varkey, P., Li, Y., Qu, Q., and Tujkovic, D. (2018). Deep learning coordinated beamforming for highly-mobile millimeter wave systems. *IEEE Access*, 6:37328–37348. [1](#), [24](#), [25](#), [27](#), [31](#), [32](#), [33](#)
- [13] Andrenko, S., Provalov, S., and Sidorenko, Y. (2004). Multibeam millimeter wave antenna. In *The Fifth International Kharkov Symposium on Physics and Engineering of Microwaves, Millimeter, and Submillimeter Waves (IEEE Cat. No. 04EX828)*, volume 2, pages 677–679. IEEE. [75](#)
- [14] Bettstetter, C., Resta, G., and Santi, P. (2003). The node distribution of the random waypoint mobility model for wireless ad hoc networks. *IEEE Transactions on mobile computing*, 2(3):257–269. [93](#)
- [15] Cai, L. X., Hwang, H., Shen, X., Mark, J. W., and Cai, L. (2009). Optimizing geographic routing for millimeter-wave wireless networks with directional antenna. In *2009 Sixth International Conference on Broadband Communications, Networks, and Systems*, pages 1–8. IEEE. [12](#), [92](#), [96](#), [97](#), [101](#), [103](#)
- [16] Cawley, G. C. and Talbot, N. L. (2007). Preventing over-fitting during model selection via bayesian regularisation of the hyper-parameters. *Journal of Machine Learning Research*, 8(Apr):841–861. [27](#)
- [17] Çivicioğlu, P., Alçı, M., and Bedok, E. (2004). Using an exact radial basis function artificial neural network for impulsive noise suppression from highly distorted image databases. In *International Conference on Advances in Information Systems*, pages 383–391. Springer. [27](#)

- [18] Clausen, T., Jacquet, P., Adjih, C., Laouiti, A., Minet, P., Muhlethaler, P., Qayyum, A., and Viennot, L. (2003). Optimized link state routing protocol (olsr). [11](#), [77](#), [78](#), [82](#)
- [19] Corless, R. M. and Jeffrey, D. J. (1997). The turing factorization of a rectangular matrix. *ACM SIGSAM Bulletin*, 31(3):20–30. [17](#)
- [20] Das, S. R., Belding-Royer, E. M., and Perkins, C. E. (2003). Ad hoc on-demand distance vector (aodv) routing. [11](#), [77](#), [78](#), [82](#)
- [21] Day, K., Touzene, A., Arafeh, B., and Alzeidi, N. (2011). Parallel routing in mobile ad-hoc networks. *arXiv preprint arXiv:1110.1563*. [11](#)
- [22] Dua, A., Kumar, N., and Bawa, S. (2015). Qos-aware data dissemination for dense urban regions in vehicular ad hoc networks. *Mobile Networks and Applications*, 20(6):773–780. [10](#)
- [23] Dutta, S., Zhang, M., Mezzavilla, M., Akdeniz, M. R., and Rangan, S. (2015). Millimeter wave module for ns-3 network simulator. [82](#)
- [24] El Ayach, O., Rajagopal, S., Abu-Surra, S., Pi, Z., and Heath, R. W. (2014). Spatially sparse precoding in millimeter wave mimo systems. *IEEE transactions on wireless communications*, 13(3):1499–1513. [3](#), [16](#), [19](#), [27](#), [30](#)
- [25] Fakhereddin, M. J., Sharif, M., and Hassibi, B. (2009). Reduced feedback and random beamforming for ofdm mimo broadcast channels. *IEEE Transactions on Communications*, 57(12):3827–3835. [5](#)
- [26] Ford, R., Zhang, M., Dutta, S., Mezzavilla, M., Rangan, S., and Zorzi, M. (2016). A framework for end-to-end evaluation of 5g mmwave cellular networks in ns-3. In *Proceedings of the Workshop on ns-3*, pages 85–92. ACM. [82](#)
- [27] Friis, H. T. (1946). A note on a simple transmission formula. *Proceedings of the IRE*, 34(5):254–256. [79](#)
- [28] Gander, W. (1980). Algorithms for the qr decomposition. *Res. Rep*, 80(02):1251–1268. [19](#)

- [29] Gao, Z., Dai, L., Mi, D., Wang, Z., Imran, M. A., and Shakir, M. Z. (2015). Mmwave massive-mimo-based wireless backhaul for the 5g ultra-dense network. *IEEE Wireless Communications*, 22(5):13–21. [30](#), [78](#), [88](#), [95](#)
- [30] Ge, X., Tu, S., Mao, G., Wang, C.-X., and Han, T. (2016). 5g ultra-dense cellular networks. *IEEE Wireless Communications*, 23(1):72–79. [8](#)
- [31] Grant, M. and Boyd, S. (2008). Graph implementations for nonsmooth convex programs. In Blondel, V., Boyd, S., and Kimura, H., editors, *Recent Advances in Learning and Control*, Lecture Notes in Control and Information Sciences, pages 95–110. Springer-Verlag Limited. http://stanford.edu/~boyd/graph_dcp.html. [25](#)
- [32] Grant, M. and Boyd, S. (2014). CVX: Matlab software for disciplined convex programming, version 2.1. <http://cvxr.com/cvx>. [25](#)
- [33] Grant, M., Boyd, S., and Ye, Y. (2008). Cvx: Matlab software for disciplined convex programming. [70](#)
- [34] Hamilton, B. R. and Ma, X. (2007). Noncooperative routing with cooperative diversity. In *2007 IEEE International Conference on Communications*, pages 4237–4242. IEEE. [92](#), [96](#), [97](#), [103](#)
- [35] Hassibi, B. and Marzetta, T. L. (2002). Multiple-antennas and isotropically random unitary inputs: The received signal density in closed form. *IEEE Transactions on Information Theory*, 48(6):1473–1484. [49](#)
- [36] Hayajna, T., Kadoch, M., and Rong, B. (2017). Ensuring reliable and stable communications in mobile ad-hoc networks. In *2017 IEEE 86th Vehicular Technology Conference (VTC-Fall)*, pages 1–6. IEEE. [11](#)
- [37] Hayajna, T. and Kadoch, M. (2017). Ensuring two routes connectivity in mobile ad hoc networks with random waypoint mobility. In *2017 IFIP/IEEE Symposium on Integrated Network and Service Management (IM)*, pages 636–639. IEEE. [11](#)
- [38] Hedrick, C. L. (1988). Routing information protocol. [78](#)

- [39] Higham, N. J. (2008). *Functions of matrices: theory and computation*, volume 104. Siam. [19](#)
- [40] Huo, Y., Dong, X., and Xu, W. (2017). 5g cellular user equipment: From theory to practical hardware design. *IEEE Access*, 5:13992–14010. [79](#), [88](#), [101](#)
- [41] Hyytiä, E. and Virtamo, J. (2007). Random waypoint mobility model in cellular networks. *Wireless Networks*, 13(2):177–188. [70](#)
- [42] Iida, N., Nishio, T., Morikura, M., Yamamoto, K., Nabetanit, T., and Aoki, T. (2015). Frame length optimization for in-band full-duplex wireless lans. In *2015 21st Asia-Pacific Conference on Communications (APCC)*, pages 354–358. IEEE. [8](#), [9](#)
- [43] Islam, M. S., Riaz, A., and Tarique, M. (2012). Performance analysis of the routing protocols for video streaming over mobile ad hoc networks. *International Journal of Computer Networks & Communications*, 4(3):133. [11](#)
- [44] Jayaprakasam, S., Ma, X., Choi, J. W., and Kim, S. (2017). Robust beam-tracking for mmwave mobile communications. *IEEE Communications Letters*, 21(12):2654–2657. [75](#)
- [45] Johnson, D. (1997). The triangular distribution as a proxy for the beta distribution in risk analysis. *Journal of the Royal Statistical Society: Series D (The Statistician)*, 46(3):387–398. [55](#)
- [46] Jwo, D.-J. and Lai, C.-C. (2007). Neural network-based gps gdop approximation and classification. *GPS Solutions*, 11(1):51–60. [27](#)
- [47] Kutty, S. and Sen, D. (2015). Beamforming for millimeter wave communications: An inclusive survey. *IEEE Communications Surveys & Tutorials*, 18(2):949–973. [2](#), [3](#)
- [48] Lee, G., Sung, Y., and Kountouris, M. (2016). On the performance of random beamforming in sparse millimeter wave channels. *IEEE Journal of Selected Topics in Signal Processing*, 10(3):560–575. [5](#), [8](#)

- [49] Lee, G., Sung, Y., and Seo, J. (2015). Randomly-directional beamforming in millimeter-wave multiuser miso downlink. *IEEE Transactions on Wireless Communications*, 15(2):1086–1100. [2](#), [5](#), [50](#), [92](#), [93](#)
- [50] MacCartney, G. R. and Rappaport, T. S. (2017). Rural macrocell path loss models for millimeter wave wireless communications. *IEEE Journal on selected areas in communications*, 35(7):1663–1677. [79](#), [80](#)
- [51] Maltsev, A., Bolotin, I., Lomayev, A., Puduev, A., and Danchenko, M. (2016). User mobility impact on millimeter-wave system performance. In *2016 10th European Conference on Antennas and Propagation (EuCAP)*, pages 1–5. IEEE. [6](#)
- [52] Maltsev, A., Puduev, A., Karls, I., Bolotin, I., Morozov, G., Weiler, R., Peter, M., and Keusgen, W. (2014). Quasi-deterministic approach to mmwave channel modeling in a non-stationary environment. In *2014 IEEE Globecom Workshops (GC Wkshps)*, pages 966–971. IEEE. [6](#)
- [53] Mezzavilla, M., Dutta, S., Zhang, M., Akdeniz, M. R., and Rangan, S. (2015). 5g mmwave module for the ns-3 network simulator. In *Proceedings of the 18th ACM International Conference on Modeling, Analysis and Simulation of Wireless and Mobile Systems*, pages 283–290. ACM. [82](#)
- [54] Mezzavilla, M., Zhang, M., Polese, M., Ford, R., Dutta, S., Rangan, S., and Zorzi, M. (2018). End-to-end simulation of 5g mmwave networks. *IEEE Communications Surveys & Tutorials*, 20(3):2237–2263. [10](#)
- [55] Mitra, P. and Poellabauer, C. (2013). Opportunistic routing in mobile ad hoc networks. In *Routing in Opportunistic Networks*, pages 145–178. Springer. [10](#), [11](#), [77](#)
- [56] Molisch, A. F., Ratnam, V. V., Han, S., Li, Z., Nguyen, S. L. H., Li, L., and Haneda, K. (2017). Hybrid beamforming for massive mimo: A survey. *IEEE Communications Magazine*, 55(9):134–141. [3](#), [4](#)

- [57] Moulines, E. and Bach, F. R. (2011). Non-asymptotic analysis of stochastic approximation algorithms for machine learning. In *Advances in Neural Information Processing Systems*, pages 451–459. [27](#)
- [58] Nasipuri, A., Mandava, J., Manchala, H., and Hiromoto, R. E. (2000a). On-demand routing using directional antennas in mobile ad hoc networks. In *Proceedings Ninth International Conference on Computer Communications and Networks (Cat. No. 00EX440)*, pages 535–541. IEEE. [92](#), [96](#), [97](#)
- [59] Nasipuri, A., Ye, S., You, J., and Hiromoto, R. E. (2000b). A mac protocol for mobile ad hoc networks using directional antennas. In *WCNC*, volume 3, pages 1214–1219. [92](#)
- [60] Ni, W., Dong, X., and Lu, W.-S. (2017). Near-optimal hybrid processing for massive mimo systems via matrix decomposition. *IEEE transactions on signal processing*, 65(15):3922–3933. [4](#)
- [61] Olivier, P. and Simonian, A. (2016). User performance in small cells networks with inter-cell mobility. *arXiv preprint arXiv:1605.08353*. [6](#), [70](#), [75](#)
- [62] Perfecto, C., Del Ser, J., Ashraf, M. I., Bilbao, M. N., and Bennis, M. (2016). Beamwidth optimization in millimeter wave small cell networks with relay nodes: A swarm intelligence approach. In *European Wireless 2016; 22th European Wireless Conference*, pages 1–6. VDE. [9](#)
- [63] Perfecto, C., Del Ser, J., and Bennis, M. (2017). Millimeter-wave v2v communications: Distributed association and beam alignment. *IEEE Journal on Selected Areas in Communications*, 35(9):2148–2162. [9](#), [10](#)
- [64] Perkins, C. E. and Bhagwat, P. (1994). Highly dynamic destination-sequenced distance-vector routing (dsv) for mobile computers. In *ACM SIGCOMM computer communication review*, volume 24, pages 234–244. ACM. [11](#), [77](#), [78](#), [82](#)
- [65] Pinkus, A. (1999). Approximation theory of the mlp model in neural networks. *Acta numerica*, 8:143–195. [27](#)

- [66] Rappaport, T. S., Sun, S., Mayzus, R., Zhao, H., Azar, Y., Wang, K., Wong, G. N., Schulz, J. K., Samimi, M., and Gutierrez, F. (2013). Millimeter wave mobile communications for 5g cellular: It will work! *IEEE access*, 1:335–349. [10](#)
- [67] Richter, Y. and Bergel, I. (2015). Optimal and suboptimal routing based on partial csi in wireless ad-hoc networks. In *2015 IEEE 16th International Workshop on Signal Processing Advances in Wireless Communications (SPAWC)*, pages 191–195. IEEE. [11](#)
- [68] Riley, G. F. and Henderson, T. R. (2010). The ns-3 network simulator. In *Modeling and tools for network simulation*, pages 15–34. Springer. [82](#)
- [69] Roh, W., Seol, J.-Y., Park, J., Lee, B., Lee, J., Kim, Y., Cho, J., Cheun, K., and Aryanfar, F. (2014). Millimeter-wave beamforming as an enabling technology for 5g cellular communications: Theoretical feasibility and prototype results. *IEEE communications magazine*, 52(2):106–113. [11](#)
- [70] Sakaguchi, K., Haustein, T., Barbarossa, S., Strinati, E. C., Clemente, A., Destino, G., Pärssinen, A., Kim, I., Chung, H., Kim, J., et al. (2017). Where, when, and how mmwave is used in 5g and beyond. *IEICE Transactions on Electronics*, 100(10):790–808. [1](#)
- [71] Schnabel, R. B. and Eskow, E. (1990). A new modified cholesky factorization. *SIAM Journal on Scientific and Statistical Computing*, 11(6):1136–1158. [19](#)
- [72] Seber, G. A. and Lee, A. J. (2012). *Linear regression analysis*, volume 329. John Wiley & Sons. [27](#)
- [73] Sharif, M. and Hassibi, B. (2005). On the capacity of mimo broadcast channels with partial side information. *IEEE Transactions on information Theory*, 51(2):506–522. [5](#), [8](#), [48](#), [49](#), [51](#), [59](#), [94](#)
- [74] Sohrabi, F. and Yu, W. (2015). Hybrid beamforming with finite-resolution phase shifters for large-scale mimo systems. In *2015 IEEE 16th International Workshop on Signal Processing Advances in Wireless Communications (SPAWC)*, pages 136–140. IEEE. [3](#), [4](#)

- [75] Sohrabi, F. and Yu, W. (2016). Hybrid digital and analog beamforming design for large-scale antenna arrays. *IEEE Journal of Selected Topics in Signal Processing*, 10(3):501–513. [3](#), [4](#)
- [76] Song, J., Choi, J., and Love, D. J. (2015). Codebook design for hybrid beamforming in millimeter wave systems. In *2015 IEEE International Conference on Communications (ICC)*, pages 1298–1303. IEEE. [3](#), [4](#)
- [77] Sun, S., Rappaport, T. S., Rangan, S., Thomas, T. A., Ghosh, A., Kovacs, I. Z., Rodriguez, I., Koymen, O., Partyka, A., and Jarvelainen, J. (2016). Propagation path loss models for 5g urban micro-and macro-cellular scenarios. In *2016 IEEE 83rd Vehicular Technology Conference (VTC Spring)*, pages 1–6. IEEE. [80](#), [94](#)
- [78] Telatar, E. (1999). Capacity of multi-antenna gaussian channels. *European transactions on telecommunications*, 10(6):585–595. [49](#)
- [79] Thornburg, A., Bai, T., and Heath, R. W. (2016). Performance analysis of outdoor mmwave ad hoc networks. *IEEE Transactions on Signal Processing*, 64(15):4065–4079. [11](#), [92](#), [101](#)
- [80] Tomaszewski, A. and Pióro, M. (2016). Packet routing and frame length optimization in wireless mesh networks with multicast communications. In *2016 17th International Telecommunications Network Strategy and Planning Symposium (Networks)*, pages 1–6. IEEE. [8](#)
- [81] Va, V., Vikalo, H., and Heath, R. W. (2016). Beam tracking for mobile millimeter wave communication systems. In *2016 IEEE Global Conference on Signal and Information Processing (GlobalSIP)*, pages 743–747. IEEE. [75](#)
- [82] Vural, S. and Ekici, E. (2009). On multihop distances in wireless sensor networks with random node locations. *IEEE Transactions on Mobile Computing*, 9(4):540–552. [100](#)
- [83] Wang, Z., Li, M., Liu, Q., and Swindlehurst, A. L. (2018). Hybrid precoder and combiner design with low-resolution phase shifters in mmwave mimo systems. *IEEE Journal of Selected Topics in Signal Processing*, 12(2):256–269. [3](#), [4](#)

- [84] Yifei, Y. and Xinhui, W. (2017). 5g new radio: Physical layer overview. *ZTE Communications*, 15(S1):3–10. [10](#)
- [85] Yu, X., Shen, J.-C., Zhang, J., and Letaief, K. B. (2016a). Alternating minimization algorithms for hybrid precoding in millimeter wave mimo systems. *IEEE Journal of Selected Topics in Signal Processing*, 10(3):485–500. [3](#), [14](#), [16](#), [19](#), [27](#), [28](#), [30](#)
- [86] Yu, X., Zhang, J., and Letaief, K. B. (2016b). Alternating minimization for hybrid precoding in multiuser ofdm mmwave systems. In *2016 50th Asilomar Conference on Signals, Systems and Computers*, pages 281–285. IEEE. [3](#), [4](#), [14](#), [16](#), [17](#), [19](#), [26](#), [27](#), [28](#), [30](#)
- [87] Yu, X., Zhang, J., and Letaief, K. B. (2017). Hybrid precoding in millimeter wave systems: How many phase shifters are needed? In *GLOBECOM 2017-2017 IEEE Global Communications Conference*, pages 1–6. IEEE. [3](#), [4](#)
- [88] Zhu, G., Huang, K., Lau, V. K., Xia, B., Li, X., and Zhang, S. (2017). Hybrid beamforming via the kronecker decomposition for the millimeter-wave massive mimo systems. *IEEE Journal on Selected Areas in Communications*, 35(9):2097–2114. [4](#), [5](#)

Vita

After graduating from the Computer Engineering department in the University of Basrah-Iraq with Bsc degree in 2007, Mustafa S. Aljumaily joined the MSc studies in the same department and completed the MSc requirements with honor in 2010. Meanwhile, he worked in many places as an IT Engineer with many duties ranging from data entry, LAN management, Enterprise Network administration, Data Base management, Coding, to GIS Section supervision. In the Spring of 2015, he joined the UTK English Language Institute (ELI) to prepare for the the TOEFL and GRE requirements. After finishing all the conditional admission's requirements, he started his PhD program in the University of Tennessee in the Summer of 2015. During his PhD study, he attended more than 10 classes about all different kinds of EECS topics with special focus on machine learning, wireless communications and networking.

Some of the projects he worked on include Human Gestures Recognition using WiFi CSI signals, Wireless communications using mmWave signals, designing and implementing a VPN and photo sharing websites, designing routing protocols for ad hoc wireless networks, designing hybrid beamforming systems for mmWave wireless networks using convex optimization, matrix factorization, and machine learning, and many other projects. His research got accepted and published in some excellent conferences includes ICICT, VTC-2018, VTC-2019, Globecom, and DySPAN. Some journals that has his publications include IJPC, IJCSI, IJCNC. He reviewed more than 30 papers for many journals and conferences.